

UTRECHT UNIVERSITY

INSTITUTE FOR THEORETICAL PHYSICS

MASTER THESIS

---

# Holographic Massive Fermions

---

*Author:*

Francisco GARCÍA FLÓREZ

*Supervisors:*

PROF. DR. IR. H. T. C. STOOF  
N. W. M. PLANTZ, MSc

June 27, 2017

**Abstract.** In this thesis we will focus on developing a systematic model for describing the behavior of a gas of cold fermionic atoms using semi-holographic methods. Specifically we will make use of the AdS<sub>5</sub>/CFT<sub>4</sub> correspondence, focusing on introducing a scalar field in the bulk that encodes the mass of the boundary fermions. Then, working in the probe limit, we will develop a method involving two fermionic bulk fields for describing massive fermions in the boundary, and analyze their behavior by computing the spectral function. Finally, we will discuss the physical interpretation of the dependence of the spectral function with the parameters of the theory.

# Contents

<b>1</b>	<b>Introduction</b>	<b>1</b>
1.1	Motivation . . . . .	1
1.2	Outline . . . . .	3
1.3	Conventions . . . . .	3
<b>2</b>	<b>Holography in Condensed Matter Physics</b>	<b>4</b>
2.1	The Anti-de Sitter/Conformal Field Theory correspondence . . . . .	4
2.1.1	The Dictionary and the GKPW master rule . . . . .	4
2.1.2	The Bulk Geometry . . . . .	6
2.2	Beyond the Basic Dictionary . . . . .	8
2.2.1	Introducing a Mass . . . . .	8
<b>3</b>	<b>Background Bulk Model</b>	<b>10</b>
3.1	Introduction . . . . .	10
3.2	Chemical Potential . . . . .	11
3.3	Mass Scale . . . . .	12
3.3.1	Bosonic Action and Equations of Motion . . . . .	12
3.3.2	Bosonic Asymptotic Behavior . . . . .	14
3.3.3	Numerically Solving the Equations of Motion . . . . .	17
<b>4</b>	<b>Fermionic Bulk Model</b>	<b>23</b>
4.1	Introduction . . . . .	23
4.1.1	Dirac Formalism in a Flat Background . . . . .	23
4.1.2	Dirac Formalism in a Curved Background . . . . .	25
4.2	Bulk Model for Chiral Fermions . . . . .	27
4.2.1	Dirac's Action and Boundary Effective Action . . . . .	27
4.2.2	Equation for the Proportionality Factor $\xi$ . . . . .	30
4.2.3	Green's Function and Spectral Function . . . . .	33
4.3	Bulk Model for Dirac Fermions . . . . .	35
4.3.1	Dirac's Action and Boundary Effective Action . . . . .	35
4.3.2	Equation for the Proportionality Factor $\xi$ . . . . .	37
4.3.3	Green's Function and Spectral Function . . . . .	40
4.3.4	Symmetries of the System . . . . .	44
4.3.5	Numerical Solution for $\xi$ . . . . .	45
4.4	Fixing the Bare Mass . . . . .	48
4.4.1	Renormalization Group Equations for $\phi$ . . . . .	49
4.4.2	Renormalization Group Equations for $M_0$ and $\langle i\bar{\psi}\psi \rangle$ . . . . .	50
<b>5</b>	<b>Results</b>	<b>53</b>
5.1	Holographic limit . . . . .	53
5.1.1	Dependence on $\tilde{g}$ . . . . .	53
5.1.2	Dependence on $\mu$ . . . . .	56
5.2	Semi-holography . . . . .	60
5.2.1	Dependence on $g$ . . . . .	60
5.2.2	Dependence on $\tilde{g}$ . . . . .	62
5.2.3	Dependence on $\mu$ . . . . .	65
<b>6</b>	<b>Conclusion</b>	<b>70</b>
6.1	Discussion . . . . .	70
6.2	Outlook . . . . .	70
	<b>Bibliography</b>	<b>72</b>

# 1 Introduction

## 1.1 Motivation

The study of Condensed Matter systems using string-theoretical methods is indeed a fairly recent field of research, but it has been very fruitful in its predictions and it definitely has the potential to describe complex systems in a systematic way, giving further physical insights. We will use the AdS/CFT correspondence to find a theoretical description of cold atomic gases, focusing on expressing the behavior of the system living in the CFT as the dual of the Anti-de Sitter geometry.

In the field of AdS/CFT research there are many possible paths to follow, but one of them that has been studied widely is the case of Anti-de Sitter<sub>5</sub>/CFT<sub>4</sub>, meaning that we will consider a geometry of five space-time dimensions in which fields propagate, with a 4-dimensional boundary in which the condensed matter theory lives. This is one of the simplest correspondences we can consider, and even though by itself does not provide the necessary tools we require to describe a gas of cold atoms, we can make additions to it which indeed fix these limitations.

As we just mentioned, the first motivation for using this theoretical apparatus is to correctly describe a gas of cold atoms, that is, an atomic Fermi gas at unitarity. The study of these systems has had a great progress in the last decade, with many different applications possible because of the generality of the results. These atomic Fermi gases, also called Fermi mixtures, can behave in two very different ways depending on the regime they are in: the BCS limit or the BEC (Bose-Einstein condensate) limit.

The BCS limit is characterized by the formation of loosely bound pairs of fermions with a size much larger than the usual interparticle distance. This is indeed the theory developed by Bardeen, Cooper and Schrieffer [1] describing the behavior of electron pairs. However this approach is way more general than it was thought, since it can also describe the regime in which there are strong interactions between fermions, therefore producing tightly bound molecules. This is the BEC limit, and in [2] Leggett predicted that these two limits are connected continuously by a crossover, which was verified in cold atom experiments by several groups such as [3, 4] and others.

Experiments probing the BCS-BEC crossover use Fermi mixtures, composed of one single atomic species but with two spin states, which can be balanced in the population of each spin states and thus it can Bose-condense by pairing each spin-up particle with another spin-down particle, called *balanced mixture* when the amount of particles in each state is the same. However, when the mixture is unbalanced it is not clear how the system can be described, and the solution is not only important for ultra cold atoms, but also for many other fields such as condensed matter physics, nuclear physics and even some applications in quantum chromodynamics. The importance of ultra cold Fermi gases for experiments lies in that it is possible to probe the unbalanced regime in the laboratory.

Specifically, the crossover experiments are possible because in these Fermi mixtures there are Feshbach resonances, characterized by allowing the interaction strength to vary in a basically infinite range of values by adjusting the difference in energy between free atoms and bound states. It is possible then to make all the atoms transition to the bound state by modifying the magnetic field through the Feshbach resonance, then cool them down, for example using evaporative cooling, and then taking the magnetic field back so that the Cooper pairs are now Bose-condensed. Indeed, this procedure would not been possible had these two limits not be connected by the crossover.

It was not until 2006 that [5, 6] experiments involving imbalanced Fermi mixtures were performed at the unitarity limit, that is, when the magnetic field is set in a way that the interactions are on resonance and thus its strength diverges. These experiments show the existence of several superfluid phases in the Temperature-Polarization phase diagram, as well as a tricritical point. Phase transitions around this point have been studied using several

techniques, [7, 8, 9], not all of them successfully.

At this point is when the AdS/CFT correspondence can make a significant difference in describing these theories. The goal is to derive an expression for a quantity that we can compare with experiments using Radio-Frequency Spectroscopy, which is the equivalent of ARPES, a widely use tool in condensed matter physics. Specifically, RF spectroscopy can measure the correlation function of the target system related to the single-particle Green's function. As we will see later, in AdS/CFT the Green's function is computed by considering a probe field propagating in an appropriate bulk geometry.

Interactions between the bulk geometry, and the fields propagating there, and the boundary system can be easily interpreted as follows. Consider a chiral fermion in the boundary, which we can consider is in either the IR or the UV regime. When the non-zero chiral component propagates in the boundary, the opposite chirality component can go inside the geometry, interact classically with the other fields in the bulk and come back to the boundary where it continues propagating. In the UV regime however, because of the short wavelengths involved it cannot go very far into the interior, so it will only probe the high-energy region near the boundary. However, in the IR regime the long wavelengths allow it to probe near the horizon, where the geometry is less Anti-de Sitter-like because of the black brane, and thus it will be dominated by the interactions.

Out of the many different experiments that can be performed, in this thesis we are going to focus on studying ultra-cold Fermi gases, which involve massive boundary fermions. In this case we are only considering one type of particles in the boundary, but the fact that they have a finite temperature, chemical potential and mass means that we will need to develop new techniques to derive the spectral function that can be checked in ARPES experiments.

As we mentioned earlier, chiral fermions in the boundary is the simplest possible situation we can consider, because the bulk model only involves the usual black brane giving a finite temperature, a gauge field associated with the chemical potential and a probe fermion field propagating on that geometry. Clearly this is not a good approach since atoms are not chiral particles, so our first goal is to introduce a new field in the bulk whose dual in the boundary will be associated with the mass term in Dirac's action.

Once we have figured this problem out, we have to realize that it is not possible to have massive chiral fermions, making that our second goal. As we have mentioned before, only one of the chiralities can propagate inside the geometry, while the other one stays in the boundary. This behavior occurs because, for the holography contribution to appear, we need to integrate out half of the degrees of freedom ("DoF" from now on) of the fermionic field. Therefore, with only one probe field in the bulk, that is with four DoF, we can have up to two non-zero components in the boundary. One way of dealing with this problem is to introduce another probe field in the bulk, coupled together with the other one and the scalar field that gives mass to the particles, so that combining their degrees of freedom remaining in the boundary we can have one full Dirac fermion.

Even though the technical aspect of this procedure is important, our third and most important goal is to correctly analyze and interpret the physical consequences of changing the parameters introduced by these fields. Successfully extracting the relevant information from the results, in a way that can be compared to experiments is the main motivation of this thesis.

## 1.2 Outline

1. **Section 2: Holography in Condensed Matter Systems.** We will begin with a more detailed introduction to the field of holography in condensed matter physics, starting with its fundamental idea of duality and what it means in terms of fields and boundary operators. The main goal of section 2 is to briefly review the general picture of the AdS/CFT correspondence, and at the same time qualitatively introduce several concepts that we will use in the remainder of the thesis.

Finally, we will introduce the concept of semi-holography, which is absolutely required to make physically meaningful predictions which can be contrasted with experiments, mainly using RF spectroscopy as we mentioned previously.

2. **Section 3. Background Bulk Model.** In section 3 we will take the qualitative ideas we presented in the previous one and expand on them with the specific mathematics. Starting with the basic Anti-de Sitter geometry in the bulk, we will introduce the features of the boundary system one by one, explaining how each of them appear in the holography dictionary related to their dual operators.

Once the fundamental ideas are introduced, we can proceed to the most important feature of this thesis: introducing a mass energy scale in the bulk. For that we will need to use some of the already known dictionary entries in a different way, finding that indeed the boundary particles have now a mass.

3. **Section 4: Fermionic Bulk Model** We proceed then to the main topic of the thesis, in which the goal is to derive an expression for the spectral function in terms of the bulk fields. For that, we will begin by introducing some necessary mathematical machinery in the form of Dirac formalism, which we will generalize to curved backgrounds.

Next, we will derive an expression for the Green's function in the simpler case of massless boundary fermions. This way, we can focus on explaining the tools used to derive the more general result of massive boundary fermions, without complicating the calculations too much.

4. **Section 5: Results.** Lastly we will present some of the most interesting results obtained from the contents derived in the previous sections, and discuss their significance and physical interpretation. We will both consider the holographic limit and the semi-holographic answer, focusing mainly in the dependence of the spectral function and mass gap as a function of the free parameters of the theory.

## 1.3 Conventions

There are several convention we will follow in this thesis, which we will enumerate below.

1. We will refer to the dimensionality of the space-time in the boundary theory by  $d$ , meaning  $d - 1$  space coordinates and 1 time dimension. Similarly, the dimensionality of the bulk will be  $d + 1$ , including both time and space coordinates.
2. The sign convention for the metric is  $\text{diag}(-, +, \dots)$ , in  $d = 4$  or  $d = 5$  dimensions depending on if we are working in the boundary or in the bulk.
3. Everything will be expressed in natural units, meaning  $\hbar = c = k_B = 1$ , but also we will express distances in units of  $L$ , the Anti-de Sitter radius.
4. The coordinates in the boundary will be denoted by 0, 1, 2, 3. The radial dimension index will always be  $r$ , and similarly any  $r$  used as a coordinate variable is referring to the extra dimension.

## 2 Holography in Condensed Matter Physics

In this section we will introduce the fundamental ideas behind the application of holographic methods to condensed matter systems. We will start by broadly stating some of the more general concepts, and then narrowing our focus towards the contents of this thesis.

Since the point of this section is not to be a very thorough review of AdS/CFT applied to condensed matter, references [10, 19] are better suited to fulfil further curiosity from the reader.

### 2.1 The Anti-de Sitter/Conformal Field Theory correspondence

We will begin visiting the main goal of any AdS/CFT research in condensed matter physics: the building of a dictionary that relates fields in the bulk with operators in the CFT. Understanding this dualities is a crucial step to gaining deeper insights into the boundary theory, and therefore the basis of this thesis.

Next, we will briefly look at the string-theoretical arguments that actually allow us to associate the bulk and the boundary theory, known as the GPKW rule. Here we will also mention the two possible approaches to Anti-de Sitter/CMT, either *top-down* or *bottom-up*.

Finally, we will study more in detail the bulk geometry and some of the properties of the Anti-de Sitter space-time, as well as briefly mentioning the non-equilibrium case.

#### 2.1.1 The Dictionary and the GKPW master rule

The idea of dualities is not strange to any physicist, since we have been using them in one form or another to describe a very large amount of systems in nature, such as the KW-duality in the 2d Ising model. At its core, the AdS/CFT correspondence is just another way of relating two theories, one that behaves in a very non-perturbative, strongly interacting regime, and another one weakly interacting in the classical limit. These two sides of the duality correspond to the boundary and bulk of some non-trivial geometry, in which the information about the boundary theory is encoded using classical general relativity.

This correspondence, as opposed to many others, comes from string theory as a limit case of a more general case. Significant research has been done in this direction, but one of the earliest versions of AdS/CFT, done by Maldacena in [11], came from a compactification of a 10-dimensional theory down to a manifold like  $\text{AdS}_5 \times S^5$ , which in practice means a general relativity background with added black holes (or black branes, as they would be called in this context), gauge, scalar and fermion fields.

There is however a fundamental difference between the boundary theories described by the early approaches from String Theory and the ones we will be considering. Because getting rid of the extra five dimensions requires a process of compactification, any simplistic approach will result in maximally supersymmetric Yang-Mills gauge theories in the boundary, which we cannot use to describe any real world condensed matter system such as cold atom gases. Any non-trivial compactification that should result in less symmetric systems is indeed very complicated, but the research is ongoing.

There are other limitations that we are glossing over, such as the large- $N$  limit and the 't Hooft limit. The latter is related to the interaction strength, and it is not discouraging for us because taking the limit of large interaction strength means that we are working in the strongly coupled limit of the boundary theory, precisely the regime we are interested in studying. In a similar way, supersymmetric theories are not the only ones that can be described in the boundaries, since there are explicit examples which indeed break supersymmetry.

The large- $N$  limit however is more important, since it can affect the results. In a nutshell, what this limit physically represents in the string theory context of describing gluons in QCD, is related to the number of

gluons in the theory ( $N^2 - 1$  to be precise). As we know, the Standard Model includes only three types of gluons, so this limit would mean considering a very large amount of them. Most importantly, moving away from this limit is not trivial, but in condensed matter physics there had been several attempts to study the possible effect of these  $1/N$  corrections by studying Gaussian fluctuations of the bulk fields.

With these requisites in mind, we can move on to the actual rules this holography dictionary contains. Summarizing in the following table the basic building blocks are listed:

<b>Bulk in <math>d + 1</math> dimensions</b>	<b>Boundary in <math>d</math> dimensions</b>
Scalar field $\phi$	Scalar composite operator $\mathcal{O}_\phi$
Vector field $A_\mu$	Current operator $J_\mu$
Space-time metric $g_{\mu\nu}$	Stress-energy tensor $T_{\mu\nu}$
Dirac field $\psi$	Chiral composite operator $\mathcal{O}_\psi$
Boundary value of field	Source of operator
Mass of the field	Conformal dimension of operator
$U(1)$ gauge field	Global $U(1)$ symmetry
Black hole Hawking temperature	Temperature of thermal equilibrium

Table 1: These dictionary entries will be used repeatedly throughout the thesis.

Let us study them in more detail. Consider first a partition function in the CFT,

$$Z_{\text{CFT}}[\mathcal{F}_s] = \int \mathcal{D}\mathcal{F} \exp \left[ i \left( S_{\text{QFT}} + \int d^d x \mathcal{F}_s(x) \mathcal{O}_{\mathcal{F}}(x) \right) \right] , \quad (2.1)$$

where  $\mathcal{F}$  is any given field of the boundary theory. Here, differentiating with respect to  $\mathcal{F}_s(x)$  we can obtain the expectation values of the operator  $\mathcal{O}_{\mathcal{F}}(x)$ , and therefore  $\mathcal{F}_s(x)$  is considered to be the *source* of the operator  $\mathcal{O}_{\mathcal{F}}(x)$ .

In usual CFTs this source field is fixed, but in our context we will consider it to be dynamical, allowing it to propagate deep into the bulk. Connecting the asymptotic behavior of these bulk fields with the source operators is what the AdS/CFT correspondence lets us do because of the GKPW rule [12, 13], which fundamentally states that

$$\left\langle \exp \left[ i \int d^d x \mathcal{F}_s(x) \mathcal{O}_{\mathcal{F}}(x) \right] \right\rangle_{\text{QFT}} = \exp \left[ i S_{\text{bulk}}[\mathcal{F}(x, r \rightarrow \infty) \rightarrow \mathcal{F}_s(x)] \right] . \quad (2.2)$$

This expression fundamentally relates the full quantum content of the boundary CFT to the classical action in the bulk, though only in the  $N \rightarrow \infty$  limit. This is the step in which considering a finite  $N$  can be introduced, one possible method being to introduce higher order loop contributions to the gravity theory, given by some approximation to a full Quantum Gravity action. This procedure can be made systematic, but it significantly increases the difficulty of finding solutions.

Associating bulk fields to sources in the boundary is but one tool this mechanism provides. In addition to this, symmetries of the boundary theory can also be encoded in the geometry of the bulk. Specifically, a conserved quantity in the CFT, such as the electric charge, is associated with a  $U(1)$  symmetry which is dual to a  $U(1)$  gauge field  $A_\mu$  in the bulk. Similarly, if instead we consider the global invariance of the stress-energy tensor in the boundary, it has to be dual to the diffeomorphism invariance of the bulk.

Closely related to these dualities, the mass of the bulk fields is directly connected to the dimensionality of the associated boundary operator. Therefore, they are not usual parameters of the theory, but instead *define* the

boundary theory we are considering. A simple example of this is to compute the critical exponents of some quantities in the boundary, and see that indeed they depend in parameters like the mass.

Finally, spinors in the bulk behave in a slightly different way compared to bosons, and we will focus one section later to explain their details. On the other hand, the last entry in the table, it is an intuitive result that the temperature of the boundary system would be related to the Hawking radiation emitted by the black hole in the bulk. This idea also points at the fact that systems out of equilibrium, with a time-dependent  $T$ , are related to changes in the geometry of the bulk over time.

To conclude, we can take a look at two fundamentally different approaches to this problem that we have briefly mentioned. Maldacena and others in the early days of AdS/CFT followed a procedure denominated *top-down* to find the boundary theory, which means taking the full 10 (or 11)-dimensional string theory and compactify the extra dimensions in a very non-trivial way, so that the boundary theory is not supersymmetric and thus can be used to describe the systems we are interested in.

Our approach to the problem is the opposite, we will consider a bulk geometry with fields classically interacting, described by some action  $S_{\text{bulk}}$ . Then, assuming that indeed there exists at least one boundary theory that is consistent with our bulk, we can proceed to extract the information it predicts comparing it with experiments. This approach is known as *bottom-up*, and even though it is only conjectured that it is possible to obtain any physically meaningful results from it, it definitely has the potential to provide many meaningful results and insights. Usually, this branch of AdS/CFT is called AdS/CMT.

The main goal of AdS/CMT is therefore to find these dualities between bulk fields and boundary operators since, opposed to the *top-down* approach, we cannot know the dual CFT to the bulk theory. Instead, we can only choose the correct dimensionality of the conformal operator and check that it behaves as expected.

### 2.1.2 The Bulk Geometry

Now that the idea of the dictionary has been introduced, we can take a slightly closer look at the Anti-de Sitter space-time. We can start from the Einstein-Hilbert action with a cosmological constant  $\Lambda$ :

$$S = \frac{1}{16\pi G} \int d^{d+1} \sqrt{-g} [R - 2\Lambda] \quad . \quad (2.3)$$

Here the cosmological constant  $\Lambda$  is related to the AdS radius  $L$  as

$$\Lambda = -\frac{d(d-1)}{2L^2} \quad , \quad (2.4)$$

and we find that the AdS metric is a solution of the field equations:

$$ds^2 = -\frac{r^2}{L^2} dt^2 + \frac{L^2}{r^2} dr^2 + \frac{r^2}{L^2} d\mathbf{x}^2 \quad . \quad (2.5)$$

As we mentioned in the conventions, we will express every length distance in units of this quantity  $L$ , so it will not appear again in the remainder of the thesis. Specifically, the coordinate transformation is

$$r \rightarrow Lr \quad , \quad t \rightarrow Lt \quad , \quad \mathbf{x} \rightarrow L\mathbf{x} \quad , \quad s \rightarrow Ls \quad . \quad (2.6)$$

Here we can see that this metric has  $d+1$  coordinates, with  $r$  defined as the radial coordinate in the bulk. The simplest physical interpretation of this is to consider the usual  $d$  coordinates in our system as the limit  $r \rightarrow \infty$ . In Figure 2.1 we can see a visual representation of this.

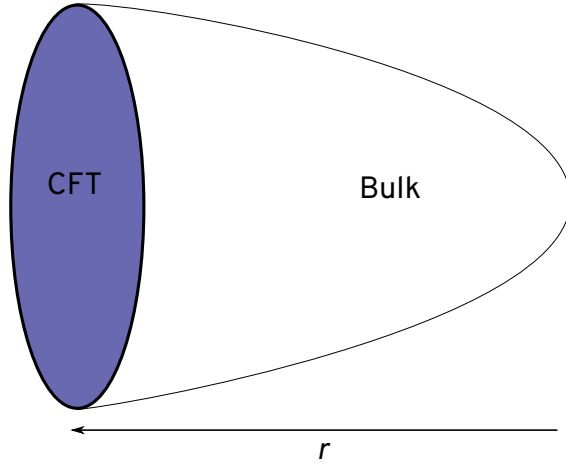


Figure 2.1: Visual representation of the CFT as the limit  $r \rightarrow \infty$  of the radial coordinate in the bulk.

However, this radial coordinate is different from the others, in the sense that its curvature has to encode the energy scale information of the theory. In this regard the Anti-de Sitter metric by itself is fairly simplistic, since it is invariant under the following scaling of coordinates:

$$r \rightarrow \frac{r}{\lambda} , \quad t \rightarrow \lambda t , \quad \mathbf{x} \rightarrow \lambda \mathbf{x} , \quad (2.7)$$

meaning that any boundary theory described using this metric has to be invariant at all energy scales. Clearly this is not sufficient to model most of the real systems we are interested in, so the only possibility is to consider the most general static solution to the field equations with planar symmetry, which contains the two functions  $f(r)$  and  $\chi(r)$ . This new metric breaks the scaling invariance while maintaining Lorentz invariance. It reads:

$$ds^2 = -f(r)e^{-\chi(r)}dt^2 + \frac{dr^2}{f(r)} + r^2d\mathbf{x}^2 . \quad (2.8)$$

As we will see, these two functions  $f(r)$  and  $\chi(r)$  will have a very relevant physical interpretation, but they have to satisfy one condition regardless of the model. We are interested in studying the behavior of cold Fermi gases in the strongly interacting limit, which means that interactions in the IR regime will be driving the physics of the system. Therefore,  $f(r)$  and  $\chi(r)$  should only deviate from the Anti-de Sitter solution deep in the geometry, and reduce to the previous metric at the boundary.

We have mentioned before the existence of black holes in the geometry, as a way to introduce a temperature in the boundary theory. This is one of the simplest examples of how the Anti-de Sitter metric is deformed near the, now horizon, of the black hole while the limit  $r \rightarrow \infty$  is kept unchanged.

Another option, this time considering a boundary system at exactly zero temperature, involves introducing an electron star in the bulk. This specific solution has several advantages, for example being suitable for studying back-reactions of the fields on the geometry. It is necessary however to consider the electrons in the fluid limit, also called the hydrodynamic limit, so that they can be described by the General Relativity version of the Navier-Stokes equations. Under these conditions, it is possible to solve the coupled system of equations, including the fermionic back-reaction on the background.

This is especially important for studying phase transitions in the boundary theory, and therefore the stability of the solution. We will however only focus on the probe limit of the theory, considering back-reactions one of the next possible step in the research of this field.

## 2.2 Beyond the Basic Dictionary

Now that we have presented the fundamental concepts of the AdS/CFT correspondence, it is time to briefly introduce how exactly this thesis and subsequent works will expand on them. Our most important goal is, because of the atomic system we want to describe, to introduce a new energy scale in the bulk theory that will be related to the mass of the boundary particles.

There are several different approaches that we will mention, and some alternatives to these such as particles being bosons or fermions. As before, the goal of this section is not to be a thorough review but to present succinctly the most important ideas.

Then, we will present some ideas related to the next logical step in this topic, namely considering the non-relativistic limit of the theory. Since atoms in these Fermi gases are very massive compared to their kinetic energy, as in  $M_0 \gg T$ , better insights into their behavior can be derived from this limit.

### 2.2.1 Introducing a Mass

In the context of AdS/CFT, introducing massive particles corresponds to a specific low-energy behavior of the spectral function: a mass gap. Considering the dispersion relation for classical massive particles,

$$\omega(k) = \sqrt{|\mathbf{k}|^2 + m^2} \quad , \quad (2.9)$$

our results should also reproduce this parabolic behavior. There are however several possible ways to introduce deviations from the relativistic dispersion relation  $\omega = |\mathbf{k}|$  characteristic of particles interacting in the usual Anti-de Sitter backgrounds, one of them being *Lifshitz Holography*.

This approach is based on introducing a critical exponent  $z$  to the energy scale near the critical point. Fundamentally, this exponent is introducing an anisotropy between time and space which results in systems that satisfy the following scaling symmetry

$$t \rightarrow \lambda^z t \quad , \quad \mathbf{x} \rightarrow \lambda \mathbf{x} \quad . \quad (2.10)$$

Clearly the case  $z = 1$  reduces to our previous discussion for normal Anti-de Sitter geometries, the main difference being that in the case  $z = 2$  the dispersion relation is now  $\omega(k) \propto k^2$ . This is indeed the case for non-relativistic theories, but it requires a different type of bulk space-time:

$$ds^2 = -\frac{r^{2z}}{L^{2z}} dt^2 + \frac{L^2}{r^2} dr^2 + \frac{r^2}{L^2} d\mathbf{x}^2 \quad . \quad (2.11)$$

Physically, when we approach the boundary as  $r \rightarrow \infty$ , the  $tt$  component of the metric diverges faster than the  $ii$  components, therefore generating the effect of a diverging speed of light at the boundary.

On the other hand, we can work with  $z = 1$  Lorentz invariant Anti-de Sitter geometry. This approach forces us to work in a relativistic formulation of the problem from the beginning, which in turn means that the low-energy behavior of the boundary particles associated with a mass requires extra fields, as we will see. Analogue to encoding the energy scale information of the theory in the bulk, we are interested in introducing a field in the bulk that is asymptotically dual to a mass contribution for the boundary particles.

The duality dictionary already has an answer for this: because we are interested in a boundary operator with some specific dimensionality, we should add a scalar field  $\phi$  to the bulk with a mass  $m^2$  of a specific value so

that it is dual to the mass of an operator in the boundary. At this point we can consider the boundary particles to be bosons or fermions, for whose the boundary action would be

$$\begin{aligned}
\text{bosons:} \quad S_{\text{bdy}} &\propto \int d^4x [(\partial\phi_{\text{bdy}})^2 + M_{\text{bdy}}^2\phi^2] \\
\text{fermions:} \quad S_{\text{bdy}} &\propto \int d^4x [\bar{\psi}_{\text{bdy}}\not{\partial}\psi_{\text{bdy}} - M_{\text{bdy}}\bar{\psi}_{\text{bdy}}\psi_{\text{bdy}}]
\end{aligned}
, \quad \text{“bdy”} \sim \text{boundary} . \quad (2.12)$$

Therefore, in the case of bosons we want the dimensionality of the operator to be 2 (because of  $\phi_{\text{bdy}}^2$ ) and the source also to be 2 (because of  $M_{\text{bdy}}^2$ ). However, in the case of fermions the operator dimension is 3, and the source has dimensionality 1. This difference means that the process to extract the asymptotic behavior of the bulk scalar field slightly deviates from each other, but the core idea of matching dimensionalities remains the same.

Extracting the spectral function in each case is a very different procedure however, and in this thesis we will focus on developing a general method to compute it for massive fermions in the boundary. Finding an expression for the single particle Green’s function that depends on  $\omega$  and  $\mathbf{k}$  requires *semi-holography*, which is equivalent to promoting the boundary source to a dynamical field. In Section 4 we will cover this for the derivation of the spectral function.

### 3 Background Bulk Model

In the following section we will dive deeper into the concepts introduced in the previous one, and specifically expanding on the relevant topics for the next part. We will begin working with just the bare relativistic background and then proceed to add other fields to the bulk, arguing what is that we want to find at the boundary. Finally, we will explain the key step of introducing a mass scale in the geometry, and set everything up for the introduction of fermionic fields.

#### 3.1 Introduction

In the previous section we have seen that it is certainly possible to derive physically relevant results by considering only small perturbations of the Anti-de Sitter metric. However, we are more interested in working with a more general geometry that allows us to introduce other effects in the boundary, such as temperature, for which we need to consider a different bulk metric. As we have seen, the normal Anti-de Sitter metric can be written in the following coordinates:

$$ds^2 = -r^2 dt^2 + \frac{dr^2}{r^2} + r^2 d\mathbf{x}^2 \quad , \quad (3.1)$$

where  $r$  is the radial dimension of the bulk. As we mentioned, a more general metric that is also a solution of the field equations contains the functions  $f(r)$  and  $\chi(r)$  as follows:

$$ds^2 = -f(r)e^{-\chi(r)} dt^2 + \frac{dr^2}{f(r)} + r^2 d\mathbf{x}^2 \quad . \quad (3.2)$$

It is clear to see that, if we compare these two metrics, for the geometry to be *asymptotically* Anti-de Sitter these two fields have to satisfy the following

$$\begin{aligned} \lim_{r \rightarrow \infty} f(r) &= r^2 \\ \lim_{r \rightarrow \infty} \chi(r) &= 0 \end{aligned} \quad . \quad (3.3)$$

The main goal we seek with this more general background is to provide a way to encode in the bulk information about the boundary temperature. As we have seen earlier in the duality dictionary, a temperature in the CFT can be introduced in the bulk by creating Hawking radiation with a black hole (also called black brane).

In an usual General Relativity context, we know that the simplest black hole is defined by the Schwarzschild's metric, although defined in four space-time dimensions. It is possible to rewrite this background in our situation with only one curved dimension and asymptotically approaching the Anti-de Sitter metric by using the Ansatz for the fields

$$\begin{aligned} f(r) &= r^2 \left( 1 - \left( \frac{r_h}{r} \right)^d \right) \quad , \\ \chi(r) &= 0 \end{aligned} \quad (3.4)$$

where  $r_h$  is the horizon radius. We can now compute the temperature of the Hawking radiation associated with this black hole, which is in general given by

$$T = \frac{1}{4\pi} f'(r_h) e^{-\chi(r_h)/2} \longrightarrow T_{\text{Sch}} = \frac{d}{4\pi r_h} , \quad (3.5)$$

which we will use to compute the temperature of the boundary system given a specific background.

Even though it is certainly possible to derive a great amount of physics just considering small perturbations of the metric (3.1), we will only work with the numerical solution to the equations of motion for the background coupled to other fields. Consider then the following Einstein-Hilbert action:

$$S_0 = \frac{1}{16\pi G} \int d^{d+1}x \sqrt{-g} (R - 2\Lambda) , \quad (3.6)$$

where  $G$  is the gravitational constant and  $\Lambda$  is the cosmological constant. To find the metric shown in equation (3.1),  $\Lambda$  has to be fixed to:

$$\Lambda = -\frac{d(d-1)}{2L^2} . \quad (3.7)$$

Now we can proceed to obtain the equations of motion for  $f(r)$  and  $\chi(r)$  from the variation of  $S_0$ , giving as a result Einstein's field equations in the general case

$$R_{\mu\nu} - \frac{1}{2} R g_{\mu\nu} + \Lambda g_{\mu\nu} = 8\pi G T_{\mu\nu} , \quad (3.8)$$

where once we introduce other fields they will contribute to  $T_{\mu\nu}$  by

$$T_{\mu\nu} = \frac{-2}{\sqrt{-g}} \frac{\delta \mathcal{L}_{\text{matter}}}{\delta g^{\mu\nu}} . \quad (3.9)$$

Here  $\mathcal{L}_{\text{matter}}$  refers to the matter contribution in the action, which in the case of equation (3.6) is clearly zero. In the remainder of this section we will introduce new fields that will indeed appear in the matter contribution to the action. Instead of working with the covariant form of the field equations shown in (3.8), we will substitute the Ansatz from (3.2) in the left hand side of (3.8), and by combining them we can extract two equations of motion for  $f(r)$  and  $\chi(r)$ .

## 3.2 Chemical Potential

In this section we will proceed by introducing a chemical potential in the boundary theory by adding a new field in the bulk. As we have mentioned before, global symmetries in the CFT translate to local ones in the geometry, which in this case corresponds to a conserved electric charge. It is a global  $U(1)$  symmetry, so the corresponding field in the bulk is a  $U(1)$  gauge field, or in other words, the usual  $A_\mu$  electromagnetic potential.

In this case however we still need to consider the curved background in which  $A_\mu$  propagates, so we need a new term in the action that accounts for this contribution, as follows

$$S_A = -\frac{1}{4\mu_0} \int d^{d+1}x \sqrt{-g} F_{\mu\nu} F^{\mu\nu} . \quad (3.10)$$

In the following, we will take  $\mu_0 = 1$ . Adding  $S_A$  to  $S_0$ , as defined in equation (3.6), gives the Einstein-Maxwell action. This is the simplest possible combination of classical gravity and electromagnetism and, similarly to the

previous Schwarzschild solution, it is possible to find an analytic solution that asymptotically resembles Anti-de Sitter and is known as the AdS Reissner-Nordström black hole.

The solution this time is the following, as we can see in [19],

$$\begin{aligned}
 f(r) &= r^2 + \frac{Q^2}{r^{2d}} - \frac{M}{r^{d-2}} & \mu &= \frac{\sqrt{2}Q}{c_d r_h^{d-2}} \\
 \chi(r) &= 0 & c_d &= \sqrt{\frac{2(d-2)}{d-1}} \\
 A_t(r) &= \mu \left( 1 - \frac{r_h^{d-2}}{r^{d-2}} \right) & M &= r_h^d + \frac{Q^2}{r_h^{d+2}}
 \end{aligned} \tag{3.11}$$

Here  $M$  and  $Q$  the mass and charge of the black hole, respectively. We can see here that we still do not need the degree of freedom introduced by the field  $\chi(r)$  to find a solution, however in the next section it will become very relevant. Another detail we see here is that we have chosen a specific gauge for the  $A_\mu$  field, in which we take all components other than  $t$  to zero, so that only the dependence shown above contributes.

This solution has more interesting characteristics than the Schwarzschild one, that we can make more obvious by looking at the condition we find for the mass of this black hole

$$M^{\frac{2d-2}{d-2}} \geq \frac{2d-2}{d-2} \left( \frac{2d-2}{d} \right)^{\frac{d}{d-2}} Q^{\frac{2d}{d-2}} \tag{3.12}$$

obtained by computing  $f(r_h) = 0$  and considering the case  $r_h \geq 0$ . When this inequality becomes an true equality we find quite an interesting solution, in which the temperature of the black hole is exactly zero but with a nonzero entropy. That we can see from the fact that since  $r_h$  is nonzero the area of the black hole is also going to be nonzero and therefore, since the Hawking entropy of the black hole is proportional to its area, it will not be zero.

As we know from classical thermodynamics, this is a very strange result for a classical system. We have found however other quantum systems, like frustrated lattices, that behave in a similar way. Finding this situation in such a simple system is nevertheless remarkable, and ongoing research on this topic will provide more answers.

In this thesis these thermodynamic problems will not arise, since once we introduce a scalar field in the bulk the limit  $T \rightarrow 0$  does indeed correspond to the black hole radius  $r_h \rightarrow 0$ . Therefore, for a finite  $r_h$  the temperature will always be non-zero.

### 3.3 Mass Scale

We will now proceed to finally introduce the field that conveys information about the mass of the particles in the boundary. We consider first the complete bulk action — including geometry, gauge field and scalar field — and proceed to compute the equations of motion from there. Then, we will introduce the asymptotic behavior of this field at the boundary and what operator it can represent.

#### 3.3.1 Bosonic Action and Equations of Motion

Our goal now is to introduce a field in the bulk that is dual to a mass term for fermions in the boundary. Let us start by remembering that the action describing massive fermions has to contain the following term

$$S_M \sim \int d^4x [M_0 \bar{\psi} \psi] \quad , \quad (3.13)$$

where  $M_0$  is the bare mass of the particle. Here we have specified  $d = 4$  for simplicity. Later, in Section 4, we will reintroduce this effective boundary action more in detail, but knowing that  $S_M$  is the term we need is enough for now. Notice that if we compare this equation with the one we presented in the introduction,  $\mathcal{F}_s(x) \mathcal{O}_{\mathcal{F}}(x)$ , we can associate  $M_0$  with the source of a field  $\mathcal{F}$  in the bulk, and  $\bar{\psi} \psi$  with the boundary operator.

The simplest field we can introduce here is a real scalar field  $\phi(r)$ , however not any field will be dual to the correct boundary term. Before solving this problem, let us consider the bulk action, in which we added the gravitational contribution, the gauge field and now the scalar field:

$$S = \int d^{d+1}x \sqrt{-g} \left[ \frac{1}{16\pi G} (R - 2\Lambda) - \frac{1}{4} F^2 - g_b \frac{1}{2} (D_\mu \phi D^\mu \phi + m^2 \phi^2) \right] \quad , \quad (3.14)$$

where  $D_\mu$  is the usual gravitational covariant derivative, and  $g_b$  is the coupling strength of the bosonic field. Notice as well that we have introduced a *bulk* mass for the scalar field,  $m^2$ , which fixes the scaling dimension of the source and vev terms in the boundary. In Section 3.3.2 we will show exactly how  $m^2$  sets the scaling dimension of those, however for this procedure we need to derive the equations of motion for  $f(r)$ ,  $\chi(r)$ ,  $A_\mu(r)$  and  $\phi(r)$ , which we will do now.

First, we will derive the stress-energy tensor  $T_{\mu\nu}$  from the variation of the action (3.14) with respect to the metric, which results in:

$$T_{\mu\nu} = g_b \left[ \frac{1}{2} \partial_\mu \phi \partial_\nu \phi - \frac{1}{4} g_{\mu\nu} (D_\rho \phi D^\rho \phi + m^2 \phi^2) \right] + F_{\mu\alpha} F_{\nu\beta} g^{\alpha\beta} - \frac{1}{4} g_{\mu\nu} F^2 \quad . \quad (3.15)$$

This covariant expression, as general as it is, contains more equations that we need. Since the metric shown in equation (3.2) only contains two functions, we can extract two independent differential equations that we can solve to find  $f(r)$  and  $\chi(r)$ . Now, for further simplifications, we will fix the gauge of the  $A_\mu$  field, so that only  $h(r) \equiv A_t(r)$  is non-zero. The two equations we can extract are the following:

$$\begin{aligned} \chi'(r) + \frac{16\pi G}{d-1} r \phi'^2(r) &= 0 \\ f'(r) + \left( \frac{d-2}{r} - \frac{\chi'(r)}{2} \right) f(r) + \frac{8\pi G}{d-1} \left( e^{\chi(r)} h'^2(r) + m^2 \phi^2(r) \right) r - rd &= 0 \end{aligned} \quad , \quad (3.16)$$

where  $'$  denotes derivatives with respect to  $r$ , and we can take  $g_b = 1$  without loss of generality. Now, proceeding to compute the equations of motion for the gauge field by computing the variation of the action with respect to  $h(r)$ , we find

$$h''(r) + \left( \frac{d-1}{r} + \frac{\chi'(r)}{2} \right) h'(r) = 0 \quad . \quad (3.17)$$

Finally, for the scalar field we have

$$(D^2 - m^2)\phi(r) = 0 \longrightarrow \phi''(r) + \left( \frac{f'(r)}{f(r)} + \frac{d-1}{r} - \frac{\chi'(r)}{2} \right) \phi'(r) - \frac{m^2}{f(r)} \phi(r) = 0 \quad . \quad (3.18)$$

These four equations describe, besides the dimensionful parameters temperature  $T$  and chemical potential  $\mu$ , a third parameter that in the next section we will show how to extract from the scalar field  $\phi(r)$ . The latter, which we will denote as  $M_0$ , will set the bare mass of the boundary fermions. Because the CFT is scale invariant, physically meaningful quantities, that we can relate with the physical system, are dimensionless ratios of parameters, such as  $\mu/T$ . Since now we will introduce a new energy scale, the number of free meaningful parameters will be two, and those are:

$$\frac{T}{M_0} \quad \text{and} \quad \frac{\mu}{M_0} . \quad (3.19)$$

### 3.3.2 Bosonic Asymptotic Behavior

In the last section we derived the non-linear coupled system of equations that describe the propagation of four fields in the bulk:  $f(r)$  and  $\chi(r)$  for the metric,  $h(r)$  as the gauge field and  $\phi(r)$  as the scalar field. These four equations are summarized next:

$$\chi'(r) + \frac{16\pi G}{d-1} r \phi'^2(r) = 0 , \quad (3.20)$$

$$f'(r) + \left( \frac{d-2}{r} - \frac{\chi'(r)}{2} \right) f(r) + \frac{8\pi G}{d-1} r \left( e^{\chi(r)} h'^2(r) + m^2 \phi^2(r) \right) - rd = 0 , \quad (3.21)$$

$$h''(r) + \left( \frac{d-1}{r} + \frac{\chi'(r)}{2} \right) h'(r) = 0 , \quad (3.22)$$

$$\phi''(r) + \left( \frac{f'(r)}{f(r)} + \frac{d-1}{r} - \frac{\chi'(r)}{2} \right) \phi'(r) - \frac{m^2}{f(r)} \phi(r) = 0 . \quad (3.23)$$

Let us go back now to the effective boundary action term shown in equation (3.13). For  $\phi(r)$  to have the same scaling dimensions as this term, we need its expansion near the boundary to be

$$\phi(r) \approx \phi_s r^{-\Delta_-} + \phi_v r^{-\Delta_+} , \quad r \rightarrow \infty , \quad (3.24)$$

where  $\Delta_{\pm}$  are the dimensionalities of the source and vev respectively. Substituting this expression in equation (3.23) and solving for  $\Delta_{\pm}$  we find

$$\Delta_{\pm} = \frac{1}{2} \left( d \pm \sqrt{d^2 + 4m^2} \right) . \quad (3.25)$$

We still need to determine  $\Delta_{\pm}$  however, which we can extract from the mass term  $S_M$ . Fixing  $d = 4$ , the dimensionality of  $\bar{\psi}\psi$  is 3, and the dimensionality of  $M_0$  is 1. Thus, if we want the source and vev of the field  $\phi(r)$  to have the correct scaling in the boundary we need to fix  $\Delta_{\pm}$  in this manner. Therefore, for  $\Delta_- = 1$  and  $\Delta_+ = 3$  we find  $m^2 = -3$ .

Equation (3.24) does not contain all the possible terms of the boundary expansion, and even though the value we derived for  $m^2$  is correct, we will now use the following expansion (see equation (4.1) in [14]):

$$\mathcal{F}(\rho) = \rho^{n_1} \left( f_{(0)} + f_{(2)}\rho^2 + \cdots + \rho^{2n} (f_{(2n)} + \tilde{f}_{(2n)} \log \rho) + \cdots \right) . \quad (3.26)$$

Here  $\mathcal{F}(\rho)$  is again any bulk field, expressed in the variable  $\rho \equiv r_h/r$ ,  $n$  are integers, and  $n_1$  is any constant. Notice that because of symmetries of the system explained in [14] there are only even powers of  $\rho$  inside the

bracket.. Fixing  $n_1 = 1$  and all  $f_{(i)} = 0$ , for  $i \neq 2$ , it reduces to equation (3.24), as expected. However, since we have to consider all terms up to order  $\rho^3$ , the expansion that we will use is the following

$$\phi(\rho) \approx \rho \left( \phi_s + \rho^2 \left( \phi_v - \tilde{\phi}_v \log \rho \right) \right) . \quad (3.27)$$

This extra coefficient,  $\tilde{\phi}_v$ , is not physically relevant, since it will be completely fixed by the equations of motion as a function of the source  $\phi_s$ . Notice however that it is *more* significant than the second because of the logarithm, but it is only important for the extraction of the numerical value, as it does not carry any physical information. To determine  $\tilde{\phi}_v$  as a function of the source, we have to substitute this expansion in equations (3.20-3.23) and solve the resulting system of algebraic equations for the coefficients. However, since we only care about terms of order up to  $\rho^3$  we can get rid of equation (3.22), thus simplifying the calculation, as we will show now.

Notice that the only term containing  $h(r)$  that is not in equation (3.22) appears in equation (3.21) as

$$\frac{8\pi G}{d-1} r e^{\chi(r)} h'^2(r) . \quad (3.28)$$

Therefore, if we show that it is of a higher order than  $r^{-3}$  we can neglect it and proceed with only three equations. First, rewriting this in terms of  $\rho$  and expanding  $\exp[\chi(r)]$ :

$$r e^{\chi(r)} h'^2(r) \sim e^{\chi(\rho)} \rho^3 h'^2(\rho) \sim \rho^3 h'^2(\rho) . \quad (3.29)$$

Here we have only focused on the  $r$  and  $\rho$  dependence, ignoring the numerical prefactor. Consider now the solution for the gauge field we presented for the AdS Reissner-Nordström Black Hole:

$$h(r) \approx \mu - n_d \rho^2 , \quad \rho \rightarrow 0 . \quad (3.30)$$

Because of the different action we are considering, this expansion will only be an approximation near the boundary, with contributions due to the new scalar field of higher order than  $\rho^2$ . Therefore, we can clearly see that the term  $\rho^3 h'^2(\rho)$  will be of a higher order than  $\rho^3$ , and thus it can be safely removed from the equation of motion. Since equation (3.23) is now decoupled from the others, it can be ignored in this calculation.

In conclusion, the system of equations we have to use is the following

$$\chi'(r) + \frac{16\pi G}{d-1} r \phi'^2(r) = 0 , \quad (3.31)$$

$$f'(r) + \left( \frac{d-2}{r} - \frac{\chi'(r)}{2} \right) f(r) + \frac{8\pi G}{d-1} m^2 r \phi^2(r) - r d = 0 , \quad (3.32)$$

$$\phi''(r) + \left( \frac{f'(r)}{f(r)} + \frac{d-1}{r} - \frac{\chi'(r)}{2} \right) \phi'(r) - \frac{m^2}{f(r)} \phi(r) = 0 . \quad (3.33)$$

Since we are considering terms up to order  $\rho^3$  in  $\phi(\rho)$ , the expansion of  $f(\rho)$  and  $\chi(\rho)$  also have to contain terms up to the same order in  $\rho$ . Let us consider  $f(\rho)$  in first place. From the Anti-de Sitter metric we already know that it has to be proportional to  $r^2$  near the boundary, therefore matching with equation (3.26) we can set  $n_1 = 0$  to find that

$$F(\rho) \equiv \rho^2 f(\rho) = f_{(0)} + f_{(2)} \rho^2 . \quad (3.34)$$

In the case of  $\chi(\rho)$ , instead of a  $r^2$  leading order behavior it should be zero in the boundary so that the scale invariance is conserved. Therefore,  $n_1 = 0$  for  $\chi(\rho)$ :

$$\chi(\rho) = \chi_{(0)} + \chi_{(2)}\rho^2 \quad . \quad (3.35)$$

Although we will not need the expansion of  $\chi(\rho)$ , we will compute it to check the consistency of the procedure. We will start first by substituting the expansion of  $\phi(\rho)$ , equation (3.27), in equation (3.31) and solving for  $\chi'(\rho)$  we find an expression that we can then substitute in equation (3.32). Neglecting terms of order higher than  $\rho^3 \log \rho$ , we have now the following system of algebraic equations for  $f_{(0)}$  and  $f_{(2)}$ :

$$\begin{cases} f_{(0)} = 1 \\ 12f_{(2)} + (f_{(0)} + m^2)\phi_s^2 = 0 \end{cases} \longrightarrow \begin{cases} f_{(0)} = 1 \\ f_{(2)} = -(1 + m^2)\frac{\phi_s^2}{12} \end{cases} \longrightarrow F(\rho) = 1 - (1 + m^2)\frac{\phi_s^2}{12}\rho^2 \quad . \quad (3.36)$$

Here we have made the contribution of  $m^2$  explicit, and will later check that indeed this procedure gives the same answer we computed before. Notice as well that  $f_{(0)} = 1$ , in agreement with the AdS metric behavior. Proceeding now by substituting this expansion for  $F(\rho)$  in equation (3.33) we can find a similar system of algebraic equations that relate  $\phi_s$  and  $\tilde{\phi}_v$ :

$$\begin{aligned} -6(3 + m^2)\phi_s &= 0 \\ \frac{1}{2}(-1 + m^2)\phi_s^3 - 6((3 + m^2)\phi_v + 2\tilde{\phi}_v) &= 0 \end{aligned} \quad . \quad (3.37)$$

After solving the system, we get:

$$\begin{aligned} m^2 &= -3 \\ \tilde{\phi}_v &= -\frac{1}{6}\phi_s^3 \end{aligned} \quad . \quad (3.38)$$

Indeed, as we expected we find that  $m^2 = -3$ , and the relation between the source and  $\tilde{\phi}_v$ . The expansion of  $\phi(\rho)$  and  $\chi(\rho)$  can be computed from here:

$$\begin{aligned} \phi(\rho) &= \rho \left( \phi_s + \rho^2 \left( \phi_v + \frac{1}{6}\phi_s^3 \log \rho \right) \right) \\ \chi(\rho) &= \frac{1}{6}\phi_s^2 \rho^2 \end{aligned} \quad , \quad \rho \rightarrow 0 \quad . \quad (3.39)$$

Here  $\chi(\rho)$  shows the expected behavior near the boundary, approaching zero with a power of  $\rho^2$ . Notice that the result we found for  $\tilde{\phi}_v$  is different than the expression found in equation (5.12) of [14], because in our case we are considering the back-reaction of the geometry in the scalar field, otherwise it would be zero.

Summarizing, up to this point we have worked in what we call the background of the theory, in other words, describing the behavior of the bulk fields. We chose the simplest model we know, just gravity, and saw that there is one analytic solution, analogous to Schwarzschild's black hole solution in 3+1 General Relativity, that introduced a finite temperature in the system related to the Hawking radiation emitted by the black brane.

Then we introduced a chemical potential in the boundary by adding a gauge field to the bulk, which can be solved analytically so find, as before, a solution analogous to Reissner-Nordström's black hole. These two solutions showed us important details about the behavior of the bulk, which we then used when we added the last contribution to the bulk, a scalar field.

Since it is not possible to find an analytic solution in this more general case, we had to resort to study the asymptotic behavior of the scalar field and relate it to the boundary operator we expect to find. After fixing every parameter we can, we are only left with  $\phi_s$  and  $\phi_v$  which will be fixed by looking at the value of the numerical solution near the boundary, as we will see in the next section.

This bundle of fields is the background we will use later, for which we need another field propagating *on top* of the background fields. This approach assuming a fixed background can be used to compute the spectral function of the boundary field using semi-holography, however it can be generalized by including the back-reaction of the probe field in the geometry. In the bosonic case this can be done without too many complications, however if the boundary field we are interested in is fermionic, we find more problems.

The root of these complications comes from the fact that fermions, as opposed to bosons, cannot be in the same state. Therefore, operators like  $\langle\psi\rangle$  are no longer well behaved and other techniques need to be used. In [16] we can see an example of this, using a specific ground state for the fermions known as the perfect fluid, allowing for the study of these back-reactions in the geometry. There is new interesting physics involved in this, for example testing the stability of the black hole and possible phase transitions. In this thesis however we will focus only on the probe field case, without any back-reactions.

### 3.3.3 Numerically Solving the Equations of Motion

To conclude this section we will delve deeper into the specifics of numerically solving equations (3.20-3.23), describing the general procedure and showing some results. We will first compute the values of the fields near the horizon, deep in the geometry, using a method very similar to what we have used before near the boundary. However, in this case the need of performing this expansion near the horizon comes from problems with the value of  $f(r)$  when  $r$  approaches  $r_h$ , since as we have seen in Schwarzschild's solution

$$f(r) = r^2 \left( 1 - \frac{r_h^{d-2}}{r^{d-2}} \right) , \quad (3.40)$$

which by definition has to satisfy  $f(r \rightarrow r_h) \rightarrow 0$ , so the system of ODEs is singular at this point. Therefore, instead of evaluating these functions exactly at the horizon, we will perform a Taylor expansion a distance  $\epsilon$  from it, and fix most of the coefficients using the equations of motion. We can only fix some of them because there are parameters of the boundary theory, such as the temperature and chemical potential, that we need to relate to the initial conditions, and therefore not all of the Taylor coefficients can be fixed by the equations of motion.

Firstly, we will transform our fields slightly so that the numerical solution is more stable and easier to handle. Taking the fields  $f(r)$  and  $\chi(r)$  we see that near the boundary,  $r \rightarrow \infty$ , it diverges like  $r^2$ . Thus, transforming

$$f(r) \longrightarrow F(r) = \frac{1}{r^2} f(r) \quad (3.41)$$

ensures that  $F(r)$  will be finite in this limit. In the case of  $\chi(r)$ , because it already has to be a constant at the boundary, we will define  $X(r) \equiv \chi(r)$  without any changes. Since we will be using these fields later, we need to keep track of those powers of  $r$  by redefining them. Also, as introduced in the previous section, instead of using the variable  $r$  we define

$$\rho \equiv \frac{r_h}{r} \quad , \quad (3.42)$$

so that the final fields are  $F(\rho)$ ,  $X(\rho)$ ,  $\Phi(\rho)$  and  $H(\rho)$ . Since we are redefining fields and variables, we also need to change the equations of motion (3.20-3.23) to reflect this, which involves using the chain rule repeatedly and multiplying the metric fields by the appropriate power of  $\rho$ . This procedure, easily performed using any suite of symbolic calculus, returns a new set of equations that we will use and denoted by  $\mathcal{E}_{\mathcal{F}}$ , with  $\mathcal{F} \in \{X, F, H, \Phi\}$ , related to equations (3.20-3.23) respectively:

$$\mathcal{E}_{\mathcal{F}} = (1 - \rho)^{m_{\mathcal{F}}} \times (\text{equation of motion})_{\mathcal{F}} \quad , \quad \text{with } m_X = m_F = m_H = 0 \quad \text{and } m_{\Phi} = 1 \quad . \quad (3.43)$$

Here we have introduced a power of  $1 - \rho$  for one of the equations, so that we can shift the overall power in the Taylor expansion for the fields. Since we are using the variable  $\rho$ , the boundary sits at  $\rho \rightarrow 0$  and the horizon at  $\rho \rightarrow 1$ . Therefore, the Taylor expansion of the fields will be centered around  $1 - \rho$  as follows

$$\mathcal{F}(\rho) = \sum_{n=0}^{\infty} C_{\mathcal{F}n} (1 - \rho)^n \approx \sum_{n=0}^{N_{\text{exp}}-1} C_{\mathcal{F}n} (1 - \rho)^n \quad , \quad (3.44)$$

where  $\mathcal{F}$  is any bulk field and the coefficients can be specified for each field and expansion order, as  $C_{\Phi 0}$  or  $C_{H1}$ . In this general expansion we are considering a sum from  $n = 0$  to  $\infty$ , however in practice the upper bound will be no higher than  $N_{\text{exp}} = 4$ , since the system of algebraic equations we will have to solve becomes increasingly difficult, while only improving the approximation slightly.

Now that we have defined the equations of motion we will be using, we can proceed to compute the system of algebraic equations for the coefficients. By substituting each field expansion  $\mathcal{F}(\rho)$  into the equations of motion  $\{\mathcal{E}_{\mathcal{F}}\}$  and neglecting higher order terms we find the system of nonlinear equations with  $4N_{\text{exp}}$  variables. It is possible however to fix some of them and since we need two free parameters the actual number of variables we can solve for is going to be smaller.

First, we can consider  $F(\rho)$ , which by definition has to satisfy  $F(1) = 0$ , and the only way to achieve that is by having  $C_{F0} = 0$ .

Secondly, consider  $H(\rho)$ . In this case we can argue that it has to be zero when  $\rho = 1$  by computing the product  $A_{\mu}A^{\mu}$ :

$$A_{\mu}A^{\mu} = g^{tt}(r)h^2(r) \quad , \quad (3.45)$$

where  $g^{tt} = (f(r))^{-1} e^{\chi(r)}$ , which by the definition of  $f(r)$  diverges as  $r \rightarrow r_h$ . Therefore, for the norm of  $A_{\mu}$  not to diverge,  $h(r_h) = 0$ , thus fixing  $C_{H0} = 0$ . Let us now consider the order of each differential equation shown in (3.20-3.23), since that will fix the number of initial condition we need.

Since we have already fixed  $C_{F0}$ , we can start with equation (3.21), which is a first order differential equation in  $f(r)$ . Therefore, to completely fix the solution only one parameter is necessary,  $f(r_h)$ , which indeed corresponds to fixing the first coefficient of the Taylor expansion. Therefore, there are no other free parameters associated with  $f(r)$ .

Consider next equation (3.22), the equation of motion for  $h(r)$ . It is a second order differential equation, and therefore both  $h(r_h)$  and  $h'(r_h)$  have to be fixed to find a specific solution. Since we have already determined a value for  $C_{H0}$ , there is one free parameter associated with  $h'(r_h)$ , which in terms of the Taylor expansion is  $C_{H1}$ . This coefficient will be one of the initial conditions we can choose in the numerical solution.

Equation (3.20), describing  $\chi(r)$ , is a bit different from the others. It is a first order differential equation, and therefore it has one free parameter:  $\chi(r_h)$ . However, because of a symmetry of the problem we will show later in this section, it is possible to add a constant to  $\chi(r)$  and it will still be a solution of the system. Therefore, its value at the horizon is not important and we can safely set  $C_{X0} = 0$ , knowing that after we have found a solution we can shift it to the value we need.

Finally, in equation (3.22), describing the scalar field  $\phi(r)$ , we can see that it is a second order differential equation. In the previous section we saw that the expansion near the boundary contains two parameters,  $\phi_s$  and  $\phi_v$ , that clearly have to be related to the two initial conditions at the horizon. However, these initial conditions are not independent and therefore only one parameter,  $\phi(r_h)$ , is necessary to fix the solution. We can derive this by evaluating equation (3.33) at the horizon, finding the relation

$$f'(r_h)\phi'(r_h) = m^2\phi(r_h) \quad . \quad (3.46)$$

The Taylor expansion coefficient  $C_{\Phi 0}$  will then be the second initial condition of the system.

The fact that we have two initial conditions is not a coincidence. Because we have introduced two boundary parameters,  $T/M_0$  and  $\mu/M_0$ , we will need at least two initial conditions to change them independently. The other parameters that we have not fixed by considering the order of the differential equations will be fixed by substituting the Taylor expansion in the equations of motion and solving the resulting system of algebraic equations for the coefficients. Because of the two free parameters, this is an under-determined system, and the solution will depend on  $C_{\Phi 0}$  and  $C_{H1}$ . This is however the only difficulty of this procedure, since once we know the field expansions near the horizon we can compute the initial conditions for the equations of motion and integrate them from  $\rho = 1 - \epsilon_1$  to  $\rho = \epsilon_2$ , with  $\epsilon_{1,2}$  being some small constants.

In Figure 3.1 we can see an example of solving the equations of motion numerically after following the previous procedure.

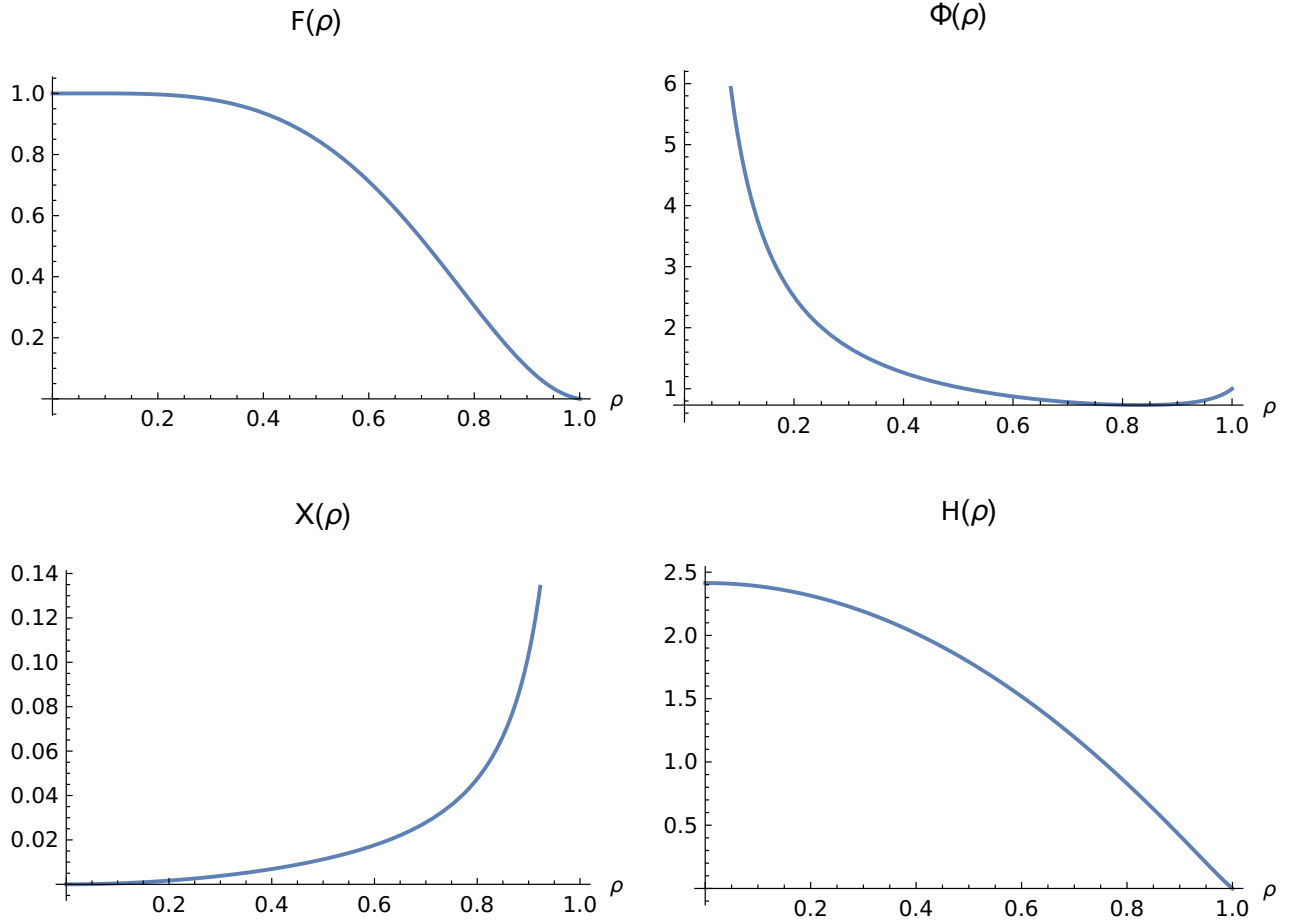


Figure 3.1: Numerical solution for the background fields, using  $C_{\Phi_0} = 1$  and  $C_{H1} = 5$  as initial conditions at the horizon. In the x-axis we can see the radial coordinate  $\rho$  and in the y-axis the value of the field. Note that  $\rho = 0$  is the boundary and  $\rho = 1$  is the horizon.

Here we can see the effect of some transformations we have performed, for example  $F(\rho)$  goes to a constant at the boundary and  $\Phi(1 - \epsilon)$  is close to  $C_{\Phi_0} = 1$ . However, there is one difference in what we were expecting from  $X(\rho)$ , since its value at the horizon is clearly not zero. This is because we have performed another transformation of the field after solving the system. Using a symmetry of the theory, as explained in [17] around equation (15), we can rescale as follows

$$\begin{aligned}
 e^{X(\rho)} &\longrightarrow C^2 e^{X(\rho)} \\
 t &\longrightarrow Ct \\
 H(\rho) &\longrightarrow C^{-1} H(\rho)
 \end{aligned}
 \quad . \quad (3.47)$$

Therefore, after solving the system we can choose  $C = e^{-X(\rho \rightarrow 0)/2}$  so that  $X(\rho \rightarrow 0)$  cancels out, recovering the behavior consistent with the Anti-de Sitter metric.  $H(\rho)$  is also transformed and thus changing the final value of the chemical potential, which we have also done in Figure 3.1.

Finally, we can proceed to extract the source and vev coefficients,  $\phi_s$  and  $\phi_v$  respectively, from the scalar field. We can compute this using the following system of equations, each coming from the asymptotic behavior of the respective field

$$\begin{aligned}
\Phi_{\text{bdy}}(\rho) &= \rho(\phi_s + \rho^2(\phi_v - \tilde{\phi}_v \log \rho)) \\
H_{\text{bdy}}(\rho) &= \mu - n_d \rho^2 \\
\phi_s^3 + 6\tilde{\phi}_v &= 0
\end{aligned}
, \tag{3.48}$$

where  $n_d$  is the charge density at the boundary, and “bdy” references the field value at the boundary. Notice that here we denote the fields with the subscript bdy to differentiate them from the field obtained by solving the equations of motion. The first equation is the asymptotic expansion for  $\Phi(\rho)$  that we have seen previously, and the third one is the condition extracted from the equations of motion for the third coefficient  $\tilde{\phi}_v$  having specified  $m^2 = -3$ .

Since need to determine five variables and we only have three equations, we have to include  $\Phi'_{\text{bdy}}(\rho)$  and  $H'_{\text{bdy}}(\rho)$  as well, computed directly from the above expressions. Now we can solve this equations by equating them to the values the numerical solution gives,

$$\begin{aligned}
\Phi_{\text{bdy}}(\epsilon) &= \Phi(\epsilon) \\
H_{\text{bdy}}(\epsilon) &= H(\epsilon) \\
\Phi'_{\text{bdy}}(\epsilon) &= \Phi'(\epsilon) \\
H'_{\text{bdy}}(\epsilon) &= H'(\epsilon) \\
\phi_s^3 + 6\tilde{\phi}_v &= 0
\end{aligned}
. \tag{3.49}$$

And by solving this system of equations we can determine the coefficients. Since this procedure results in the parameters of the boundary theory computed in terms of the initial conditions  $C_{\Phi_0}$  and  $C_{H_1}$ , it is not ideal to derive results from the theory, as parameters will be set by the boundary theory and not the other way around. Fixing this involves “inverting” this procedure by considering a boundary value problem instead of an initial conditions problem, as we have done with the equations of motion. That way, we can use an optimizing routine to solve the background and determine the values for the initial conditions such that the boundary system has the temperature and chemical potential we want.

In Figure 3.2 we can see how well this expansion matches the real solution in terms of percentage difference. This Figure clearly shows that the expansion indeed approaches the real solution near the boundary, and even after one tenth of the distance away from the boundary it is still a very good approximation.

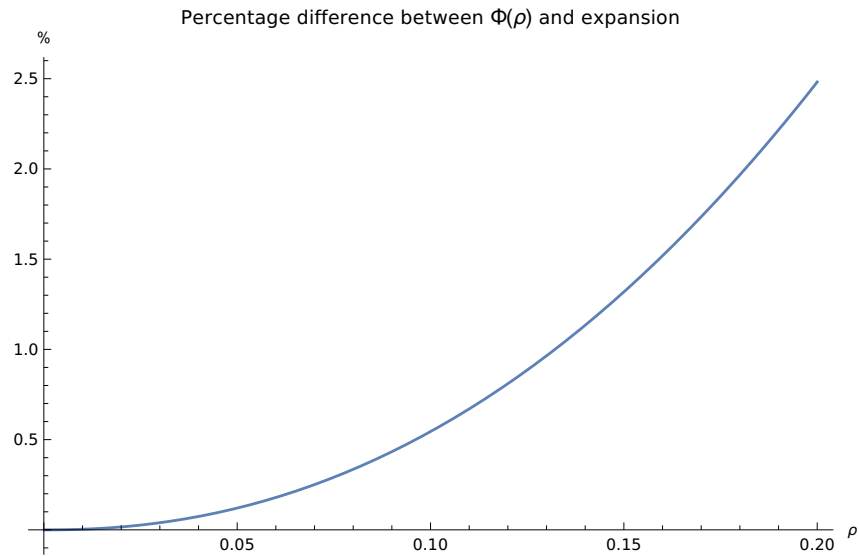


Figure 3.2: Percentage difference calculated as  $2\frac{\Phi(\rho)-\Phi_{\text{bdy}}(\rho)}{\Phi(\rho)+\Phi_{\text{bdy}}(\rho)}$  for small values of  $\rho$ . Here we have used the same parameters as in Figure 3.1, with  $\epsilon_1 = 10^{-5}$  and  $\epsilon_2 = 10^{-4}$ .

## 4 Fermionic Bulk Model

In this section we will introduce the central topic of this thesis: the fermionic probe field in the bulk that will be dual to the self-energy of the boundary system. Firstly we will introduce some conventions and generalities we will use throughout the section, so that after that we can introduce the simple case of chiral fermions. Finally, we will introduce another fermionic field in the bulk, therefore finding Dirac fermions in the boundary, using the mass deformation introduced in the previous section. See [20] for further reading.

### 4.1 Introduction

#### 4.1.1 Dirac Formalism in a Flat Background

We will in first place consider the usual Dirac action in a flat space-time, both in  $d$  and  $d + 1$  dimensions. Even though we cannot consider a truly flat space-time to have a boundary, we will consider for now two different geometries with different dimensionality. We can write the action as follows

$$S_\psi = -ig_f \int d^d x \bar{\psi}(\gamma^{\underline{a}}\partial_{\underline{a}} - M)\psi \quad . \quad (4.1)$$

Here we have introduced several pieces of notation, which will become more relevant later. Firstly, we are using here underlined indices  $\underline{a}$  instead of the usual Greek ones. Any underlined Latin index acts in a flat space-time. Therefore, in the boundary, the metric is  $g_{\underline{a}\underline{b}} \equiv \eta_{\underline{a}\underline{b}}$ , with  $\underline{a}, \underline{b} \in \{\underline{0}, \underline{1}, \underline{2}, \underline{3}\}$ , and these underlined indices can be raised and lowered using the flat metric.

Moreover, we have fixed  $d = 4$  in the previous equation and we will continue working with this for the remaining of the thesis. In [15] it is shown that the dimensionality of gamma matrices is always  $2^{\lfloor \frac{d}{2} \rfloor}$ , and thus for  $d = 4$  they are actually  $4 \times 4$  matrices. Most importantly, when we are working in  $d + 1 = 5$  gamma matrices are still  $4 \times 4$  because of the rounding down, so we will not be considering significantly different gamma matrices in the bulk and in the boundary.

In the  $d + 1$ -dimensional space-time Dirac's action can be written as

$$S_\psi = -ig_f \int d^{d+1}x \bar{\psi}(\Gamma^{\underline{a}}\partial_{\underline{a}} - M)\psi \quad , \quad (4.2)$$

where we have used a slightly different notation. Here  $\underline{a} \in \{\underline{r}, \underline{0}, \underline{1}, \underline{2}, \underline{3}\}$ , running over the  $d + 1$  bulk coordinates as we have been using in the previous section with the background fields. In this case we are implicitly working with a flat space-time, as noted by the underlined indices, but once we introduce a curved background Greek indices will always assume that  $g_{\mu\nu} \neq \eta_{\mu\nu}$ .

Besides this change in the indices, we represent  $d + 1$  gamma matrices with the capital version of the letter. Now, moving on to the general properties of gamma matrices, they are a representation of a Clifford algebra that satisfies the following property

$$\{\gamma^{\underline{a}}, \gamma^{\underline{b}}\} = 2\eta^{\underline{a}\underline{b}} \quad , \quad \text{and} \quad \{\Gamma^{\underline{a}}, \Gamma^{\underline{b}}\} = 2\eta^{\underline{a}\underline{b}} \quad , \quad (4.3)$$

where the operator  $\{*,*\}$  is the anti-commutator, defined as  $\{A, B\} = AB + BA$ . Moreover, it is important to introduce now the matrix  $\gamma^5$ , usually defined as

$$\gamma^5 \equiv i\gamma^0\gamma^1\gamma^2\gamma^3 \ , \quad (4.4)$$

where the index 5 is not underlined because this is a definition, and it satisfies

$$\{\gamma^5, \gamma^a\} = 0 \ , \quad (\gamma^5)^2 = \mathbb{1} \ . \quad (4.5)$$

In  $d = 4$  dimensions this matrix can be used to project any spinor in its left and right chiralities, using the following operators

$$\begin{aligned} L &= \frac{1}{2}(1 - \gamma^5) \ , \quad R = \frac{1}{2}(1 + \gamma^5) \\ \psi &= L\psi + R\psi = \psi_L + \psi_R \quad , \\ \gamma^5\psi_{R,L} &= \pm\psi_{R,L} \end{aligned} \quad (4.6)$$

with  $\psi_{R,L}$  defined as

$$\psi_L = \begin{pmatrix} 0 \\ \psi_- \end{pmatrix} \quad \text{and} \quad \psi_R = \begin{pmatrix} \psi_+ \\ 0 \end{pmatrix} \ . \quad (4.7)$$

Because  $\gamma^5$  is clearly not part of the other  $\gamma^a$ , this representation is called *reducible*, and it happens for every representation in an even number of dimensions. However, in  $d + 1 = 5$  it is no longer reducible, and the extra matrix we need is precisely  $\gamma^5$ . Therefore, our convention for the gamma matrices is the following

$$\begin{aligned} \Gamma^0 &= \gamma^0 = \begin{pmatrix} 0 & -\mathbb{1} \\ \mathbb{1} & 0 \end{pmatrix} \\ \Gamma^i &= \gamma^i = \begin{pmatrix} 0 & \sigma^i \\ \sigma^i & 0 \end{pmatrix} \quad , \\ \Gamma^r &= \gamma^5 = \begin{pmatrix} \mathbb{1} & 0 \\ 0 & -\mathbb{1} \end{pmatrix} = i\Gamma^0\Gamma^1\Gamma^2\Gamma^3 \end{aligned} \quad (4.8)$$

where  $\sigma^i$  are Pauli matrices, defined as

$$\sigma^i = \left( \begin{pmatrix} 0 & 1 \\ 1 & 0 \end{pmatrix} , \begin{pmatrix} 0 & -i \\ i & 0 \end{pmatrix} , \begin{pmatrix} 1 & 0 \\ 0 & -1 \end{pmatrix} \right) \ . \quad (4.9)$$

In addition to these,  $\sigma^0 \equiv \mathbb{1}_{2 \times 2}$ , since it will be necessary to write a matrix of this dimensions in terms of Pauli matrices, which can be expressed as

$$A_{2 \times 2} = a_{\underline{a}}\sigma^{\underline{a}} \ , \quad (4.10)$$

and similarly in the case of  $4 \times 4$  matrices,

$$A_{4 \times 4} = a\mathbb{1} + b^{\underline{a}}\Gamma_{\underline{a}} + c^{\underline{ab}}\sigma_{\underline{ab}} + d^{\underline{a}}\Gamma_{\underline{a}}\Gamma^r + e\Gamma^r \ , \quad (4.11)$$

where  $\sigma_{ab} \equiv \frac{i}{2}[\Gamma^a, \Gamma^b]$ , as shown in [25]. It is important to note that these two representations, both for  $2 \times 2$  and  $4 \times 4$  matrices equally, are as general as possible in terms of symmetries. This means that if the matrix  $A$  we are considering has one or more underlying symmetry some of the terms in these expressions will drop out, since the associated coefficients will always be zero.

For example, let us consider the case we will deal with of rotational symmetry. For  $2 \times 2$  matrices it is clear that this is the only symmetry that can be described, since introducing a local Lorentz transformation  $\Lambda$  will not change anything. In the case of  $4 \times 4$  matrices however, this is more complicated. In the case that we will have to deal with, it means that only the first two contributions are allowed, since all the others are non-zero only when there are other broken symmetries, but it is clear that they contain more information than the smaller ones.

As a final note, we will use  $\Gamma^0$  to define

$$\bar{\psi} = \psi^\dagger \Gamma^0 . \quad (4.12)$$

### 4.1.2 Dirac Formalism in a Curved Background

This discussion however is only valid for a flat, Minkowski-like background, which of course is not our situation. To generalize the previous results we need to introduce a way to describe local transformations of spinors using a basis of vectors on each point of the bulk. The main advantage of using this method is that we can separate the information related to the geometry from the spinor field, so that we can work with the usual gamma matrices in this curved background.

Considering the main goal of this approach, what we need is a set of basis vectors in which the metric of the space-time is locally flat, in mathematical terms

$$\hat{e}^a(x) \hat{e}_b(x) = \delta_b^a , \quad \forall x , \quad (4.13)$$

which is related to the actual basis tangent to the geometry at that point by the *vielbeins*:

$$\hat{e}_\mu(x) = e_\mu^a(x) \hat{e}_a(x) , \quad \hat{e}_a(x) = e_\underline{a}^\mu(x) \hat{e}_\mu(x) , \quad (4.14)$$

where  $e_\mu^a$  are the vielbeins, and  $e_\underline{a}^\mu$  the inverse. These functions indeed satisfy the conditions we were looking for, namely

$$\begin{aligned} e_\nu^a e_\underline{a}^\mu &= \delta_\nu^\mu & e_\mu^a e_\underline{a}^\mu &= \delta_\underline{a}^a \\ g_{\mu\nu} e_\underline{a}^\mu e_\underline{b}^\nu &= \eta_{\underline{a}\underline{b}} & \eta_{\underline{a}\underline{b}} e_\underline{a}^\mu e_\underline{b}^\nu &= g_{\mu\nu} \end{aligned} . \quad (4.15)$$

Now we can take any tensor and describe it in local or global coordinates using the vielbeins as

$$V^\mu = e_\underline{a}^\mu V^{\underline{a}} , \quad V^{\underline{a}} = e_\mu^{\underline{a}} V^\mu , \quad (4.16)$$

which therefore we can apply to the gamma matrices as follows

$$\Gamma^\mu = e_\underline{a}^\mu \Gamma^{\underline{a}} , \quad (4.17)$$

to find the curved background version of them. This transformation can also be applied to the Clifford representation property, reading now

$$\{\Gamma^\mu, \Gamma^\nu\} = 2g^{\mu\nu} \quad . \quad (4.18)$$

This is not everything we need to rewrite Dirac's action in a curved space-time, since we still need to make sure that the derivative of a spinor still transforms like a tensor. Working with a normal vector we know from any General Relativity book that the covariant derivative is

$$D_\mu V^\nu = \partial_\mu V^\nu + \Gamma_{\mu\sigma}^\nu V^\sigma \quad . \quad (4.19)$$

Here  $\Gamma_{\mu\sigma}^\nu$  are the Christoffel symbols, not gamma matrices. However a vector expressed in the locally flat basis will behave differently, as follows

$$D_\mu V^a = \partial_\mu V^a + \omega_{\mu\bar{b}}^a V^{\bar{b}} \quad , \quad (4.20)$$

where  $\omega_{\mu\bar{b}}^a$  is the *spin connection*, and it can be expressed as

$$\omega_{\mu\bar{b}}^a = e_{\bar{b}}^a e_{\nu}^\lambda \Gamma_{\mu\lambda}^\nu - e_{\bar{b}}^\lambda \partial_\mu e_\lambda^a \quad , \quad (4.21)$$

which can be derived by imposing that these two transformations, for  $V^\mu$  and  $V^a$ , have to be the same. As a final step, since spinors are not vectors in either basis, but objects that transform on their own under Lorentz transformations we need to introduce another term in the covariant derivative to account for this. Assuming a term in the covariant derivative like the following

$$D_\mu \psi = \partial_\mu \psi + \Omega_\mu \psi \quad . \quad (4.22)$$

Now, to compute  $\Omega_\mu$  we need to remember that  $\bar{\psi}\psi$  and  $\bar{\psi}\Gamma^a\psi$  transform, respectively, like a scalar and a vector under local Lorentz transformations. Therefore, by imposing that they transform as expected the following conditions have to be satisfied:

$$\begin{aligned} \Gamma^0 \Omega_\mu^\dagger \Gamma^0 &= -\Omega_\mu \\ [\Gamma^a, \Omega_\mu] &= \omega_{\mu\bar{b}}^a \Gamma^{\bar{b}} \quad , \end{aligned} \quad (4.23)$$

which indeed they are by choosing the spin connection to be

$$\Omega_\mu = \frac{1}{8} \omega_{\mu\bar{a}\bar{b}} [\Gamma^{\bar{a}}, \Gamma^{\bar{b}}] \longrightarrow D_\mu \psi = \partial_\mu \psi + \frac{1}{8} \omega_{\mu\bar{a}\bar{b}} [\Gamma^{\bar{a}}, \Gamma^{\bar{b}}] \psi \quad . \quad (4.24)$$

Finally, taking the metric

$$ds^2 = -f(r)e^{-\chi(r)} dt^2 + \frac{dr^2}{f(r)} + r^2 d\mathbf{x}^2 \quad , \quad (4.25)$$

we can easily compute the vielbeins as the square root of the inverse of it, resulting in

$$e_{\underline{0}}^0 = \sqrt{\frac{e^{\chi(r)}}{f(r)}} \ , \quad e_{\underline{i}}^i = \frac{1}{r} \ , \quad e_{\underline{r}}^r = \sqrt{f(r)} \ . \quad (4.26)$$

We need to make one extra remark about the chiral components of a spinor in a curved background here. Notice that even though we can define

$$\psi_{R,L} = \frac{1}{2}(1 \pm \Gamma^r)\psi \ , \quad (4.27)$$

we cannot change  $\underline{r} \rightarrow r$ , thus introducing a vielbein. This projection however is valid for a fixed value of  $\rho$ , so the projection into the two components will be different based on how far away we are from the horizon. In the following section we will have to fix  $\rho = \rho_0$ , focusing on only one surface of the geometry to be able to project out the spinor's components.

These are all the ingredients we need to generalize Dirac's action to curved backgrounds, so we can proceed to the actual calculation of the probe field.

## 4.2 Bulk Model for Chiral Fermions

We will now move on to apply what we have just introduced in AdS/CFT. This section is only an example of the case in which we consider chiral fermions, that is, massless, at the boundary. This approach is still valid for systems in which the kinetic energy of the particles is much higher than their mass, but clearly invalid when our main goal is to describe cold atoms. However, introducing first the mathematical tools will let us focus on the procedure, before adding the complications necessary for the description of massive fermions.

The main idea is to consider the action of a probe field propagating in the geometry described by the solution to the equations of motion we have derived previously. Given some initial condition at the horizon this field will be dual to some fermionic operator in the boundary, which we will use to compute the spectral function that we can compare with experiments to test the theory.

These two systems, one with massless and the other with massive fermions, differ in the number of degrees of freedom we have at the boundary. Since a chiral fermion only has two non-zero components, which we compute by integrating out half of the degrees of freedom of the probe field in the bulk, it seems reasonable that to find Dirac fermions we would need twice the number of DoF in the bulk. This is indeed the approach we will take, considering two probe fields coupled together with the scalar field  $\phi$  in the simplest possible way.

### 4.2.1 Dirac's Action and Boundary Effective Action

We introduce now the full action in the bulk as follows

$$S = \int d^{d+1}x \sqrt{-g} \left[ R - 2\Lambda - \frac{1}{4}F^2 - ig_f \bar{\psi} \left( \frac{1}{2} \overleftrightarrow{\mathcal{D}} - iqA - M \right) \psi - g_b (D_\mu \phi D^\mu \phi - m^2 \phi^2) \right] \ , \quad (4.28)$$

where only  $\psi$  is a dynamical field, while every other field is fixed. Here  $\overleftrightarrow{\mathcal{D}}$  is the contraction  $\Gamma^\mu D_\mu$ , each defined in the previous section, and notice that we have not included the gauge field in the covariant derivative so it is more explicit. Notice that technically we do not need the scalar field  $\phi$  here, since it does not interact with  $\psi$  in any way, but for completeness we are including it.

We have also introduced another parameter into the theory,  $M$ , playing a role similar to  $m^2$  for the bosonic field. However in this case it can only take the values  $M \in [-1/2, 1/2]$  the upper limit so that the field is not divergent in the boundary, and the lower one corresponds to the Breitenlohner-Freedman bound (see [22, 23]), although we will focus in the case  $M \neq 0$ . However, similarly as with  $m^2$ , this is not parameter like  $T$  or  $\mu$  in the sense that the boundary theory is different for each choice of  $M$ .

Computing the variation of  $\psi$  as usual we can find the equations of motion for this field and the boundary terms,

$$\delta_{\bar{\psi}, \psi} S = \dots - i \frac{gf}{2} \int d^{d+1}x \sqrt{-g} \left[ \bar{\psi} \overrightarrow{D} \delta\psi - \delta\bar{\psi} \overleftarrow{D} \psi \right] , \quad (4.29)$$

where  $\dots$  represent extra terms that contribute to the equations of motion, without any derivatives of variations. Only the terms shown above can contribute to the boundary theory directly, by using Stokes' Theorem as follows:

$$\begin{aligned} \int d^{d+1}x \sqrt{-g} \left[ \bar{\psi} \overrightarrow{D} \delta\psi - \delta\bar{\psi} \overleftarrow{D} \psi \right] &= \int d^{d+1}x \sqrt{-g} \left[ D_\mu \left( e_\alpha^\mu \left( \bar{\psi} \Gamma^\alpha \delta\psi - \delta\bar{\psi} \Gamma^\alpha \psi \right) \right) \right] + \dots \\ &= \int d^d x \sqrt{-h} n_\mu e_\alpha^\mu \left[ \bar{\psi} \Gamma^\alpha \delta\psi - \delta\bar{\psi} \Gamma^\alpha \psi \right] + \dots \\ &= \int d^d x \sqrt{-h} \left[ \bar{\psi} \Gamma^r \delta\psi - \delta\bar{\psi} \Gamma^r \psi \right] + \dots \\ &= \int d^d x \sqrt{-h} \left[ \bar{\psi}_L \delta\psi_R + \delta\bar{\psi}_R \psi_L - \bar{\psi}_R \delta\psi_L - \delta\bar{\psi}_L \psi_R \right] + \dots \end{aligned} \quad (4.30)$$

Let us go through the steps of this calculation.

1. In the first step we have rewritten the derivative of the integrand using

$$\begin{aligned} D_\mu (e_\alpha^\mu \bar{\psi} \Gamma^\alpha \delta\psi) &= D_\mu e_\alpha^\mu \bar{\psi} \Gamma^\alpha \delta\psi + e_\alpha^\mu D_\mu \bar{\psi} \Gamma^\alpha \delta\psi + \boxed{e_\alpha^\mu \bar{\psi} \Gamma^\alpha D_\mu \delta\psi} \\ D_\mu (e_\alpha^\mu \delta\bar{\psi} \Gamma^\alpha \psi) &= D_\mu e_\alpha^\mu \delta\bar{\psi} \Gamma^\alpha \psi + \boxed{e_\alpha^\mu D_\mu \delta\bar{\psi} \Gamma^\alpha \psi} + e_\alpha^\mu \delta\bar{\psi} \Gamma^\alpha D_\mu \psi \end{aligned} , \quad (4.31)$$

so that we can use Stokes' Theorem in the next step. Notice that  $D_\mu e_\alpha^\mu$  is not zero, only  $D_\mu g^{\alpha\beta} = D_\mu (e_\alpha^\alpha e_\beta^\beta \eta^{\alpha\beta}) = 0$ , by definition. Notice that the boxed terms are the ones we find in the variation of the action, therefore solving for them in the equations above and substituting back we find the full derivative, which will appear in Stokes' Theorem, and other terms that will only contribute to the equations of motion, represented by  $\dots$  above.

2. The general expression for Stokes' Theorem can be found in [18], equation (E.14):

$$\int_M d^{d+1}x \sqrt{-g} D_\mu V^\mu = \int_{\partial M} d^d x \sqrt{-h} n_\mu V^\mu , \quad (4.32)$$

where we are integrating the divergence of a vector  $V^\mu$  over a manifold  $M$  with boundary  $\partial M$ , which is equal to the integral of the normal component of the field over the boundary. Moreover,  $h$  is the determinant of the metric in the boundary. Translating to our needs,  $M$  is the whole geometry, with  $\partial M$  is the Anti-de Sitter-like boundary, and  $V^\mu = e_\alpha^\mu \left[ \bar{\psi} \Gamma^\alpha \delta\psi - \delta\bar{\psi} \Gamma^\alpha \psi \right]$  as we have extracted from step 1.

Also, since we only have one direction that asymptotically approaches the boundary, the normal vector is simply  $n_\mu = e_\mu^r \delta_r^r$ . Besides, this boundary is chosen at a fixed  $r = r_0$  that we will take to infinity later.

In this step  $\partial M$  would also include the horizon boundary, but the contribution cancels out because  $g^{rr} = 0$  at that point.

3. In this step we have used the previous expression for  $n_\mu$  and the fact that, for diagonal metrics,  $e_{\underline{r}}^r = \sqrt{g^{rr}}$ .
4. Finally, we can decompose each field in its chiral components and apply the matrix  $\Gamma^z$  using equation (4.6), to find the result above. At this point we can introduce better what are these two chiral components in the boundary since, in analogy with the background scalar field and its source and vev components,  $\psi_R$  and  $\psi_L$  will be also dual to some source and vev at the boundary. What this means is that, even though we can set  $\delta\psi_R$  or  $\delta\psi_L$  to zero, meaning that it will be a fixed field at the boundary, we cannot fix both at the same time.

Therefore, to cancel out the remaining terms we will have to add a counter-term to the action of the form

$$S_{ct} = \pm i \frac{g_f}{2} \int d^d x \sqrt{-h} [\bar{\psi}_L \psi_R + \bar{\psi}_R \psi_L] \quad , \quad (4.33)$$

since the variation of it will precisely cancel out our above result. We have freedom to decide which chirality will behave as source, thus its variation will be zero, and therefore fixing the sign of the counter-term. For simplicity, we will choose here  $\delta\psi_R = 0$ . It is important to remark at this point that we in fact are free to introduce extra terms that *only* depend on, in this case,  $\psi_R$  which we will do now.

The following step is in fact what separates semi-holography from pure holography, and will be key to find nontrivial results. Since we are fixing  $\psi_R$  in the boundary, it will behave as the source of some holographic operator that in turn will introduce what we will interpret as the self-energy in the spectral function for the boundary fermions. Therefore, to describe the dynamics of this field at the boundary we need to introduce the following ad-hoc term to the action:

$$S_{UV} = -iZ \int d^d x \sqrt{-g} [\bar{\psi}_R (\not{D} - iq\mathbb{A}) \psi_R] \quad , \quad (4.34)$$

using the freedom we mentioned previously in step 4. Collecting these two new terms we have introduced to the action, it reads now

$$\begin{aligned} S_{\text{total}} = & -ig_f \int d^{d+1} x \sqrt{-g} \left[ \bar{\psi} \left( \frac{1}{2} \overleftrightarrow{\not{D}} - iq\mathbb{A} - M \right) \psi \right] \\ & - ig_f \int d^d x \sqrt{-g} e_{\underline{r}}^r [\bar{\psi}_R \psi_L] - iZ \int d^d x \sqrt{-g} [\bar{\psi}_R (\not{D} - iq\mathbb{A}) \psi_R] \end{aligned} \quad . \quad (4.35)$$

Here we have included only one of the two terms we shown before in the counter-term, so that the Green's function is complex (see [23, 24] for a more in depth discussion). Also, we have multiplied and divided by  $e_{\underline{r}}^r$  so that instead of the determinant of the induced metric, we find  $\sqrt{-g}$ . Armed with this action we can proceed now to compute the self-energy contribution to the spectral function, for what we will need to introduce a new system of differential equations derived from Dirac's equation of motion. Even though this results are only valid for chiral fermions, as we will see it is straightforward to generalize them to the case with two fermionic fields in the bulk, which is the case we are ultimately interested in.

The second and third terms together form the effective action at the boundary, and can be rewritten in terms of the spin components  $\psi_{\pm}$  as follows

$$S_{\text{eff}} = -i \int d^d x \sqrt{-g} \left[ Z \psi_+^\dagger e_{\underline{a}}^\mu \sigma^a (\partial_\mu - iqA_\mu) \psi_+ + g_f e_{\underline{r}}^r \psi_+^\dagger \psi_- \right] \quad . \quad (4.36)$$

Here the index  $\mu$  runs over  $d$  dimensions, and this contraction includes vielbeins. We will come back to this expression when computing the spectral function from the Green's function. Notice that we have switched from  $\bar{\psi}$  to  $\psi^\dagger$ , since we are not interested in computing the relativistic Green's function for this, even though at a later point we will do the calculation.

### 4.2.2 Equation for the Proportionality Factor $\xi$

Because we have introduced this boundary condition  $\delta\psi_R = 0$ , only  $\psi_R$  terms should appear in the boundary theory, with  $\psi_L$  being integrated out of the action. We can rewrite  $\psi_L$  in terms of  $\psi_R$  introducing the following ratio

$$\psi_L = -i\xi\psi_R \quad . \quad (4.37)$$

Here  $\xi$  is a  $4 \times 4$  complex matrix. In the previous section, when we computed the asymptotic behavior of the scalar field  $\phi$  we saw the first step in computing this ratio. Given that we know the source and vev coefficients, we can compare that expansion with the actual solution and extract their values, and if we had an analytic solution for the fields we could write it in a compact expression.

Fermionic fields are slightly different though, because even though we could follow a similar procedure computing the asymptotic expansion of  $\psi$  and extracting  $\psi_R$  and  $\psi_L$  there is a better way. Instead, we can write a system of differential equations for the matrix  $\xi$ , which will be derived from the equations of motion for  $\psi$  and will themselves act as equations of motion for  $\xi$ . Here we are introducing some complexity into the problem, since these are no longer going to be linear equations, but nonlinear, and since in general  $\xi$  will have several components unless the problem has symmetries the general solution will involve up to  $4 \times 4 = 16$  coupled nonlinear differential equations.

Fortunately, our case is not this complicated and in the end we will find only one equation for chiral fermions and three for Dirac fermions. First we need Dirac's field equations for  $\psi$ , that we can compute from the action in equation (4.28), resulting in the following:

$$(\not{D} - iq\mathcal{A} - M)\psi = 0 \quad , \quad (4.38)$$

and another, for  $\bar{\psi}$  that we will not use. In this equation however we are actually hiding several important terms in  $\not{D}\psi$  that are quite relevant for the computation.

Considering that the covariant derivative of a spinor involves the spin connection, so expanding the equation above gives

$$\left( \Gamma^\mu \partial_\mu + \frac{1}{8} e_{\underline{c}}^\mu \omega_{\mu\overline{ab}} \Gamma^{\underline{c}}[\Gamma^{\underline{a}}, \Gamma^{\underline{b}}] - iq\mathcal{A} - M \right) \psi = 0 \quad . \quad (4.39)$$

Even though it is certainly possible to solve the equations of motion with this extra term, we would prefer to simplify them as much as possible before introducing any numerical methods. For this we can redefine the field  $\psi$  in a way that the spin connection is cancelled. We will focus in the case that  $\psi$  is of the form

$$\psi(r, x) = \psi(r) e^{ikx} \quad , \quad (4.40)$$

in other words, that it is a plane-wave solution. This indeed exactly what we need, because since there are no other terms depending directly on  $x$  we can Fourier transform the boundary coordinates to momentum space

and leave only the radial coordinate in the amplitude. We will perform this computation explicitly later, for now we assume that it is possible to act on each plane-wave independently of the others.

Now, focusing only on the terms involving the radial coordinate  $r$  means that only the component  $\mu = r$  of the first and second terms will contribute. Explicitly, only the following terms are important

$$\left( e_r^r \Gamma^r \partial_r + e_r^r \frac{1}{8} \omega_{rab} \Gamma^r [\Gamma^a, \Gamma^b] \right) \psi(r) + \dots = 0 \quad . \quad (4.41)$$

Here  $\dots$  represents the terms contributed from the derivatives with respect to the boundary coordinates, as well as the gauge field contribution and the mass term. Now, we need to assume that  $\frac{1}{8} \omega_{rab} [\Gamma^a, \Gamma^b] \Gamma^r = p(r) \Gamma^r$ , where  $p(r)$  is any function of the radial coordinate, which is indeed our case:

$$p(r) = \frac{r f'(r) + f(r)(6 - r \chi'(r))}{4r \sqrt{f(r)}} \quad . \quad (4.42)$$

Here we have commuted  $\Gamma^r$  with the commutator using that property of  $\gamma^5$  as shown in [25]. It may be possible to find a more general condition for this to work, however this is more than enough for our purposes.

Therefore, this is the equation that we are dealing with, and what we need to transform it into

$$(e_r^r \Gamma^r \partial_r + e_r^r \Gamma^r p(r)) \psi(r) \longrightarrow e_r^r \Gamma^r \partial_r \psi(r) \quad , \quad (4.43)$$

which we can do by transforming

$$\psi(r) \longrightarrow \psi(r) \exp \left[ - \int^r dr' p(r') \right] \quad , \quad (4.44)$$

so that  $\partial_r \psi(r)$  will introduce the derivative of the exponent,  $p(r)$ , which cancels out the spin connection. Therefore, using this transformed field the equations of motion simplify to

$$(\not{\partial} - iq\mathcal{A} - M) \psi = 0 \quad . \quad (4.45)$$

This procedure is directly generalizable to the case with two fermionic fields, as long as the spin connection remains the same for each, and the equations of motion also remain linear in the fields. In the next section we will explicitly check this calculation.

Before getting back to the proportionality factor  $\xi$  again, let us introduce the Fourier transform of  $\psi$  as follows

$$\psi(r, x) = \int \frac{d^d k}{(2\pi)^d} \psi(r, k) e^{ikx} \quad , \quad (4.46)$$

so that, written in components, the equations of motions are

$$-e_r^r \partial_r \begin{pmatrix} \psi_+ \\ \psi_- \end{pmatrix} - ie_0^0 \tilde{\omega} \begin{pmatrix} \psi_- \\ \psi_+ \end{pmatrix} + ie_3^3 k_3 \begin{pmatrix} -\sigma^3 \psi_- \\ \sigma^3 \psi_+ \end{pmatrix} - M \begin{pmatrix} -\psi_+ \\ \psi_- \end{pmatrix} = 0 \quad , \quad \tilde{\omega} \equiv \omega + qh(r) \quad . \quad (4.47)$$

Here we have multiplied by  $-\Gamma^r$  so that the first term is  $-e_r^r \partial_r \psi$ . However, and most importantly, we have used the rotational symmetry of the system to chose the  $k$  vector to be in the  $z$ -axis:  $(\omega, 0, 0, k_3)$ . As we will see later,

this allows us to simplify significantly our calculations without loss of generality. Using only  $2 \times 2$  matrices we can rewrite these equations as follows

$$e_{\underline{r}}^x \partial_r \psi_{\pm} = i \hat{F}(\omega, \mp k_3) \psi_{\mp} \pm M \psi_{\pm} \quad , \quad \hat{F}(\omega, k_3) = -e_0^0 \sigma^0 \tilde{\omega} + e_2^3 \sigma^3 k_3 \rightarrow \hat{F}(k) = e_a^\mu \sigma^a k_\mu \quad . \quad (4.48)$$

In the definition of  $\hat{F}(k)$  it is clearly shown the rotational invariance and how it is affected by our choice of axis. We can now actually get back to the proportionality factor equation, that in term of chiral components reads

$$\psi_L = -i \hat{\xi} \psi_R \rightarrow \begin{pmatrix} 0 \\ \psi_- \end{pmatrix} = -i \hat{\xi} \begin{pmatrix} \psi_+ \\ 0 \end{pmatrix} \rightarrow \psi_- = -i \hat{\xi} \psi_+ \quad , \quad (4.49)$$

where  $\hat{\xi}$  is a  $2 \times 2$  matrix, that corresponds to the bottom left block of  $\xi$ . Therefore, performing this substitution we find

$$\begin{aligned} e_{\underline{r}}^x \partial_r \psi_+ &= \hat{F}(\omega, k_3) \hat{\xi} \psi_+ + M \psi_+ \\ e_{\underline{r}}^x \partial_r \psi_- &= i \hat{F}(\omega, -k_3) \psi_+ + i M \hat{\xi} \psi_+ \end{aligned} \quad . \quad (4.50)$$

Now, to use this equations we have to look again at (4.49) and compute the derivative of it with respect to  $r$ :

$$e_{\underline{r}}^x \partial_r \hat{\xi} \psi_+ = i e_{\underline{r}}^x \partial_r \psi_- - \hat{\xi} e_{\underline{r}}^x \partial_r \psi_+ \quad , \quad (4.51)$$

where we have multiplied by  $e_{\underline{r}}^x$ , making now clear how the previous equations fit in this derivation. Substituting we find

$$\left( e_{\underline{r}}^x \partial_r \hat{\xi} + 2M \hat{\xi} + \hat{F}(\omega, -k_3) + \hat{\xi} \hat{F}(\omega, k_3) \hat{\xi} \right) \psi_+ = 0 \quad . \quad (4.52)$$

There are several important remarks that we can make from this expression. Let us go through them

1. As we have mentioned previously, this is indeed a system of nonlinear differential equations for  $\hat{\xi}$ , a matrix of dimensionality  $2 \times 2$ . Notice that the only nonlinear term is the last one, and there are some regimes in which the solution to this equation can be approximated analytically. This is especially true if we consider the limit  $r \rightarrow \infty$ , because only  $e_{\underline{r}}^x$  will have a non-negligible contribution.

Solving this equation near the boundary easily shows that the leading order term in the expansion of  $\hat{\xi}$  goes like  $r^{-2M}$ .

2. On the other hand, taking  $r \rightarrow r_h$  means that only the other two terms survive. Since  $f(r_h) = 0$ , the vielbein  $e_0^0$  is the only one that contributes, and then it is straightforward to see that

$$\omega \left( \mathbb{1} + \hat{\xi}^2(r_h) \right) = 0 \rightarrow \hat{\xi}^2(r_h) = -1 \quad , \quad \omega \neq 0 \quad . \quad (4.53)$$

This is the initial condition at the horizon we will use in the numerical solution, and in the next section we will check that it is still the same after introducing the second fermionic field in the bulk. As noted, this is only valid for  $\omega \neq 0$ , but we will not be focusing on this point in the results. Moreover, we will always consider  $\omega + i\epsilon$  in the numerical solution to avoid poles in the spectral function.

Notice that, in complete opposition of what we had to do with the scalar field in the background we do not need to expand around the horizon and evaluate the field at a point close to it. Instead, this value

is precisely the initial condition at  $r = r_h$ . It is still possible to do an expansion so that we can evaluate  $\hat{\xi}(r_h + \epsilon)$ , but we will take the previous result as the initial condition.

3. This choice of the initial condition is not arbitrary, since clearly we have two options:  $\hat{\xi}(r_h) = \pm i$ . These two options correspond to infalling or outgoing boundary conditions at the horizon, meaning that the field  $\psi$  propagates outwards or inwards at the point  $r = r_h$ . Because this is a normal black hole, in which matter *falls* but does not get out, we are required to use infalling boundary conditions, associated with the positive sign. We can check that this is indeed the case by substituting the plane-wave solution for  $\psi$  at the horizon and indeed this choice corresponds to propagating into the horizon. This initial condition also corresponds to the physically interesting retarded Green's function.
4. Notice that because of our choice of axis  $\hat{F}(k)$  is a diagonal matrix, and therefore the off-diagonal terms of  $\hat{\xi}$  are not coupled with the diagonal ones. Expanding this equation component by component, a tedious but straightforward calculation, we will see that the off-diagonal terms can be taken to be zero, and only the diagonal ones will contribute to the final solution.

Defining  $\hat{\xi}$  by components as follows,

$$\hat{\xi} \equiv \begin{pmatrix} \hat{\xi}_+ & 0 \\ 0 & \hat{\xi}_- \end{pmatrix} \quad (4.54)$$

and extracting the two remaining equations we find one symmetry of the system, namely that  $\hat{\xi}_+(k_3) = \hat{\xi}_-(-k_3)$ .

As a significant difference when compared to the background fields, this initial condition has no free parameters that we can set, even if we perform the expansion near the horizon these will be fixed by the infalling boundary conditions.

5. As a final remark, we will see in the next section that we find a similar equation when dealing with two fermionic fields, with another extra field to account for their coupling. However it should be clear that by setting the coupling constant to zero we should recover two exact copies of this equation, a condition that we will check later.

With this differential equation we can proceed and solve the propagation of  $\hat{\xi}$  from the horizon to the boundary, but we still need a way to relate it directly with the system described by the CFT. We will explore this option in the next section.

### 4.2.3 Green's Function and Spectral Function

To conclude our work with chiral fermions, we will compute the spectral function using the effective action in the boundary from equation (4.36). Introducing a Fourier transform of the fields similar to equation (4.46), the effective action results in

$$S_{\text{eff}} = - \int \frac{d^d k}{(2\pi)^d} \sqrt{-g} \left[ -Z \psi_+^\dagger \hat{F}(k) \psi_+ + i g_f e_\tau^r \psi_+^\dagger \psi_- \right] , \quad (4.55)$$

and rewriting  $\psi_-$  using  $\hat{\xi}$ ,

$$S_{\text{eff}} = - \int \frac{d^d k}{(2\pi)^d} \sqrt{-g} \psi_+^\dagger \left[ -Z \hat{F}(k) + g_f e_\tau^r \hat{\xi} \right] \psi_+ . \quad (4.56)$$

Now, considering that when  $r \rightarrow \infty$  all vielbeins  $e_{\underline{\mu}}^{\mu}$ , with  $\mu \in \{0, 1, 2, 3\}$ , go like  $1/r$ , we can extract that from  $\hat{F}(k)$  as follows

$$S_{\text{eff}} = -Z \int \frac{d^d k}{(2\pi)^d} \sqrt{-g} \psi_+^\dagger \frac{1}{r} \left[ \tilde{\omega} - \sigma^i k_{\underline{i}} + \frac{gf}{Z} r^2 \hat{\xi} \right] \psi_+ . \quad (4.57)$$

Here we have also substituted  $e_{\underline{r}}^r$  with its value at the boundary,  $r$ , and extracted  $Z$  from the integrand. Also, we have restored the rotational symmetry by writing the term  $\sigma^i k_{\underline{i}}$ . Now we can redefine the  $\psi_+$  field to get rid of these terms:

$$\psi_+ \longrightarrow \psi_+ [Zr^{-1}\sqrt{-g}]^{-\frac{1}{2}} , \quad (4.58)$$

so that the final expression reads

$$S_{\text{eff}} = - \int \frac{d^d k}{(2\pi)^d} \psi_+^\dagger \left[ \tilde{\omega} - \sigma^i k_{\underline{i}} + \frac{gf}{Z} r^2 \hat{\xi} \right] \psi_+ . \quad (4.59)$$

This is not the final expression we will use however, since we want to write it in terms of constant terms at the boundary. We have seen that  $\hat{\xi} \propto r^{-2M}$ , and therefore by multiplying it by  $r^{2M}$  we indeed find a constant value when  $r \rightarrow \infty$ . In other words,

$$\lim_{r \rightarrow \infty} r^{2M} \hat{\xi} = \text{constant} , \quad (4.60)$$

and since the full term should remain a constant, we impose that the following also remains constant at the boundary

$$g \equiv \frac{gf}{Z} r^{2-2M} \longrightarrow \text{constant} . \quad (4.61)$$

Getting everything together, we can extract the inverse Green's function from the action rewritten as

$$G_R^{-1}(k) = \tilde{\omega} - \sigma^i k_{\underline{i}} - \Sigma , \quad \Sigma = -g \lim_{r \rightarrow \infty} r^{2M} \hat{\xi} . \quad (4.62)$$

Here  $\Sigma$  can be directly interpreted as the self-energy of the particles. Using the following definition of the spectral function,

$$\rho(\omega, k_3) = -\frac{1}{2\pi} \text{Im}[\text{Tr}[G_R(\omega, k_3)]] . \quad (4.63)$$

It has to satisfy the ARPES sum-rule

$$\int_{-\infty}^{\infty} d\omega \rho(\omega, k_3) = 1 , \quad (4.64)$$

thus guaranteeing that the anti-commutation relations for the fermionic single particle operators work as expected, and it is only possible by introducing the ad-hoc term  $S_{UV}$  to the boundary action. Because the procedure to compute the spectral function when having more than one field is fundamentally different to the one involving one field, we will only briefly cover the latter here.

As we can see from equation (4.63), we need to compute the trace of the Green's function, meaning that we need to invert the matrix  $G_R^{-1}$  we just computed. Restoring again our choice of  $\mathbf{k} = (0, 0, k_3)$ , it is only a  $2 \times 2$  diagonal matrix, thus we can use the general expression

$$A^{-1} = \begin{pmatrix} a_+ & 0 \\ 0 & a_- \end{pmatrix}^{-1} = 2 \frac{A^{\text{sym}} \sigma^0 + A^{\text{asym}} \sigma^3}{(A^{\text{sym}})^2 - (A^{\text{asym}})^2}, \quad A^{\text{sym}} = a_+ + a_- \quad , \quad A^{\text{asym}} = a_+ - a_- \quad . \quad (4.65)$$

Here  $A^{\text{sym}}$  and  $A^{\text{asym}}$  are the symmetric and antisymmetric coefficients of the matrix, so that the inverse can be written in terms of the identity,  $\sigma^0$ , and  $\sigma^3$ . Using this representation of the matrix, the spectral density can be written as

$$\rho(\omega, k_3) = -\frac{1}{\pi} \text{Im} \left[ \frac{\tilde{\omega} - \Sigma_0}{(\tilde{\omega} - \Sigma_0)^2 - (k_3 + \Sigma_3)^2} \right], \quad (4.66)$$

which we mention explicitly because we will check in the next section that we indeed recover this expression in the case the two fermionic fields are not coupled together. Here  $\Sigma_0$  and  $\Sigma_3$  are the symmetric and antisymmetric parts of the self-energy, similarly to the coefficients for the matrix  $A$  we mentioned.

Summarizing what we have done until now, we started by introducing basic concepts related to Dirac's gamma matrices, and how the choice of space-time can affect them. At the same time we introduced some of the properties of the Clifford algebra for gamma matrices, as well as the chiral projectors using  $\gamma^5$ .

Then we moved on to the more interesting case of a curved geometry as a background, which introduces several problems that we mostly solve by introducing vielbeins, a basis that allows using locally flat coordinates in which we can define the normal gamma matrices. Then, by connecting these local coordinates in a consistent manner we can compute the covariant derivative and thus the spin connection.

Having introduced all the necessary components to continue, we proceed to introduce the bulk action for one fermionic field and compute the boundary terms which are canceled out by the counter-term. Then, taking a modified version of Dirac's equation we find a differential equation describing how the proportionality factor  $\hat{\xi}$  propagates from the horizon to the boundary, which will be central to computing the self-energy given by holography.

Taking again the boundary effective action and the proportionality factor, we can derive the spectral function from the Green's function, finally finding a closed expression for  $\rho(\omega, k_3)$ . We will proceed now with the central topic of this thesis, that we have been pointing at in this section. Until now we introduced all the important information we need in a simpler context, which we will generalize later and therefore will need a slightly different handling.

### 4.3 Bulk Model for Dirac Fermions

Following a similar structure as we have done for chiral fermions, we will do the complete calculation now for two fermionic fields in the bulk coupled together and with the scalar field. This coupling term in the action is what will give mass to the fermions in the boundary, and since it is mostly affected by the scalar field, our choice of initial conditions for the background will have a significant impact in the final value of the mass.

#### 4.3.1 Dirac's Action and Boundary Effective Action

As before, we will start by considering the action for a fermionic probe field propagating in the bulk from the horizon of the black hole towards the boundary. The key difference now is that instead of working only with  $\psi$

we will introduce  $\psi^{(1)}$  and  $\psi^{(2)}$  as follows

$$\begin{aligned}
S = \int d^{d+1}x \sqrt{-g} & \left[ R - 2\Lambda - \frac{1}{4}F^2 \right. \\
& - ig_f \left( \bar{\psi}^{(1)} \left( \frac{1}{2} \overleftrightarrow{\mathcal{D}} - i\mathcal{A} \right) \psi^{(1)} - M\bar{\psi}^{(1)}\psi^{(1)} + \bar{\psi}^{(2)} \left( \frac{1}{2} \overleftrightarrow{\mathcal{D}} - i\mathcal{A} \right) \psi^{(2)} + M\bar{\psi}^{(2)}\psi^{(2)} \right) \\
& - g_b (D_\mu \phi D^\mu \phi - m^2 \phi^2) \\
& \left. - ig_c \phi \left( \bar{\psi}^{(1)} \psi^{(2)} + \bar{\psi}^{(2)} \psi^{(1)} \right) \right] . \quad (4.67)
\end{aligned}$$

Here we can make several comments about this action.

1. Notice that if we take  $g_c = 0$  this action is fundamentally the same as the one for chiral fermions, the only difference being that there are two copies of the probe field. However, since they are not coupled in this case, they both should be the same with opposite mass  $M$ . It is possible to consider two masses for each field,  $M_1 \neq -M_2$ , which will introduce a new term in the self-energy proportional to  $\Gamma^z$ . For simplicity, we will only consider the case  $M_1 = -M_2$ .
2. Regarding the bulk mass  $M$ , we have chosen these two fields to have the same value for the mass with opposite sign. This choice will simplify the calculations and make both fields have the same asymptotic behavior near the boundary.
3. These two probe fields are coupled using the scalar field  $\phi$  in a very specific way. This is the simplest term we can think of, since a priori there are no reasons against adding something like

$$- ig_c D_\mu \phi \left( \bar{\psi}^{(1)} \Gamma^\mu \psi^{(2)} + \bar{\psi}^{(2)} \Gamma^\mu \psi^{(1)} \right) , \quad (4.68)$$

and even though these coupling terms could generate interesting physics in the boundary we will focus in the simplest one. These are of course restricted to real Lorentz scalars, but we can easily think of other terms in the action that satisfy this condition.

The next step in the calculation is to compute the boundary action using the variational principle. As before, focusing only on terms involving derivatives of the variation, we find

$$\delta_{\bar{\psi}^{(i)}, \psi^{(i)}} = \dots - i \frac{g_f}{2} \int d^{d+1}x \sqrt{-g} \left[ \bar{\psi}^{(1)} \overrightarrow{\mathcal{D}} \delta \psi^{(1)} - \delta \bar{\psi}^{(1)} \overleftarrow{\mathcal{D}} \psi^{(1)} + \bar{\psi}^{(2)} \overrightarrow{\mathcal{D}} \delta \psi^{(2)} - \delta \bar{\psi}^{(2)} \overleftarrow{\mathcal{D}} \psi^{(2)} \right] . \quad (4.69)$$

Comparing this variation with the one found for chiral fermions, we can notice that it is a duplicate of it for each field. This is completely expected, since the coupling term we have introduced does not involve any derivatives and therefore it will only contribute to the equation of motion, but not to the boundary terms. In other words, this coupling will only affect in the IR regime of the theory, as we can expect from introducing a mass, while for higher momentum we should recover the behavior of free particles.

Because this is the same as before, we only need to pick which chirality will act as source for each field. In the previous case we chose  $\delta \psi_R = 0$ , which corresponds to  $\delta \psi_R^{(1)} = 0$ . For  $\psi^{(2)}$  however we will pick the opposite, since both chiralities can act as source, thus having  $\delta \psi_L^{(2)} = 0$ . This way, as we will see later in equation (4.72), the boundary fermionic field will be  $\psi_+ \equiv \psi_R^{(1)} + \psi_L^{(2)}$ .

The counter-term for this combination therefore reads

$$S_{ct} = -ig_f \int d^d x \sqrt{-h} \left[ \bar{\psi}_R^{(1)} \psi_L^{(1)} - \bar{\psi}_L^{(2)} \psi_R^{(2)} \right] . \quad (4.70)$$

As before, the dynamics of these fields in the boundary are given by

$$S_{UV} = -iZ \int d^d x \sqrt{-g} \left[ \bar{\psi}_R^{(1)} (\not{D} - iq\mathcal{A}) \psi_R^{(1)} + \bar{\psi}_L^{(2)} (\not{D} - iq\mathcal{A}) \psi_L^{(2)} \right] . \quad (4.71)$$

Before we can continue, we will introduce one important difference from the chiral case. Previously we were only dealing with one Dirac field in the bulk, and after integrating out two of its components only a 2-component spinor remains in the boundary. We simplified our notation by, instead of working with  $\psi_R$ , writing our equations in terms of  $\psi_+$ . Now however this approach is no longer possible, since we have eight components in the bulk and four in the boundary.

Instead, we will combine  $\psi_R^{(1)}$  and  $\psi_L^{(2)}$  in such a way that we can work with them as if they were just one spinor. Defining  $\psi_{\pm}$  as follows,

$$\psi^{(i)} = \begin{pmatrix} \psi_+^{(i)} \\ \psi_-^{(i)} \end{pmatrix} \longrightarrow \psi_- \equiv \begin{pmatrix} \psi_-^{(1)} \\ \psi_+^{(2)} \end{pmatrix} , \quad \psi_+ \equiv \begin{pmatrix} \psi_+^{(1)} \\ \psi_-^{(2)} \end{pmatrix} , \quad (4.72)$$

where now  $\psi_{\pm}$  are 4-component spinors instead of the 2-component ones defined in the previous section. This notation will allow us to write several of the equations found previously in the exact same way, the only difference now matrices are going to be  $4 \times 4$ .

Indeed, notice that  $\psi_+ = \psi_R^{(1)} + \psi_L^{(2)}$ , while  $\psi_-$  contains the components we will integrate out. For completeness, we will also define the components of  $\psi_{\pm}^{(i)}$  as

$$\psi_{\pm}^{(i)} = \begin{pmatrix} u_{\pm}^{(i)} \\ d_{\pm}^{(i)} \end{pmatrix} , \quad (4.73)$$

where  $u$  and  $d$  reference the spin up and down components.

### 4.3.2 Equation for the Proportionality Factor $\xi$

Moving forward to the proportionality factor, we want to derive again a differential equation that describes how it propagates from the horizon to the boundary using the equations of motion for the probe fields. As before, using variational calculus and this time focusing on the terms that do not contribute only at the boundary, we find the following system of differential equations

$$\begin{aligned} (\not{\partial} - i\mathcal{A})\psi^{(1)} &= M\psi^{(1)} - \tilde{g}\phi\psi^{(2)} \\ (\not{\partial} - i\mathcal{A})\psi^{(2)} &= -M\psi^{(2)} - \tilde{g}\phi\psi^{(1)} \end{aligned} , \quad \tilde{g} = \frac{g_c}{g_f} . \quad (4.74)$$

Here we have already transformed both fields as

$$\psi^{(i)} \longrightarrow \psi^{(i)} \exp \left[ - \int^r dr' p(r') \right] , \quad p(r)\Gamma^r = \frac{1}{8} \omega_{r\bar{a}\bar{b}} [\Gamma^{\bar{a}}, \Gamma^{\bar{b}}] \Gamma^r , \quad (4.75)$$

and canceled out the extra exponential from both equations. It is clear now that, even though both equations are coupled as long as any extra terms are linear in the fields this transformation will remove the spin connection successfully.

Now, introducing the Fourier transform of  $\psi^{(i)}$  as

$$\psi^{(i)}(r, x) = \int \frac{d^d k}{(2\pi)^d} \psi^{(i)}(r, k) e^{ikx} \quad , \quad (4.76)$$

and substituting back in equation (4.74) we find

$$-e_{\underline{r}}^r \partial_r \begin{pmatrix} \psi_+^{(1)} \\ \psi_-^{(1)} \end{pmatrix} - ie_{\underline{0}}^0 \tilde{\omega} \begin{pmatrix} \psi_-^{(1)} \\ \psi_+^{(1)} \end{pmatrix} + ie_{\underline{3}}^3 k_3 \begin{pmatrix} -\sigma^3 \psi_-^{(1)} \\ \sigma^3 \psi_+^{(1)} \end{pmatrix} + M \begin{pmatrix} -\psi_+^{(1)} \\ \psi_-^{(1)} \end{pmatrix} + \tilde{g} \phi \begin{pmatrix} -\psi_+^{(2)} \\ \psi_-^{(2)} \end{pmatrix} = 0 \quad , \quad (4.77)$$

$$-e_{\underline{r}}^r \partial_r \begin{pmatrix} \psi_+^{(2)} \\ \psi_-^{(2)} \end{pmatrix} - ie_{\underline{0}}^0 \tilde{\omega} \begin{pmatrix} \psi_-^{(2)} \\ \psi_+^{(2)} \end{pmatrix} + ie_{\underline{3}}^3 k_3 \begin{pmatrix} -\sigma^3 \psi_-^{(2)} \\ \sigma^3 \psi_+^{(2)} \end{pmatrix} - M \begin{pmatrix} -\psi_+^{(2)} \\ \psi_-^{(2)} \end{pmatrix} + \tilde{g} \phi \begin{pmatrix} -\psi_+^{(1)} \\ \psi_-^{(1)} \end{pmatrix} = 0 \quad . \quad (4.78)$$

Here we have again multiplied by  $-\Gamma^r$ , and  $\tilde{\omega}$  is the same as before. However, as we have said before, we do not want to deal with the field components in this basis, but rather in terms of  $\psi_{\pm}$ , so we can take the second component of (4.77) and interchange it with the second of (4.78). Then, multiplying the latter by  $-\Gamma^r \Gamma^0$  we can rewrite them as

$$-e_{\underline{r}}^r \partial_r \psi_{\pm} - ie_{\underline{0}}^0 \tilde{\omega} \psi_{\mp} \pm ie_{\underline{3}}^3 k_3 \Gamma^0 \Gamma^3 \psi_{\mp} \pm M \psi_{\pm} \mp \tilde{g} \phi \Gamma^0 \psi_{\mp} = 0 \quad . \quad (4.79)$$

Notice that here we are dealing with 4-component spinors, and therefore we are using gamma matrices instead of Pauli matrices as we did in the chiral case. By defining  $\tilde{F}(k)$  we can rewrite this expression as follows

$$e_{\underline{r}}^r \partial_r \psi_{\pm} = i\tilde{F}(\omega, \mp k_3) \psi_{\mp} \pm M \psi_{\pm} \mp \tilde{g} \phi \Gamma^0 \psi_{\mp} \quad , \quad \tilde{F}(\omega, k_3) = -e_{\underline{0}}^0 \tilde{\omega} \mathbb{1} - e_{\underline{3}}^3 k_3 \Gamma^0 \Gamma^3 \longrightarrow \Gamma^0 \tilde{F}(k) = \tilde{k} \quad . \quad (4.80)$$

Comparing this expression with equation (4.48) we can see a few differences in signs, however it can be easily explained by the gamma matrices, especially  $\Gamma^0$ , which contain already this information. By setting  $\tilde{g} = 0$  we indeed find two almost identical copies of equation (4.48), as we expected. There is one slight difference here however, and is that instead of  $\tilde{F}(k)$  being diagonal now it is block diagonal.

We can now introduce the proportionality factor as

$$\psi_- = -i\xi \psi_+ \quad , \quad (4.81)$$

where  $\xi$  is now a full  $4 \times 4$  matrix. Even though we could derive an equation for this  $\xi$ , it will not be suited for numerically solving the system, since it will contain up to 16 components fully coupled together. To avoid this we will change our basis again, decoupling up and down spin components, as follows

$$\psi_{\mp} = \begin{pmatrix} \psi_{\mp}^{(1)} \\ \psi_{\mp}^{(2)} \end{pmatrix} = \begin{pmatrix} u_{\mp}^{(1)} \\ d_{\mp}^{(1)} \\ u_{\mp}^{(2)} \\ d_{\mp}^{(2)} \end{pmatrix} \longrightarrow \begin{pmatrix} u_{\mp}^{(1)} \\ u_{\mp}^{(2)} \\ d_{\mp}^{(1)} \\ d_{\mp}^{(2)} \end{pmatrix} = \begin{pmatrix} \psi_{\mp}^u \\ \psi_{\mp}^d \end{pmatrix} = \hat{\psi}_{\mp} \quad . \quad (4.82)$$

From here it is clear that the basis change matrix is

$$T \equiv \begin{pmatrix} 1 & 0 & 0 & 0 \\ 0 & 0 & 1 & 0 \\ 0 & 1 & 0 & 0 \\ 0 & 0 & 0 & 1 \end{pmatrix} \longrightarrow \hat{\psi}_{\mp} = T\psi_{\mp} \quad , \quad (4.83)$$

so that

$$\begin{aligned} \psi_- &= -i\xi\psi_+ \\ T^{-1}\hat{\psi}_- &= -i\xi T^{-1}\hat{\psi}_+ \quad , \\ \hat{\psi}_- &= -i(T\xi T^{-1})\hat{\psi}_+ \end{aligned} \quad (4.84)$$

and finally redefining  $\hat{\xi} \equiv T\xi T$  (notice that  $T^2 = \mathbb{1}$ ), we find the new identity

$$\hat{\psi}_- = -i\hat{\xi}\hat{\psi}_+ \quad . \quad (4.85)$$

Notice that  $\hat{\xi}$  here is not the same as in the chiral case: this is a  $4 \times 4$  matrix. Multiplying equation (4.80) by  $T$  from the left in both sides we find that the products  $T\Gamma^a$  separate the up and down components of  $\psi_{\pm}$ , and therefore we can extract two uncoupled equations for both  $\psi_{\pm}^u$  and  $\psi_{\pm}^d$ :

$$e_{\underline{r}}^r \partial_r \hat{\psi}_{\pm} = i\tilde{F}(\omega, \mp k_3) \hat{\psi}_{\mp} \pm M \hat{\psi}_{\pm} \mp i\tilde{g}\phi\Gamma^r\Gamma^0\Gamma^z \hat{\psi}_{\mp} \quad . \quad (4.86)$$

This equation might seem more complicated than the previous one, but notice that now everything is block diagonal and therefore there are no coupling terms between spin up and spin down. This is equivalent to what we found for the chiral case, but then it was as simple as only having two non-zero components of a  $2 \times 2$  matrix.

Notice as well that the coupling term has an important difference compared to the others, this being that a Pauli matrix other than  $\sigma^0$  or  $\sigma^3$  appeared. What this means is that in the final expression we will find coupling terms between the components of each block, which we will see are directly related to the fermion mass in the boundary.

For convenience, this expression written in terms of  $\psi_{\pm}^{u,d}$  reads

$$\begin{aligned} e_{\underline{r}}^r \partial_r \hat{\psi}_{\pm}^u &= i\hat{F}(\omega, \pm k_3) \hat{\psi}_{\mp}^u \pm M \hat{\psi}_{\pm}^u \pm i\tilde{g}\phi\sigma^2 \hat{\psi}_{\mp}^u \\ e_{\underline{r}}^r \partial_r \hat{\psi}_{\pm}^d &= i\hat{F}(\omega, \mp k_3) \hat{\psi}_{\mp}^d \pm M \hat{\psi}_{\pm}^d \pm i\tilde{g}\phi\sigma^2 \hat{\psi}_{\mp}^d \quad . \end{aligned} \quad (4.87)$$

Here we can clearly see one symmetry of the system, since changing  $u \leftrightarrow d$  and  $k_3 \rightarrow -k_3$  transforms one equation into the other. Because of this from now on we will only work with the  $u$  component for simplicity. Now, since these two blocks are uncoupled, we can rewrite the matrix  $\hat{\xi}$  as

$$\hat{\xi} = \begin{pmatrix} \hat{\xi}^u & 0 \\ 0 & \hat{\xi}^d \end{pmatrix} \quad , \quad (4.88)$$

where  $\hat{\xi}^{u,d}$  are  $2 \times 2$  matrices. Notice that because of the symmetry we just mentioned, these two components are related by  $\hat{\xi}^u(k_3) = \hat{\xi}^d(-k_3)$ , in clear analogy with our previous result for chiral fermions. Using this now the relation between  $\hat{\psi}_-$  and  $\hat{\psi}_+$  can be simplified to

$$\hat{\psi}_-^u = -i\hat{\xi}^u\hat{\psi}_+^u . \quad (4.89)$$

Again, taking a derivative with respect to  $r$  on both sides we find

$$\partial_r\hat{\xi}^u\hat{\psi}_+^u = i\partial_r\hat{\psi}_-^u - \hat{\xi}^u\partial_r\hat{\psi}_+^u , \quad (4.90)$$

where we can substitute equation (4.86) to find

$$e_{\underline{r}}^r\partial_r\hat{\xi}^u + 2M\hat{\xi}^u + \hat{F}(\omega, -k_3) + \hat{\xi}^u\hat{F}(\omega, k_3)\hat{\xi}^u - \tilde{g}\phi\left(\sigma^2 - \hat{\xi}^u\sigma^2\hat{\xi}^u\right) = 0 . \quad (4.91)$$

Let us go through several remarks about this equation.

1. We can clearly see here that  $\tilde{g} = 0$  or  $\phi = 0$  recovers exactly the chiral situation with double the number of fields. In this case, since everything is diagonal we can safely set the extra terms to zero. On the other hand, when the coupling term contributes the off-diagonal terms couple and this equation effectively involves the four components.
2. Since the coupling term does not include any vielbeins, the previous discussion regarding the value of  $\hat{\xi}^u$  at the horizon remains exactly the same as before. In the opposite direction, when  $r \rightarrow \infty$ , the argument also remains unchanged, since  $\phi$  goes to zero near the boundary.
3. One approach we are not considering in this thesis would involve studying analytically the regime in which this coupling term is most significant, since it may be possible to neglect some of the  $k$  dependence in  $\hat{F}(k)$ .

Now that we have derived the equation that describes  $\hat{\xi}^u$ , we can proceed to compute the spectral function. In that section however we will be working with  $\xi$ , so we will need to change basis back to the original one by multiplying it by  $T$ , as  $\xi = T\hat{\xi}T$ . Because of the block structure of  $\hat{\xi}$ ,  $\xi$  will contain certain symmetries that we will exploit to write the spectral function in a simple way.

### 4.3.3 Green's Function and Spectral Function

We will proceed now to compute the spectral function for Dirac fermions, which will involve mostly the same steps we explained in the previous section. For this, we will need to consider the effective boundary action and extract from there the inverse Green's function, but we have not considered all the necessary terms yet.

In addition to  $S_{UV}$  and  $S_{ct}$  there is another term contributed by the asymptotic behavior of the scalar field  $\phi$ , which is dual to some boundary operator with scaling dimension 3 coupled to a source term of scaling dimension 1. We have seen previously that these are precisely the dimensionalities of a term giving mass to a fermionic field, and therefore in the effective boundary action we should consider a term consistent with it, as follows

$$S_M = -i \int d^d x \sqrt{-g} M_0 \left[ \bar{\psi}_L^{(2)} \psi_R^{(1)} + \bar{\psi}_R^{(1)} \psi_L^{(2)} \right] . \quad (4.92)$$

Because deriving the final expression for the Green's function can be tricky, we are going to briefly go through it explaining the most important parts. Our final goal is to write the action in a way that we can read off the inverse Green's function directly, which means:

$$S_{\text{eff}} = - \int \frac{d^d k}{(2\pi)^d} \psi_+^\dagger G_R^{-1} \psi_+ . \quad (4.93)$$

Notice that this is not the Lorentz invariant version of the Green's function, that would be  $-\Gamma^0 G_R^{-1}$ , which we will compute once we know this one.

1. Considering  $S_{UV}$  first, we have

$$-iZ \int d^d x \sqrt{-g} \left[ \bar{\psi}_R^{(1)} (\not{\partial} - iq\not{A}) \psi_R^{(1)} + \bar{\psi}_L^{(2)} (\not{\partial} - iq\not{A}) \psi_L^{(2)} \right] . \quad (4.94)$$

Fourier transforming these fields we find

$$Z \int \frac{d^d k}{(2\pi)^d} \sqrt{-g} \left[ \bar{\psi}_R^{(1)} \not{k} \psi_R^{(1)} + \bar{\psi}_L^{(2)} \not{k} \psi_L^{(2)} \right] . \quad (4.95)$$

Using now that  $-\Gamma^0 \not{k} = \tilde{F}(k)$  and  $\bar{\psi} = \Gamma^0 \psi^\dagger$ , this expression simplifies to

$$-Z \int \frac{d^d k}{(2\pi)^d} \sqrt{-g} \left[ \psi_R^{(1)\dagger} \tilde{F}(\omega, k_3) \psi_R^{(1)} + \psi_L^{(2)\dagger} \tilde{F}(\omega, k_3) \psi_L^{(2)} \right] , \quad (4.96)$$

which, written in terms of 2-component spinors is

$$-Z \int \frac{d^d k}{(2\pi)^d} \sqrt{-g} \left[ \psi_+^{(1)\dagger} \hat{F}(\omega, k_3) \psi_+^{(1)} + \psi_-^{(2)\dagger} \hat{F}(\omega, -k_3) \psi_-^{(2)} \right] . \quad (4.97)$$

Finally, using  $\psi_+$ :

$$\int \frac{d^d k}{(2\pi)^d} \sqrt{-g} \psi_+^\dagger \begin{pmatrix} -Z \hat{F}(\omega, k_3) & 0 \\ 0 & -Z \hat{F}(\omega, -k_3) \end{pmatrix} \psi_+ . \quad (4.98)$$

We will follow the same procedure for  $S_{ct}$  and  $S_M$ , first Fourier transforming, then rewriting in components and then in terms of  $\psi_+$ .

2. Let us go through  $S_{ct}$  now,

$$-ig_f \int d^d x \sqrt{-g} e_\pm^r \left[ \bar{\psi}_R^{(1)} \psi_L^{(1)} - \bar{\psi}_R^{(2)} \psi_L^{(2)} \right] . \quad (4.99)$$

Fourier transforming and using components,

$$ig_f \int \frac{d^d k}{(2\pi)^d} \sqrt{-g} e_\pm^r \left[ \psi_+^{(1)\dagger} \psi_-^{(1)} + \psi_+^{(2)\dagger} \psi_-^{(2)} \right] . \quad (4.100)$$

Using now  $\psi_- = -i\xi \psi_+$  to rewrite this in terms of  $\psi_+$ :

$$\int \frac{d^d k}{(2\pi)^d} \sqrt{-g} \psi_+^\dagger [g_f e_\pm^r \xi] \psi_+ . \quad (4.101)$$

3. Finally,  $S_M$ :

$$-i \int d^d x \sqrt{-g} M_0 \left[ \bar{\psi}_L^{(2)} \psi_R^{(1)} + \bar{\psi}_R^{(1)} \psi_L^{(2)} \right] . \quad (4.102)$$

Same as before, Fourier transforming and writing by components,

$$-i \int \frac{d^d k}{(2\pi)^d} \sqrt{-g} M_0 \left[ \psi_-^{(2)\dagger} \psi_+^{(1)} - \psi_+^{(1)\dagger} \psi_-^{(2)} \right] . \quad (4.103)$$

Notice that this term is hermitian. Since these are all components of  $\psi_+$  we can just write

$$\int \frac{d^d k}{(2\pi)^d} \sqrt{-g} \psi_+^\dagger \begin{pmatrix} 0 & iM_0 \\ -iM_0 & 0 \end{pmatrix} \psi_+ . \quad (4.104)$$

We can now put everything together, to find that the matrix is

$$\sqrt{-g} \left[ \begin{pmatrix} -Z\hat{F}(\omega, k_3) & iM_0 \\ -iM_0 & -Z\hat{F}(\omega, -k_3) \end{pmatrix} + g_f e_r^r \xi \right] . \quad (4.105)$$

Evaluating this when  $r \rightarrow \infty$ , at the boundary, we have that  $\hat{F}(\omega, k_3) \approx (-\tilde{\omega} + \sigma^3 k_3)/r$ . Thus we need to transform  $\psi_+$  as follows to get rid of these extra factors in the diagonal

$$\psi_+ \longrightarrow \psi_+ (\sqrt{-g} Z r^{-1})^{-\frac{1}{2}} , \quad (4.106)$$

and by redefining  $M_0 \rightarrow M_0 Z/r$  we find the inverse Green's function:

$$G_R^{-1} = \begin{pmatrix} \tilde{\omega} - \sigma^3 k_3 & iM_0 \\ -iM_0 & \tilde{\omega} + \sigma^3 k_3 \end{pmatrix} + \frac{g_f}{Z} e_r^r \xi . \quad (4.107)$$

Notice that clearly the top right block is exactly the same we found for the chiral case, so this generalization contains the previous case and can be recovered when the mass is zero. As before, we can introduce the self-energy by redefining the second term to

$$g \equiv \frac{g_f}{Z} r^{2-2M} \longrightarrow \text{constant at the boundary} \\ -g \lim_{r \rightarrow \infty} r^{2M} \xi \equiv \Sigma . \quad (4.108)$$

At this point in the derivation of the spectral function for chiral fermions we decomposed  $\Sigma$  in terms of Pauli matrices, however that is not possible in this case since this matrix is  $4 \times 4$ . Our goal now is to compute the trace of  $G_R$ , from the definition of the spectral function, and we will do so by exploiting the symmetric structure of this matrix.

Considering first the first term, its structure is the following

$$A^{-1} = \begin{pmatrix} a_+ & 0 & b_+ & 0 \\ 0 & a_- & 0 & b_- \\ c_+ & 0 & d_+ & 0 \\ 0 & c_- & 0 & d_- \end{pmatrix}, \quad (4.109)$$

and by looking at the second term, we have that  $\xi = T\hat{\xi}T$ , so

$$\xi = T\hat{\xi}T = T \begin{pmatrix} \hat{\xi}_+ & 0 \\ 0 & \hat{\xi}_- \end{pmatrix} T \longrightarrow \text{has the same structure as } A^{-1}. \quad (4.110)$$

Assuming that  $\hat{\xi}_{\pm}$  are two general  $2 \times 2$  matrices with no symmetries, after this transformation we will find a matrix with the same structure as the one above, so we can work with  $A^{-1}$  as if it were  $G_R^{-1}$ . Therefore, we can derive that this type of matrices satisfy the following

$$\text{Tr}[A] = \frac{\text{Tr}[m_+]}{\det m_+} + \frac{\text{Tr}[m_-]}{\det m_-}, \quad m_{\pm} = \begin{pmatrix} a_{\pm} & b_{\pm} \\ c_{\pm} & d_{\pm} \end{pmatrix}. \quad (4.111)$$

Applying this result to  $G_R^{-1}$  means that  $m_{\pm}$  are

$$m_{\pm} = -\hat{F}(\omega, \pm k_3) - M_0 \sigma^2 - \Sigma_{\pm}, \quad \begin{aligned} \Sigma_+ &= -g \lim_{r \rightarrow \infty} r^{2M} \hat{\xi}^u \\ \Sigma_- &= -g \lim_{r \rightarrow \infty} r^{2M} \hat{\xi}^d \end{aligned}, \quad (4.112)$$

which is indeed a similar result to what we found previously, but now generalized to our case. Notice as well that these two matrices are related by the transformation  $k_3 \rightarrow -k_3$  and  $u \leftrightarrow d$ . In addition, computing the trace and determinant we find their value to be

$$\begin{aligned} \text{Tr}[m_{\pm}] &= 2(\tilde{\omega} - \Sigma_{0,\pm}) \\ \det m_{\pm} &= [\tilde{\omega} - \Sigma_{0,\pm}]^2 - [k_3 \pm \Sigma_{3,\pm}]^2 + [iM_0 + i\Sigma_{2,\pm}][iM_0 + (\Sigma_{\pm})_{21}] \\ &\text{with} \\ \Sigma_{0,\pm} &= \frac{1}{2} \left( (\Sigma_{\pm})_{11} + (\Sigma_{\pm})_{22} \right) \\ \Sigma_{2,\pm} &= i(\Sigma_{\pm})_{12} \\ \Sigma_{3,\pm} &= \frac{1}{2} \left( (\Sigma_{\pm})_{11} - (\Sigma_{\pm})_{22} \right) \end{aligned} \quad (4.113)$$

Comparing this with the expression we found for the spectral function in the chiral case,

$$\rho(\omega, k_3) = -\frac{1}{\pi} \text{Im} \left[ \frac{\tilde{\omega} - \Sigma_0}{(\tilde{\omega} - \Sigma_0)^2 - (k_3 + \Sigma_3)^2} \right], \quad (4.114)$$

we can see that each of the matrices  $m_{\pm}$  reduce to this expression when  $M_0 = 0$  and  $\Sigma_{\pm}$  is diagonal. Notice as well that the numerator is exactly the same, as new terms only appear in the denominator. However, we will not work directly with these expressions, since there are several symmetries in this system that we have not yet mentioned and that will simplify this final result for the spectral function significantly, as well as the propagation equation for  $\hat{\xi}^{u,d}$ .

### 4.3.4 Symmetries of the System

Looking back at the differential equation describing  $\hat{\xi}^{u,d}$ ,

$$\begin{aligned} e_{\underline{r}}^r \partial_r \hat{\xi}^u + 2M\hat{\xi}^u - \hat{F}(\omega, k_3) - \hat{\xi}^u \hat{F}(\omega, -k_3) \hat{\xi}^u - \tilde{g}\phi \left( \sigma^2 - \hat{\xi}^u \sigma^2 \hat{\xi}^u \right) &= 0 \\ e_{\underline{r}}^r \partial_r \hat{\xi}^d + 2M\hat{\xi}^d - \hat{F}(\omega, -k_3) - \hat{\xi}^d \hat{F}(\omega, k_3) \hat{\xi}^d - \tilde{g}\phi \left( \sigma^2 - \hat{\xi}^d \sigma^2 \hat{\xi}^d \right) &= 0 \end{aligned} \quad (4.115)$$

writing it component by component, a straightforward but tedious calculation, we can see several symmetries of the problem. Some of them are expected, as we can see

$$\begin{aligned} \hat{\xi}_{11}^u &= \hat{\xi}_{22}^d, & \hat{\xi}_{22}^u &= \hat{\xi}_{11}^d \\ \hat{\xi}_{21}^u &= \hat{\xi}_{21}^d, & \hat{\xi}_{12}^u &= \hat{\xi}_{12}^d \\ \hat{\xi}_{12}^u &= -\hat{\xi}_{21}^u, & \hat{\xi}_{12}^d &= -\hat{\xi}_{21}^d \end{aligned} \quad (4.116)$$

Using these symmetries we can rewrite some of the expressions we have derived in the previous section, for example:

$$\begin{pmatrix} \hat{\xi}_{11}^{u,d} & \hat{\xi}_{12}^{u,d} \\ -\hat{\xi}_{12}^{u,d} & \hat{\xi}_{22}^{u,d} \end{pmatrix} = \hat{\xi}^{u,d} = \frac{1}{2} \left( \hat{\xi}_{11}^{u,d} + \hat{\xi}_{22}^{u,d} \right) \sigma^0 + \frac{1}{2} \left( \hat{\xi}_{11}^{u,d} - \hat{\xi}_{22}^{u,d} \right) \sigma^3 + i \hat{\xi}_{12}^{u,d} \sigma^2, \quad (4.117)$$

which means that the self energy can be written as

$$\Sigma_{\pm} = \Sigma_{0,\pm} \sigma^0 + \Sigma_{3,\pm} \sigma^3 + \Sigma_{2,\pm} \sigma^2. \quad (4.118)$$

Therefore, the expressions for trace and determinant of the  $m_{\pm}$  matrices are

$$\begin{aligned} \text{Tr}[m_{\pm}] &= 2(\tilde{\omega} - \Sigma_{0,\pm}) \\ \det m_{\pm} &= [\tilde{\omega} - \Sigma_{0,\pm}]^2 - [k_3 \pm \Sigma_{3,\pm}]^2 - [M_0 + \Sigma_{2,\pm}]^2 \end{aligned} \quad (4.119)$$

Notice as well that, since  $\hat{\xi}_{12,21}^u = \hat{\xi}_{12,21}^d$ ,  $\Sigma_{2,+} = \Sigma_{2,-} = \Sigma_2$ . Similarly, using  $\hat{\xi}_{11,22}^u = \hat{\xi}_{22,11}^d$  implies  $\Sigma_{0,+} = \Sigma_{0,-} = \Sigma_0$  and  $\Sigma_{3,+} = -\Sigma_{3,-} = -\Sigma_3$ , so that the equation above simplifies to

$$\begin{aligned} \text{Tr}[m_{\pm}] &= 2(\tilde{\omega} - \Sigma_0) \\ \det m_{\pm} &= [\tilde{\omega} - \Sigma_0]^2 - [k_3 - \Sigma_3]^2 - [M_0 + \Sigma_2]^2 \end{aligned} \quad (4.120)$$

meaning that both terms contribute exactly the same. This is a fact of physical importance, since we have to remember that what these two terms represent are the up and down spins of the boundary fermions. Since our theory does not include any phenomena that can affect one of them more than the other, this is the result that we expect to find. In addition, notice that using this notation it perfectly resembles the chiral case but having multiplied the number of degrees of freedom by two.

We can write now the final expression for the spectral function:

$$\rho(\omega, k_3) = -\frac{2}{\pi} \text{Im} \left[ \frac{\tilde{\omega} - \Sigma_0}{(\tilde{\omega} - \Sigma_0)^2 - (k_3 - \Sigma_3)^2 - (M_0 + \Sigma_2)^2} \right] . \quad (4.121)$$

As before, the integral of this expression over all the frequencies should satisfy the ARPES sum-rule for any  $k_3$ . Since it depends on the numerically solved self-energy  $\Sigma$ , it is not trivial to compute this integral, but a possible approach would be to use the known expansion for  $\Sigma$  near the boundary for  $|k| \rightarrow \infty$ , which we can compute from the equation for  $\hat{\xi}$ . That way, choosing some high enough energy  $\Lambda$  the integrand can be computed numerically for  $\omega < \Lambda$  and analytically for  $\omega > \Lambda$ .

We can at this point also mention the case of  $g = 0$ , in which the self-energy drops out of the previous expression leaving us with the usual spectral function for a massive particle. Even though this can be thought as expected behavior, in this case we are introducing a mass only using holography, and therefore there should be a term in the self-energy that also contributes to  $M_0$ . Therefore, we can consider this limiting case as internally inconsistent, even though it is possible to compute.

Before moving on, we can look again at the relativistic inverse Green's function using these symmetries. Defining this version as  $\tilde{G}_R^{-1} \equiv -\Gamma^0 G_R^{-1}$ , it satisfies

$$S_{\text{eff}} = \int \frac{d^d k}{(2\pi)^d} \bar{\psi}_+ \tilde{G}_R^{-1} \psi_+ , \quad (4.122)$$

where instead of taking the adjoint  $\psi_+^\dagger$ , we are including a gamma matrix,  $\bar{\psi}_+$ . This is a relevant expression, because it is directly related to the 2-point correlator  $\langle i\bar{\psi}_+ \psi_+ \rangle$ . Since it is relativistic, it should be written in a covariant way using gamma matrices, and because of the symmetries and our choice of axis for  $k$  in this problem we know that it has to contain only the identity,  $\Gamma^0$  and  $\Gamma^3$ .

Taking the expression we found for  $G_R^{-1}$  and applying the symmetries we have derived from the equations of motion, we find then

$$\tilde{G}_R^{-1} = -[\tilde{\omega} - \Sigma_0] \Gamma^0 + [k_3 - \Sigma_3] \Gamma^3 + i[M_0 - \Sigma_2] \mathbb{1}_{4 \times 4} , \quad (4.123)$$

which, after taking the self-energy to zero, reduces to the usual propagator for massive fermions,

$$G_R(k) = \frac{1}{\Gamma^a k_a + iM_0 - \Sigma} \rightarrow \frac{1}{\Gamma^a k_a + iM_0} , \quad \Sigma = -\Sigma_0 \Gamma^0 + \Sigma_3 \Gamma^3 + i\Sigma_2 \mathbb{1}_{4 \times 4} . \quad (4.124)$$

From this expression for  $\tilde{G}_R^{-1}$  we can clearly see that  $\text{Tr}[G_R]$  is indeed what we computed previously, but the method we used clearly showed how the spin contributes to the final result, thus giving more physical insight.

### 4.3.5 Numerical Solution for $\hat{\xi}$

Moving on to the details of the numerical solution, we can expect less complexity than when solving for the background fields because of the fixed initial condition we are using for  $\hat{\xi}$  at the horizon. Instead we need to deal with a complex matrix of coupled coefficients, and extract the pertinent information for the spectral function.

It is possible however to decrease the complexity of these equations by using the symmetries we have shown earlier. For this we need to expand equation (4.91) component by component and after simplifying we find only three independent differential equations, since there are only three truly independent fields. In the following we define  $\xi_1 \equiv \hat{\xi}_{11}^u$ ,  $\xi_2 \equiv \hat{\xi}_{22}^u$  and  $\xi_3 \equiv \hat{\xi}_{12}^u$  for notational simplicity, and  $F(\omega, k_3) \equiv \hat{F}_{11}(\omega, k_3) = -e_0^0 \tilde{\omega} + e_3^3 k_3$ .

Then:

$$\begin{aligned}
e_r^r \partial_r \xi_1 + 2M\xi_1 - F(\omega, k_3) - \xi_1^2 F(\omega, -k_3) + \xi_3^2 F(\omega, k_3) - 2i\tilde{g}\phi\xi_1\xi_3 &= 0 \\
e_r^r \partial_r \xi_2 + 2M\xi_2 - F(\omega, -k_3) - \xi_2^2 F(\omega, k_3) + \xi_3^2 F(\omega, -k_3) - 2i\tilde{g}\phi\xi_2\xi_3 &= 0 \quad . \\
e_r^r \partial_r \xi_3 + 2M\xi_3 - \xi_1\xi_3 F(\omega, -k_3) - \xi_2\xi_3 F(\omega, k_3) - i\tilde{g}\phi(1 - \xi_1\xi_2 + \xi_3^2) &= 0
\end{aligned} \tag{4.125}$$

Here we can clearly see that  $\tilde{g}\phi$  is indeed in control of the coupling between diagonal and off-diagonal terms, so that if either of these are zero, they decouple and  $\xi_3$  can be set to zero. As we have seen, this field goes like  $r^{-2M}$  when  $r \rightarrow \infty$  so in a similar manner to how we proceed with the background metric fields, we will transform it so that it converges to a constant at the boundary, as follows

$$\Xi_i(\rho) \equiv \rho^{-2M} \xi_i(\rho) \quad , \quad i \in \{1, 2, 3\} \quad , \tag{4.126}$$

where we have also changed variables from  $r$  to  $\rho$ . Again, substituting this change in the previous equations we can find the final differential equation describing the propagation of  $\Xi_i(\rho)$ . After finding the solution, we can recover the matrix form by

$$\Xi = \begin{pmatrix} \Xi_{11} & \Xi_{12} \\ \Xi_{21} & \Xi_{22} \end{pmatrix} = \begin{pmatrix} \Xi_1 & \Xi_3 \\ -\Xi_3 & \Xi_2 \end{pmatrix} . \tag{4.127}$$

In Figure 4.1 we can see the result for one specific combination of parameters.

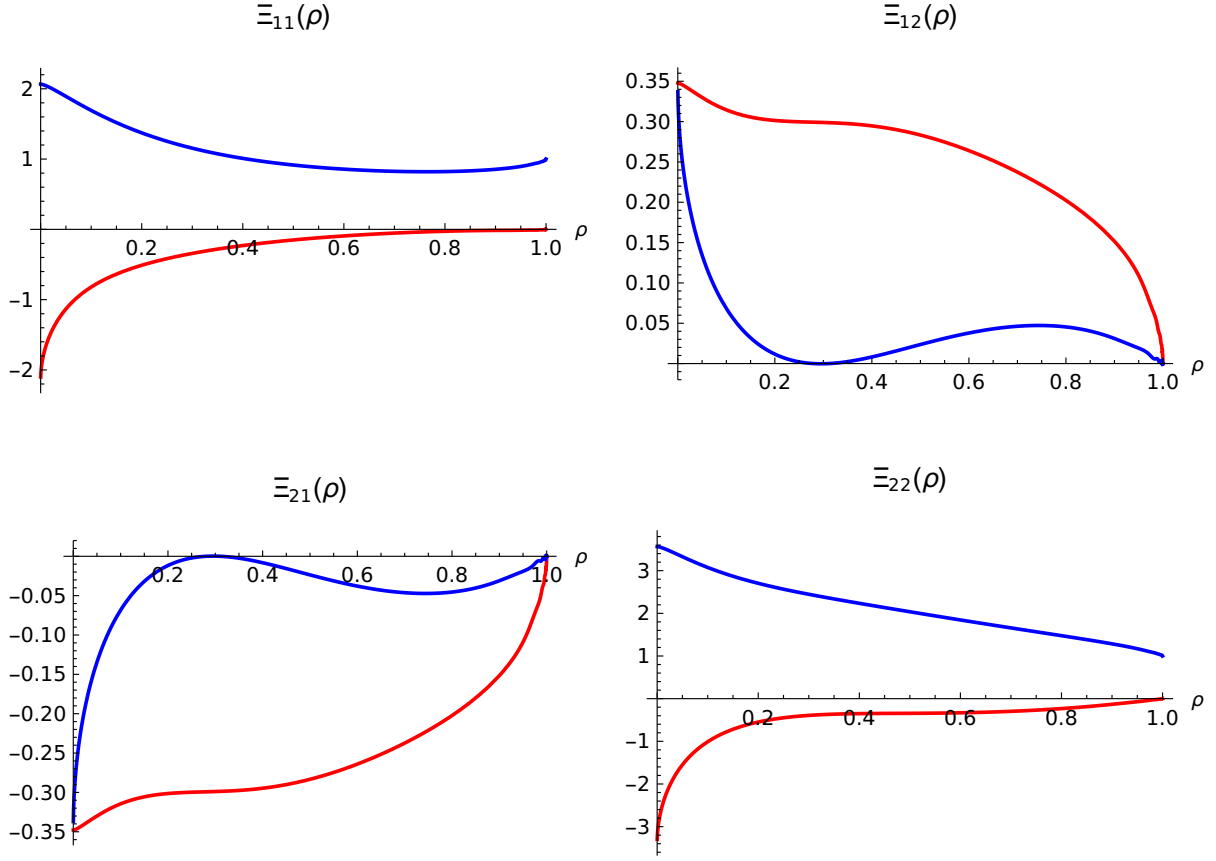


Figure 4.1: Numerical solution for the fermionic fields, using  $C_{\Phi 0} = 1$  and  $C_{H1} = 5$  as initial conditions at the horizon for the background, and  $\omega = 1 + i\epsilon$ ,  $k_3 = 1$ ,  $\tilde{g} = 1$ ,  $M = \frac{1}{4}$ ,  $q = 1$ . In the x-axis we can see the radial coordinate  $\rho$  and in the y-axis the value of each of the components of the field. Note that  $\rho = 0$  is the boundary and  $\rho = 1$  is the horizon. The red line is  $\text{Re}(\Xi)$  and the blue line is  $\text{Im}(\Xi)$ .

Notice from the caption that we are using  $M = 1/4$ , which will be our choice by default for the remaining of the results presented. Now, to compute the spectral function from here we will need to first rewrite everything in dimensionless units. In the boundary we have three parameters,  $T$ ,  $\mu$  and  $M_0$ , and since only the first two can be set freely we will express everything in units of  $M_0$ . This means that the temperature of the boundary system will be  $T/M_0$ , and similarly for the chemical potential,  $\mu/M_0$ .

However these are not the only parameters, when we introduce the probe field  $\omega$  and  $k_3$  appear, and they are dimensionful. Therefore, we will need to change the inverse Green's function and spectral function to rewrite everything in terms of dimensionless variables. Recall that the inverse Green's function is

$$G_R^{-1} = \begin{pmatrix} \tilde{\omega} - \sigma^3 k_3 & iM_0 \\ -iM_0 & \tilde{\omega} + \sigma^3 k_3 \end{pmatrix} - \Sigma \quad . \quad (4.128)$$

Transforming the field  $\psi_+ \rightarrow M_0^{-\frac{1}{2}} \psi_+$ , and the variables  $\tilde{\omega} \rightarrow \tilde{\omega} M_0$ ,  $k_3 \rightarrow k_3 M_0$ , we find

$$G_R^{-1} = \begin{pmatrix} \tilde{\omega} - \sigma^3 k_3 & i \\ -i & \tilde{\omega} + \sigma^3 k_3 \end{pmatrix} + \frac{gf}{ZM_0} r^2 \xi \quad . \quad (4.129)$$

However, now we cannot simply redefine  $g$  including this factor of  $M_0$ , since it changes with the background. Therefore, using a fixed  $g$  and changing the background means that we would be modifying the real coupling

constant which would invalidate any comparisons later in the results. To fix this, we will remove any scale dimensions from the self energy and combine them together as a power of  $M_0$ .

Since the scaling of  $M_0$  is  $r$ , we can begin by grouping the following together

$$\left(\frac{g_f r^2}{Z M_0}\right) \xi \quad , \quad (4.130)$$

where the factor between parenthesis is indeed constant. Notice that  $g_f$  is then dimensionless, and  $[Z] = [M_0] = 1$ . Removing the scaling from  $\xi$  as before, and multiplying and dividing by  $M_0$ :

$$\left(\frac{g_f r^2}{Z M_0}\right) r^{-2M} \frac{M_0^{-2M}}{M_0^{-2M}} r^{2M} \xi = \left(\frac{g_f r^{2-2M}}{Z M_0^{1-2M}}\right) M_0^{-2M} (r^{2M} \xi) \quad . \quad (4.131)$$

Here we can therefore see that the dimensionless self-energy is

$$\left(\frac{g_f r^{2-2M}}{Z M_0^{1-2M}}\right) M_0^{-2M} (r^{2M} \xi) \longrightarrow -g \lim_{r \rightarrow \infty} \frac{r^{2M}}{M_0^{2M}} \xi \equiv \Sigma \quad . \quad (4.132)$$

This is the expression for the self-energy we will use, with this new dimensionless  $g$  instead of the dimensionful one. Performing these changes in the spectral function, we find

$$\rho(\omega, k_3) = -\frac{2}{\pi} \text{Im} \left[ \frac{\tilde{\omega} - \Sigma_0}{(\tilde{\omega} - \Sigma_0)^2 - (k_3 - \Sigma_3)^2 - (1 + \Sigma_2)^2} \right] \quad , \quad (4.133)$$

where now every quantity is expressed in units of  $M_0$ . In the next section we will present and discuss our findings using this spectral function in several situations. Before that however we need to fix the value of  $M_0$ , since as we have seen it is now involved in almost every variable, by determining the value of  $\alpha$  in  $M_0 = \alpha \phi_s$ .

#### 4.4 Fixing the Bare Mass

Previously, in Section 3, we mentioned that the scalar field expansion near the boundary contains the source and vev,  $\phi_s$  and  $\phi_v$ , dual to the mass contribution for a fermion in the boundary. Namely:

$$\phi_s \phi_v \longleftrightarrow M_0 \langle \bar{\psi} \psi \rangle \quad . \quad (4.134)$$

However, there is one free parameter hidden in this duality. Transforming  $M_0 \rightarrow M_0/\alpha$  and  $\langle \bar{\psi} \psi \rangle \rightarrow \alpha \langle \bar{\psi} \psi \rangle$ , where  $\alpha$  is a constant value, shows that there is a scaling invariance that we need to fix to correctly determine  $M_0$  from  $\phi_s$ . In this section we will explain one possible way of determining its value.

We will start from the expansion near the boundary of the scalar field  $\phi$ , and from there compute some Renormalization Group Equations (“RG equations” from now on) that relate the three coefficients with a scaling parameter  $\lambda$ . Then, from  $M_0$  itself and  $\langle i\bar{\psi}\psi \rangle$ , the source and dual operator associated to  $\phi_s$  and  $\phi_v$  respectively, we will derive another set of RG equations that depend on another scaling parameter  $l$ .

Now, combining them in a meaningful way means that both  $\lambda$  and  $l$  have to have the same behavior as they flow towards the IR regime. Finally, comparing both equations considering the  $\alpha$  factor relating the expansion coefficients and the duals, we can solve an algebraic equation solving for  $\alpha$  and finding its value.

As we have said this procedure seems reasonable, however it may be proven inconsistent by studying different regimes that we will not consider in this thesis. One of these situations involves considering the non relativistic limit of this theory, by taking  $c \rightarrow \infty$ . Because of our choice of natural units we cannot see the effect of this limit, but a careful derivation shows that several quantities diverge, as they are proportional to  $c$ , which might be fixed by choosing a different  $\alpha$  constant.

These problems are outside the scope of this thesis, but a proper analysis of the specifics of this procedure is necessary given that the non relativistic limit is, after all, the regime in which cold atoms move. Some analysis using bosonic fields instead of fermionic fields reveals that indeed the value we will find for  $\alpha$  is explicitly not consistent in the non-relativistic limit.

#### 4.4.1 Renormalization Group Equations for $\phi$

First, we need to derive the RG equations using the information in the side of the bulk, which in this case means the scalar field  $\phi$ . Because we have chosen the scaling dimensions such that  $M_0 \langle i\bar{\psi}\psi \rangle$  is the dual to  $\phi_s\phi_v$ , relating these two will fix  $\alpha$ . Let us begin then by deriving the RG equations from the expansion of  $\phi$  near the boundary:

$$\phi(r) = \frac{1}{r} \left( \phi_s + \frac{1}{r^2} (\phi_v + \tilde{\phi}_v \log r) \right) , \quad (4.135)$$

where we rescale  $r \rightarrow \lambda r$ , so that

$$\phi(r) = \frac{1}{\lambda r} \left( \phi_s(\lambda) + \frac{1}{\lambda^2 r^2} (\phi_v(\lambda) + \tilde{\phi}_v(\lambda) \log(\lambda r)) \right) . \quad (4.136)$$

Comparing these two expressions we can extract the equalities between the coefficients:

$$\begin{aligned} \phi_s(\lambda) &= \lambda \phi_s \\ \phi_v(\lambda) + \tilde{\phi}_v(\lambda) \log \lambda &= \lambda^3 \phi_v , \\ \tilde{\phi}_v(\lambda) &= \lambda^3 \tilde{\phi}_v \end{aligned} \quad (4.137)$$

which we can differentiate to find the following RG equations:

$$\begin{aligned} \lambda \frac{d\phi_s(\lambda)}{d\lambda} &= \phi_s(\lambda) \\ \lambda \frac{d\phi_v(\lambda)}{d\lambda} &= 3\phi_v(\lambda) - \tilde{\phi}_v(\lambda) . \\ \lambda \frac{d\tilde{\phi}_v(\lambda)}{d\lambda} &= 3\tilde{\phi}_v(\lambda) \end{aligned} \quad (4.138)$$

The first and second ones are simple relations for the source and vev, with the corresponding scaling dimension multiplying the rhs. The second equation however relates those coefficients in a non trivial way, and we will see that from it we can extract the value of  $\alpha$ .

#### 4.4.2 Renormalization Group Equations for $M_0$ and $\langle i\bar{\psi}\psi \rangle$

Now, we will take the other side of the duality and derive a similar set of RG equations. Considering first the vev,

$$\langle i\bar{\psi}\psi \rangle = \text{Tr} \left[ \int \frac{d^d k}{(2\pi)^d} \frac{1}{-i\not{k} + M_0 - \langle O^*O \rangle} \right] , \quad (4.139)$$

with  $\langle O^*O \rangle$  given by

$$\langle O^*O \rangle = \Sigma = -\Sigma_0 \Gamma^0 + \Sigma_3 \Gamma^3 + i\Sigma_2 \mathbb{1} . \quad (4.140)$$

as we have decomposed  $\Sigma$  before. This is however not an easy to work with expression, because it is the inverse of a matrix. To fix it, we will multiply and divide by the conjugate of the denominator, so that  $\langle i\bar{\psi}\psi \rangle$  reads

$$\begin{aligned} \langle i\bar{\psi}\psi \rangle &= \text{Tr} \left[ \int \frac{d^d k}{(2\pi)^d} \frac{1}{-i\not{k} + M_0 - \Sigma} \frac{i\not{k} + M_0 - \Sigma^\dagger}{i\not{k} + M_0 - \Sigma^\dagger} \right] \\ &= \text{Tr} \left[ \int \frac{d^d k}{(2\pi)^d} \frac{i\not{k} + M_0 - \Sigma^\dagger}{k^2 + M_0^2 + |\Sigma|^2 - i(\Sigma\not{k} - \not{k}\Sigma^\dagger) + M_0(\Sigma + \Sigma^\dagger)} \right] . \end{aligned} \quad (4.141)$$

To simplify the denominator we need to use the expansion of  $\Sigma$  near the boundary, which is given by  $\Sigma = \sigma k^{2M}$ , where  $\sigma$  is a complex constant matrix. In addition, writing  $k^{2M+1} = \left(k^2\right)^{M+\frac{1}{2}} = k^{2M+1}$ , with  $k$  being the modulus of the vector, the expression above becomes:

$$\langle i\bar{\psi}\psi \rangle = \text{Tr} \left[ \int \frac{d^d k}{(2\pi)^d} \frac{i\not{k} + M_0 - k^{2M}\sigma^\dagger}{k^2 + M_0^2 + k^{4M+2}|\sigma|^2 + 2k^{2M+1}\text{Im}(\sigma) + 2k^{2M+1}M_0\text{Re}(\sigma)} \right] , \quad (4.142)$$

where we can now take the Trace of the numerator, and using that  $\text{Tr}[\not{k}] = 0$  we can get rid of every gamma matrix. Also, transforming to spherical coordinates we find an extra factor of  $2\pi^2 k^3$ . We will fix  $d = 4$  explicitly in the following.

$$\langle i\bar{\psi}\psi \rangle = 2\pi^2 \int_0^\infty \frac{dk}{(2\pi)^4} \frac{4M_0 k^3 - k^{2M+3}\text{Tr}[\sigma^\dagger]}{k^2 + M_0^2 - k^2 \hat{\sigma}} , \quad \hat{\sigma} \equiv -k^{4M-2}|\sigma|^2 - 2k^{2M-1}\text{Im}(\sigma) - 2k^{2M-1}M_0\text{Re}(\sigma) . \quad (4.143)$$

Here we have defined  $\hat{\sigma}$  for simplicity in the notation. Extracting a factor of  $k^2$  from the denominator, so that we find

$$\frac{1}{1 + k^{-2}M_0^2 - \hat{\sigma}} \approx 1 - k^{-2}M_0^2 + \hat{\sigma} , \quad (4.144)$$

where we have expanded this fraction using the geometric series. We can always do this because, since  $M \in \left(-\frac{1}{2}, \frac{1}{2}\right]$ , every term in  $\hat{\sigma}$  has a negative power of  $k$ , as well as  $M_0$  as we can clearly see. Therefore, since we are working in the limit  $k \rightarrow \infty$  this expansion is always possible. We will now introduce a cut-off  $\Lambda$  and an energy scale  $\mu$  to track of UV divergences and get rid of IR ones, respectively.

The integral we need to solve is therefore

$$2\pi^2 \int_{\mu}^{\Lambda} \frac{dk}{(2\pi)^4} \left( 4M_0 k - k^{2M+1} \text{Tr} \left[ \sigma^\dagger \right] \right) (1 - k^{-2} M_0^2 + \hat{\sigma}) \quad , \quad (4.145)$$

where most of the terms in the integrand are of the form  $Ck^\Delta$ , with  $C$  being a combination of the different constants appearing here, and  $\Delta > 0$ . There is one exception however, and we can see that term directly from the expression above:

$$- 8\pi^2 \int_{\mu}^{\Lambda} \frac{dk}{(2\pi)^4} \frac{M_0^3}{k} = - \frac{M_0^3}{2\pi^2} \log \left( \frac{\Lambda}{\mu} \right) \quad . \quad (4.146)$$

This term is special however for a very specific reason, this being that when we rescale the cut-off  $\Lambda \rightarrow \Lambda e^{-l}$ , this logarithm will produce a contribution that does not depend on  $\Lambda$ , namely

$$\langle i\bar{\psi}\psi \rangle = \frac{M_0^3}{2\pi^2} l \quad , \quad (4.147)$$

therefore every other term will be canceled out with a counter-term, only this one remaining. With this result we can finally write the RG equation for the vev, with  $l$  as the flow variable. Rescaling  $\langle i\bar{\psi}\psi \rangle \rightarrow \langle i\bar{\psi}\psi \rangle e^{-3l}$  and  $M_0 \rightarrow M_0 e^{-l}$  we have:

$$\begin{aligned} \frac{dM_0^3}{dl} = 0 & \xrightarrow{M_0 \rightarrow M_0 e^{-l}} \frac{d(M_0^3 e^{-3l})}{dl} = 0 \quad \longrightarrow \quad \frac{dM_0^3}{dl} = 3M_0^3 \\ \frac{d\langle i\bar{\psi}\psi \rangle}{dl} = \frac{M_0^3}{2\pi^2} & \xrightarrow{\langle i\bar{\psi}\psi \rangle \rightarrow \langle i\bar{\psi}\psi \rangle e^{-3l}} \frac{d(\langle i\bar{\psi}\psi \rangle e^{-3l})}{dl} = \frac{M_0^3 e^{-3l}}{2\pi^2} \quad \longrightarrow \quad \frac{d\langle i\bar{\psi}\psi \rangle}{dl} = 3\langle i\bar{\psi}\psi \rangle + \frac{M_0^3}{2\pi^2} \end{aligned}$$

Here we have used that  $M_0$  should not change under rescaling and  $\langle i\bar{\psi}\psi \rangle$  should transform following the result derived above. Let us go back now to the RG equations we derived for the scalar field and the constant  $\alpha$ .

Considering

$$\begin{aligned} \lambda \frac{d\phi_s(\lambda)}{d\lambda} &= \phi_s(\lambda) & \phi_s &= \frac{M_0}{\alpha} \\ \lambda \frac{d\phi_v(\lambda)}{d\lambda} &= 3\phi_v(\lambda) - \tilde{\phi}_v(\lambda) & \text{and} & \phi_v = \alpha \langle i\bar{\psi}\psi \rangle \quad , \quad (4.148) \\ \lambda \frac{d\tilde{\phi}_v(\lambda)}{d\lambda} &= 3\tilde{\phi}_v(\lambda) & \tilde{\phi}_v &= -\frac{1}{6}\phi_s^3 = -\frac{M_0^3}{6\alpha^3} \end{aligned}$$

we can compare with the two equations above to determine  $\alpha$ . Specifically, comparing the second equation in both terms we have

$$\begin{aligned} \frac{d\langle i\bar{\psi}\psi \rangle}{dl} = 3\langle i\bar{\psi}\psi \rangle + \frac{M_0^3}{2\pi^2} & \longrightarrow \quad \frac{\alpha M_0^3}{2\pi^2} = -\tilde{\phi}_v = \frac{1}{6}\phi_s^3 = \frac{M_0^3}{6\alpha^3} \quad \longrightarrow \quad \alpha = \left( \frac{\pi^2}{3} \right)^{\frac{1}{4}} \approx 1.34677 \quad . \quad (4.149) \\ \lambda \frac{d\phi_v(\lambda)}{d\lambda} = 3\phi_v(\lambda) - \tilde{\phi}_v(\lambda) & \end{aligned}$$

Thus fixing the relation between the source and the bare mass of the fermions. Notice here that the only way of having the term  $\tilde{\phi}_v$  in the second equation is by considering the logarithmic term in the expansion of the field near the boundary. Without that term we could not have related the bare mass term in the RG for the vev with the source term.

Notice as well that we are glossing over the fact that there are two different flow variables,  $l$  and  $\lambda$ , but assuming both of them share the same behavior we can transform in a way that  $\frac{dl}{d\lambda} = \lambda^{-1}$ , so that both equations are expressed in the same variables.

## 5 Results

Finally we will present our findings using the theory we described until now. Results will be separated in the *Holography* case, and the *Semi-holography* case. In the former we will analyse the behavior of the self-energy  $\Sigma$  alone by taking the limit  $g \rightarrow \infty$ , regardless of other terms in the spectral function. In the latter, we will consider the full expression we derived for  $\rho(\omega, k_3)$ , and by comparing these two situation we will extract some conclusions.

In every case, unless explicitly stated, we will consider  $M = \frac{1}{4}$  and  $q = 1$ , with every variable expressed in units of  $M_0$ . To avoid poles, we will always add  $i\epsilon$  to  $\omega$ , with  $\epsilon$  being a sufficiently small value. Since we need to compute the spectral function at a finite  $\rho$ , we will always integrate fields from  $\rho = 1 - \epsilon$  at the horizon to  $\rho = \epsilon$  near the boundary, and take the latter as the limit  $r \rightarrow \infty$ . Again,  $\epsilon$  is chosen to be sufficiently small. Lastly, we will fix the temperature to  $T = \frac{1}{100}$  unless specified otherwise. If we are not explicitly specifying that we are evaluating the spectral function in the  $(\omega, k_3)$  plane, it will always be with  $k_3 = 0$ . In the cases in which we introduce the chemical potential  $\mu$ , we will always plot  $\rho(\omega - \mu, k_3)$ .

Each section will be also separated in studying the dependence with one parameter alone, mainly  $\tilde{g}$  and  $\mu$ , computing the spectral function for each at different temperatures when necessary. Notice that  $g$  is the constant defined in the self-energy and  $\tilde{g}$  is the coupling constant in the bulk, between the fermionic fields  $\psi^{(i)}$  and the bosonic field  $\phi$ .

We will systematically present and discuss the effect of varying the parameters  $g$ ,  $\tilde{g}$  and  $\mu$  on the spectral function. For this, we will structure the remainder of the section in the following way: first we will focus on computing  $\rho(\omega, 0)$  for some  $\omega \in [\omega_a, \omega_b]$ , and varying one of these parameters in another interval  $[a, b]$ , while fixing the other two.

We will divide the results in the two cases we mentioned before, essentially the limit  $g \rightarrow \infty$  and finite  $g$ , each subsequently divided in the dependence on  $g$  (only in the latter case),  $\tilde{g}$  and  $\mu$ . In general, we will consider first the dependence on  $\tilde{g}$  at a fixed  $\mu$ , then we will fix  $\tilde{g}$  and change  $\mu$ , and finally we will present the spectral function in the  $(\omega, k_3)$ -plane for a few chosen values of the parameters.

### 5.1 Holographic limit

Considering the full spectral function,

$$\rho(\omega, k_3) = -\frac{2}{\pi} \text{Im} \left[ \frac{\tilde{\omega} - \Sigma_0}{(\tilde{\omega} - \Sigma_0)^2 - (k_3 - \Sigma_3)^2 - (1 + \Sigma_2)^2} \right], \quad (5.1)$$

in this first section we will take the limit  $g \rightarrow \infty$ , so that only the self-energy terms remain:

$$g\rho(\omega, k_3) = \frac{2}{\pi} \text{Im} \left[ \frac{g\Sigma_0}{(\Sigma_0)^2 - (\Sigma_3)^2 - (\Sigma_2)^2} \right]. \quad (5.2)$$

Here we have also multiplied by a factor of  $g$  so that the spectral function is finite in this limit. In practice we cannot take  $g$  to infinity, but we will choose a high enough value so that  $\omega$  and  $k_3$  are negligible compared to the self-energy contribution.

#### 5.1.1 Dependence on $\tilde{g}$

The goal of this section is to analyze the dependence of the effective mass only in terms of  $\tilde{g}$ , thus we set  $\mu = 0$  and compute the spectral function at  $k_3 = 0$ . Since this is the simplest case, in which we are only considering

the holographic contribution to the spectral function, we should extract as much information as possible from these results so that we can understand the more general case better.

We will therefore begin by computing  $\rho(\omega, 0)$  for a range of values of  $\tilde{g}$ , and compute the effective mass by measuring the position of the spectral function peaks as a function of  $\omega$ :

$$M_{\text{eff}} = \frac{1}{2}(\omega_+ - \omega_-) \quad , \quad (5.3)$$

where  $\omega_{\pm}$  refers to the positive and negative peaks, respectively. Even though in this case we could only compute the positive peak and that corresponds to the effective mass, when setting  $\mu \neq 0$  we will need to use this equation.

In Figure 5.1 we can see the result of this computation. In the left plot we can see the values the spectral function takes, which clearly shows a linear dependence between the peak and  $\tilde{g}$ . In addition, the width of this peak is kept very close to constant.

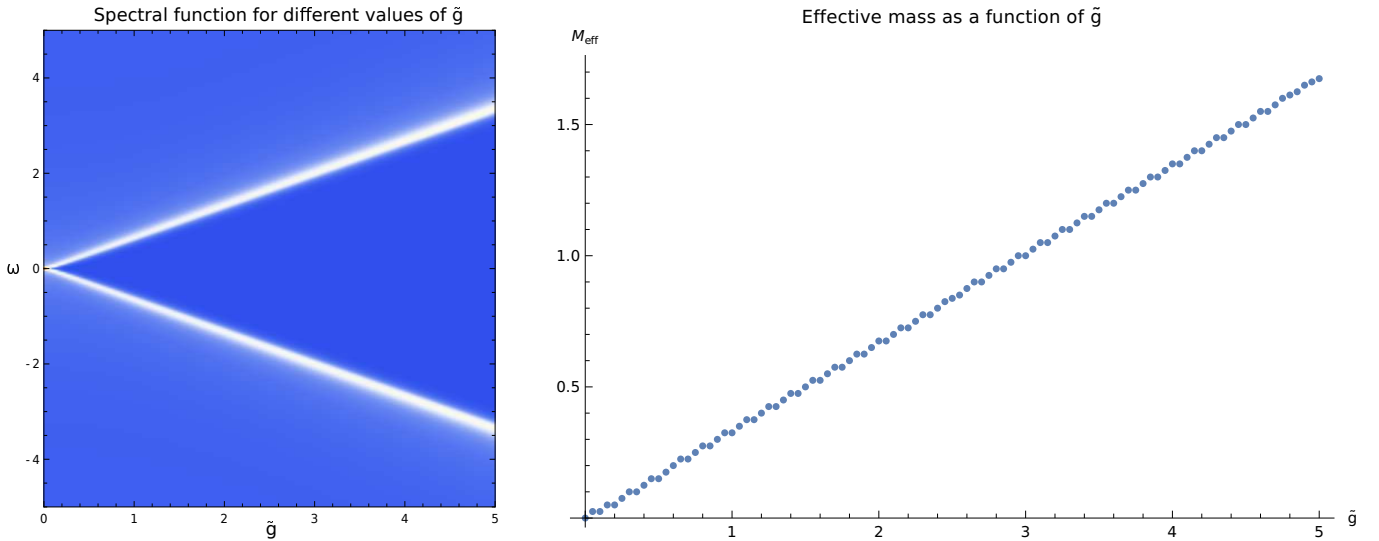


Figure 5.1: (left) Here is presented the spectral function  $\rho(\omega, 0)$ , for several values of  $\tilde{g}$ . Default values for other parameters used. Notice that when  $\tilde{g} \rightarrow 0$  there is no gap, meaning the boundary particles are massless, and increasing  $\tilde{g}$  translates to a linear increase of the mass gap. (right) Here we present the value of the mass in terms of  $\tilde{g}$ , computed from the data shown in (left).

In the left plot of Figure 5.1 we can see the result of applying equation (5.3) to the data, again clearly showing the linear dependence between the effective mass and  $\tilde{g}$ .

Since this is a surprisingly simple solution, we can fit it to an expression that can later be used to analyze the semi-holographic behavior knowing what is exactly the holographic contribution to the spectral function. Considering then the following expression,

$$\rho_{\text{approx}}(\omega, \tilde{g}) = \text{Im} \left[ \frac{A}{\omega - B\tilde{g} - i(C + D\omega + E\tilde{g})} \right] \quad , \quad (5.4)$$

we can fit the parameters  $A$ ,  $B$ ,  $C$ ,  $D$  and  $E$  using the numerical solution. Notice that  $B$  should be exactly twice the slope of the effective mass line shown in the right plot of Figure 5.1. Also we have included a possible  $\omega$  and  $\tilde{g}$  dependence in the width of the peak, so that the approximation is slightly better. It is indeed possible to consider extra higher order terms, and as we can expect the calculation shows that their coefficients are at least an order of magnitude smaller than  $D$  and  $E$ , so we can neglect them.

In Figure 5.2 we can see on the right plots the result of fitting this expression to the data, with a remarkably good agreement. The numerical result for the coefficients is summarized in the following table

$$\begin{aligned}
 A &\rightarrow 5.94687 \cdot 10^{-9} \\
 B &\rightarrow 0.686273 \\
 C &\rightarrow 0.209738 \\
 D &\rightarrow 0.532702 \\
 E &\rightarrow -0.368806
 \end{aligned}
 \tag{5.5}$$

Notice however that these coefficients ultimately also depend on  $M$  and  $T$ , although the dependence with the latter should mostly affect the widening of the peak, but not its position. Since the parameter  $M$  modifies the theory in a non-trivial way its effects are more difficult to predict, but computing a new set of coefficients for each value involves the same procedure.

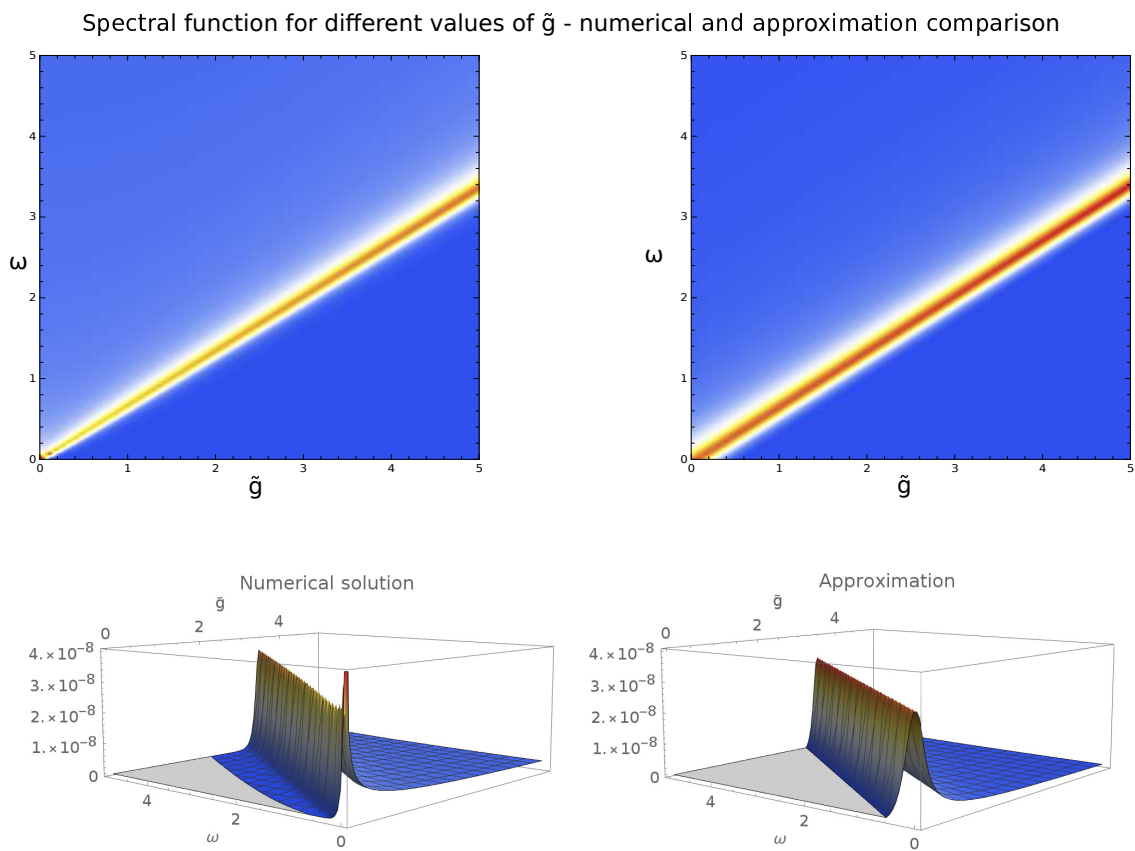


Figure 5.2: Using the same parameters as in Figure 5.1, here we compare the upper half plane,  $\omega > 0$ , with the approximation given by equation (5.4). We can notice a some details our approximation cannot capture, such as a slight widening of the peak as  $\tilde{g}$  increases, or the significant increase in value when both peaks merge near the origin. Despite these, we can say this approximation does reproduce the most important characteristics of the numerical solution.

Taking a closer look at the second row of plots in Figure 5.2, we can easily see that our approximation does not capture every detail of the numerical solution, but we can consider this an expected limitation. Firstly, notice

that near the origin, with  $\tilde{g} = 0$ , the numerical solution peaks sharply because instead of two, there is only one peak at that point. This is expected, since in the limit this should resemble a Dirac delta characteristic of massless particles.

In addition, the width is not exactly the same, specifically the shape of the fall-off outside the light cone (which corresponds to the left side of the plots). The numerical solution presents a sharp fall-off, in essence making the possibility of finding fermionic states of lower energy basically non-existent. On the other hand, considering only values of  $\tilde{g}$  slightly larger than one this approximation is significantly good.

Moving on, let us now analyze the full spectral function  $\rho(\omega, k_3)$ , evaluated in the whole plane. In these density plots we should clearly see the mass shell behavior typical of massive particles, with the parabolic dependence when  $|\mathbf{k}|$  is sufficiently close to zero. In Figure 5.3 we can see the result of this calculation for several values of  $T$  and  $\tilde{g}$ .

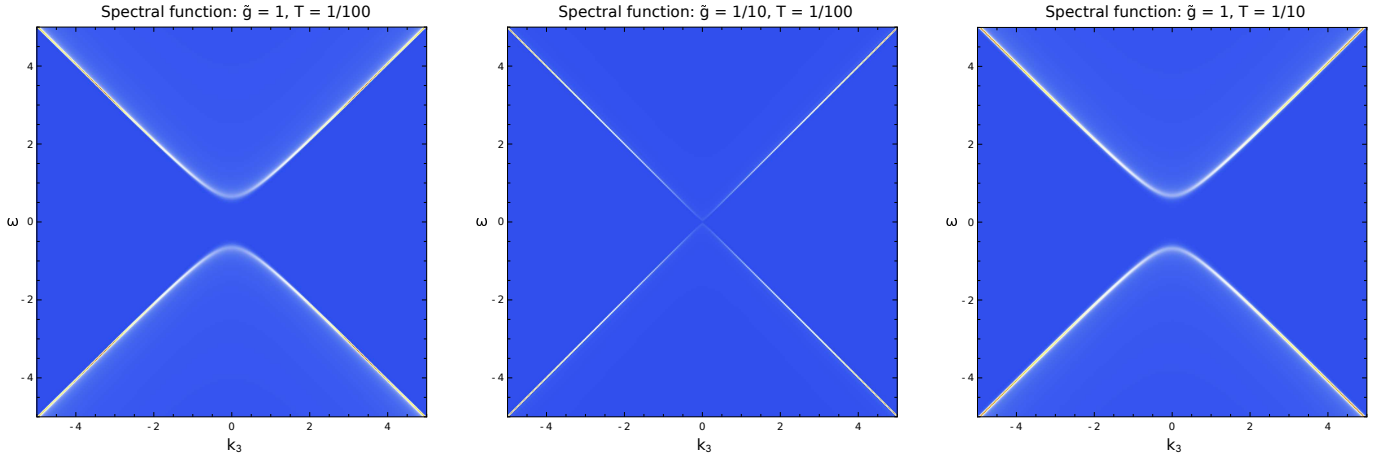


Figure 5.3: Here we can see the expected behavior of the spectral function in the  $(\omega, k_3)$ -plane, for several different values of  $T$  and  $\tilde{g}$ . All the colors are in the same scale. In the (left) panel there is the spectral function with the default parameters we are using; the (center) panel corresponds to the almost massless case, and the (right) panel shows the not-so-significant effects of increasing the temperature.

Indeed, the shape resembles exactly what we would expect of massive fermions. Besides, the width is mostly constant and very thin, so these are very stable states. Notice as well that the spectral function is basically zero below  $\omega = M_{\text{eff}}$ , meaning this is a hard gap.

On the other hand, in the case of a very small  $\tilde{g} = \frac{1}{10}$ , it is clear that the usual Dirac cone behavior is restored. The dispersion relation is therefore linear in  $k_3$ , following the light cone.

Finally, considering  $\tilde{g} = 1$  again but increasing the temperature to  $T = \frac{1}{10}$ , we can only notice a slightly wider line. This is expected behavior, since the effect of temperature is precisely to disturb the ground-state. We can also see that the mass gap does not get affected by it in a significant manner, especially the value of the mass.

### 5.1.2 Dependence on $\mu$

We will now move on to the  $\mu \neq 0$  case, in which we will study the effect of the chemical potential on the spectral function. For usual massive fermions, the effect of the chemical potential is to shift the spectral function up or down in the  $\omega$ -axis, exactly the amount  $\mu$ .

In this case however, we still expect the main shift happening but with other non-trivial effects contributing to the final result as well. To remove the shift in the spectral function, we will always plot  $\rho(\omega - \mu, k_3)$  so that the

middle of the mass gap stays close to  $\omega = 0$ .

Following a similar procedure as in the previous section, we will start by plotting the spectral function for  $k_3 = 0$  at a fixed  $\mu$ , for several values of  $\tilde{g}$ . We expect a similar general behavior to what we have already seen in Figure 5.1, except for  $\omega < \mu$ . In this regime the effects of the chemical potential should be driving the behavior of the spectral function.

In Figure 5.4 we can see the results of this computation, comparing the effects of three different values of  $\mu$ .

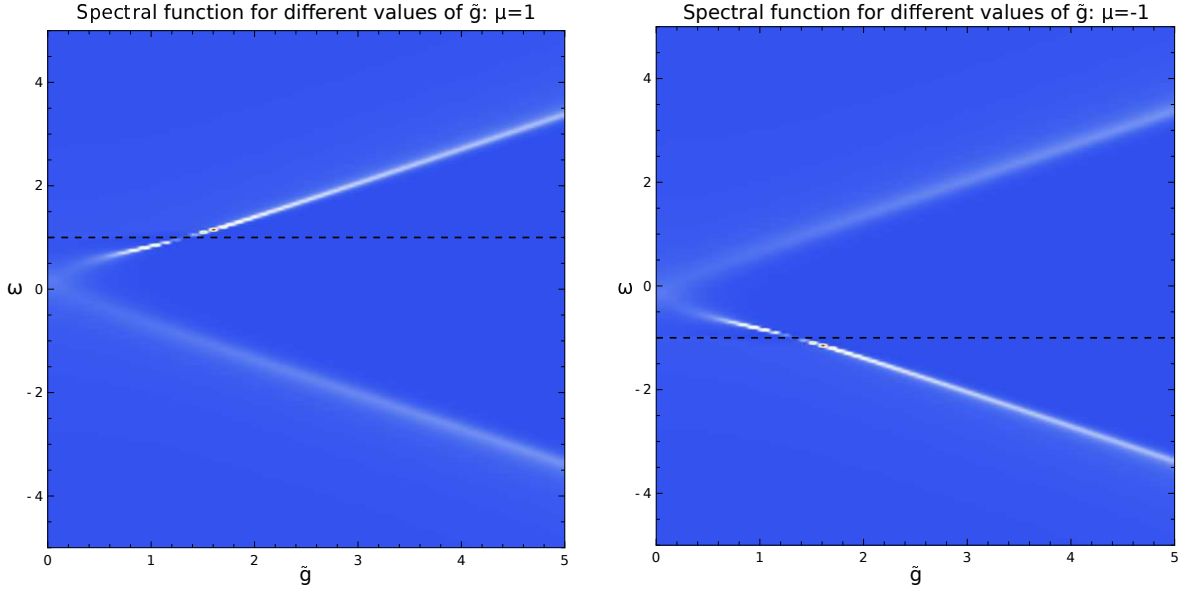


Figure 5.4: Here we present the results of computing the spectral function for  $k_3 = 0$ , for three different values of the chemical potential. The dashed line marks the line  $\omega = \mu$ .

Indeed, as we expected the general behavior of the spectral function remains unchanged, but the region  $|\omega| < |\mu|$  has definitely been modified. Notice in first place that exactly at the crossing point  $\omega = \mu$  the value of the spectral function goes to zero, which corresponds to the Fermi surface.

The behavior of the bottom branch (top for  $\mu < 0$ ) is the usual behavior we expect when the density of states shifts because of the chemical potential. Having a positive  $\mu$  creates more particles than antiparticles and vice-versa for negative  $\mu$ , which we can see as a widening and general blurriness in the plot. Notice however that the effective mass is not significantly changed, keeping the linear dependence with  $\tilde{g}$ .

Next, we will consider the opposite of Figure 5.4, by fixing  $\tilde{g}$  to some values and plotting the dependence of the spectral function for  $k_3 = 0$  over a range of values for  $\mu$ . Presenting the spectral function in this way will allow us to clearly see the behavior of the peaks as the chemical potential increases.

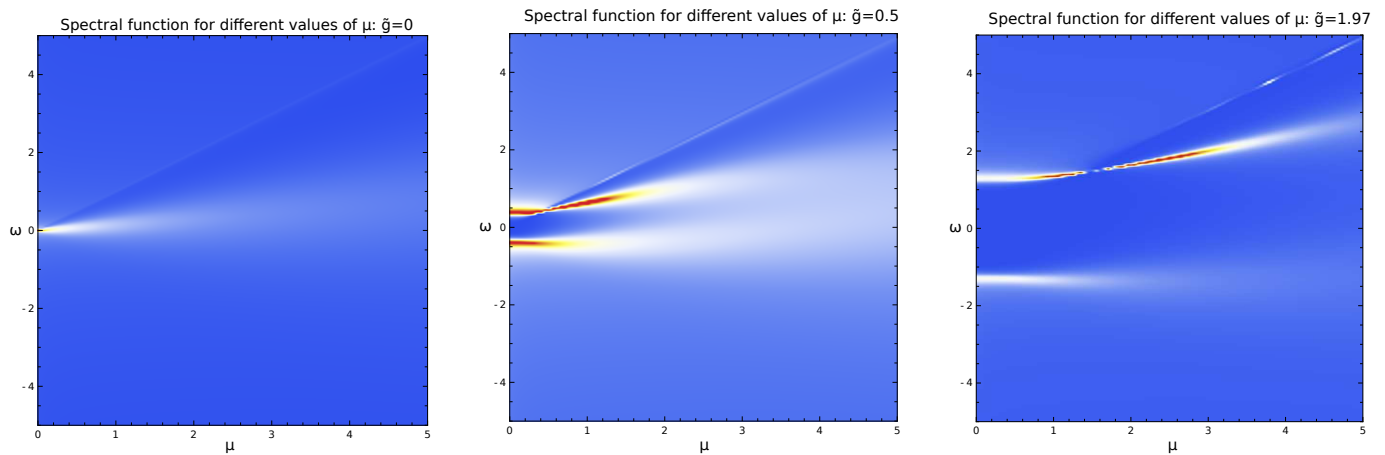


Figure 5.5: Spectral function  $\rho(\omega, 0)$  as a function of  $\mu$ , for three different values of  $\tilde{g}$ . In these plots we can see the effects of the chemical potential on the spectral function when it is lower, equal and higher than the effective mass.

Let us look first at the leftmost plot, in which we are considering just a massless fermion. There we can see, as expected, that the main shape of the spectral function does not change with  $\mu$ , however it is noticeably wider for large chemical potential. Indeed, comparing with Figure 5.4, we can see that this is the behavior we could have expected when  $\tilde{g}$  is small enough.

In the middle plot we have slightly increased  $\tilde{g}$ , so the particles are no longer massless. There we can clearly see the point in the x-axis in which  $\mu = M_{\text{eff}}$ . At this value the positive peak of the spectral function becomes zero because of the Fermi surface, and for larger  $\mu$  can see several effects happening. Firstly, the widening of the peaks actually makes them merge together once the chemical potential is high enough. This situation can be interpreted as the mass energy being negligible compared to  $\mu$ , so that the energy of the fermions is enough to be considered relativistic.

In addition to the widening of the peaks, notice as well that they are shifted towards positive  $\omega$ . This can be interpreted as the density of states moving from antiparticles to particles, since a positive chemical potential will create more of the latter than the former.

In the rightmost plot we can see more clearly the effects we discussed above when  $\mu$  is not significantly higher than the effective mass. Notice that in the three plots there is a line of slope one starting from the point  $\mu = M_{\text{eff}}$ , and increasing with  $\mu$ . It corresponds to  $\omega = \mu$ , therefore corresponding to the Fermi surface.

In Figure 5.6 we can see a close up of these effects for several values of  $\mu$ , at a fixed  $\tilde{g} = 1$ .

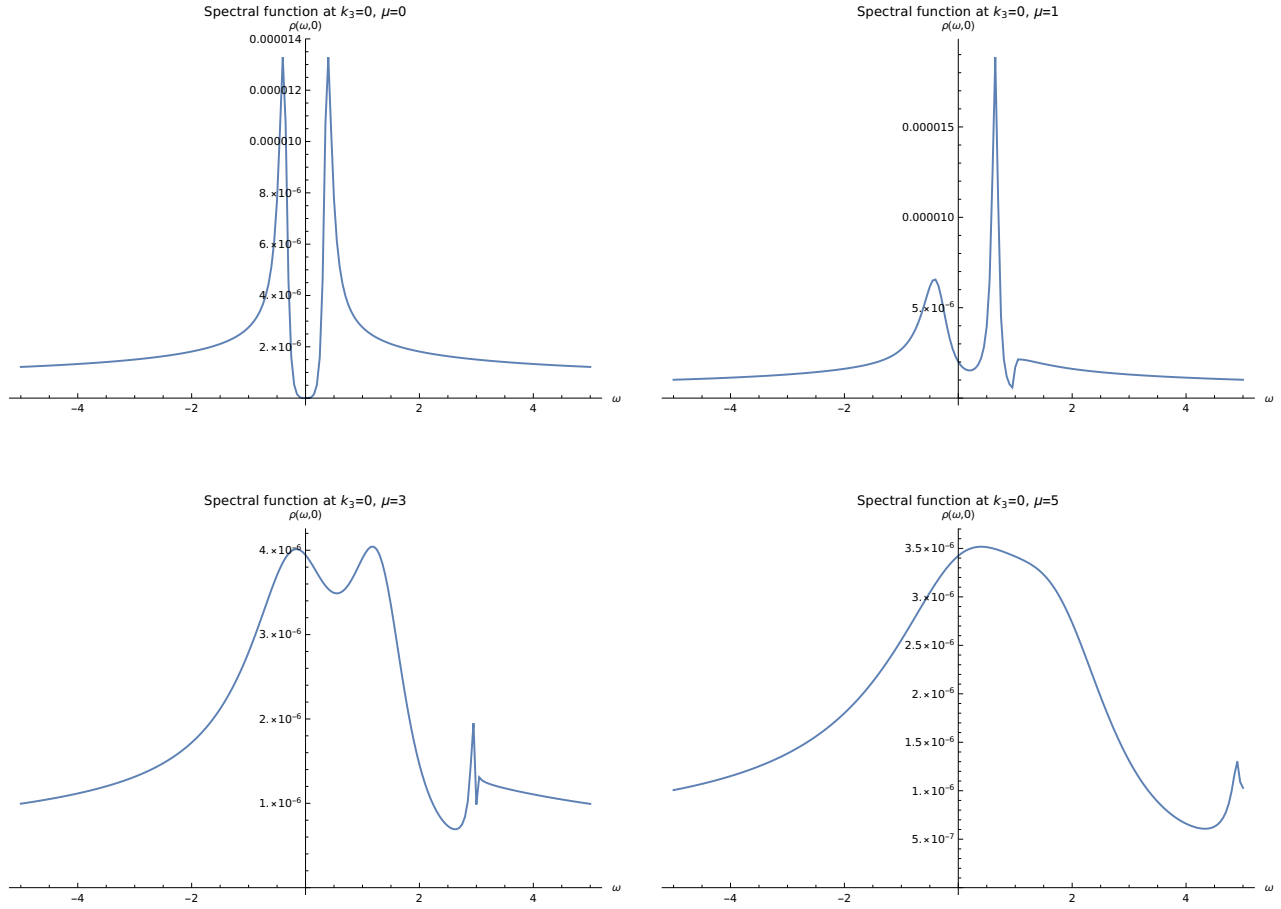


Figure 5.6: Here we show how an increase in chemical potential modifies the spectral function at  $k_3 = 0$  and for  $\tilde{g} = 1$ . We can see closely several of the effects we described from Figure 5.5, such as the Fermi surface, the merging of peaks and shifting towards positive  $\omega$ .

Notice that the behavior of the spectral function is not smooth around the Fermi surface, which could be produced because of some numerical effect of the solution. Since this is a special point, we may need to consider this case separately from the others to fix the correct convergence.

Besides that however, the spectral function is precisely how we were expecting from the previous plots. Notice that the merging of the peaks is not just a shift, instead their maximum value decreases while the density of states in between them increases.

Finally, we present the result computing the spectral function in the  $(\omega, k_3)$ -plane for several values of  $\mu$ , having fixed  $\tilde{g} = 1$ , in Figure 5.7.

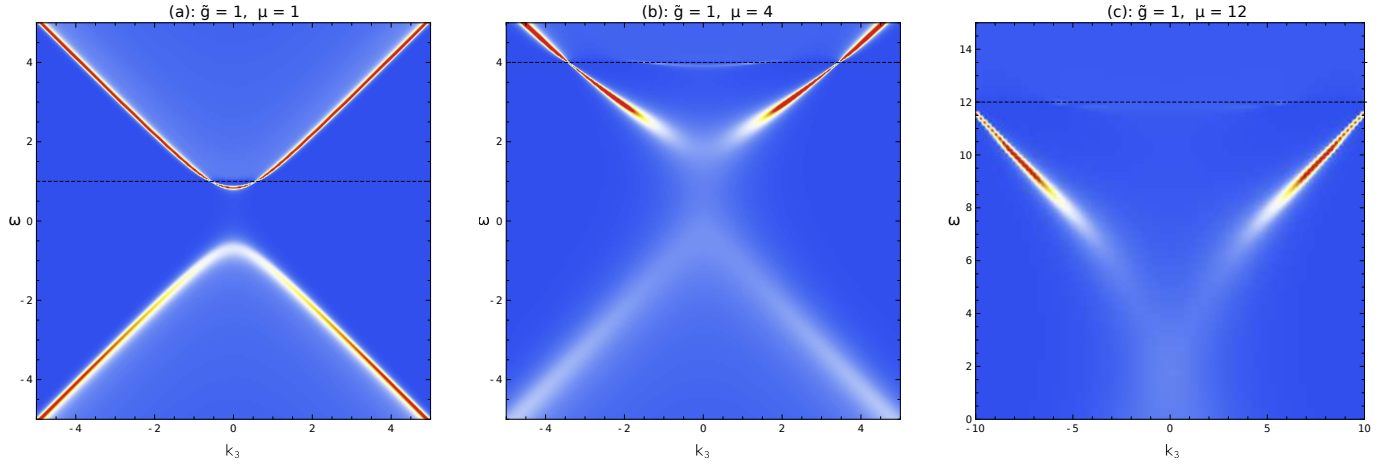


Figure 5.7: Here we can see the results of plotting the spectral function in the  $(\omega, k_3)$ -plane, for several values of  $\mu$ , with  $\tilde{g} = 1$ . The dashed line marks the points with  $\omega = \mu$ .

In 5.7(a) we can see the case in which  $\mu$  is only slightly above the effective mass, and therefore does not significantly affect the spectral function. We can notice however that the bottom branch is less sharp than the top one, as we can expect from Figures 5.5 and 5.6. Notice however that when  $k_3$  is sufficiently large the peaks are again well defined.

In (b) we have increased  $\mu$  even further, so we can clearly see its effects on the spectral function, for small enough  $|\mathbf{k}|$ . Indeed, similarly as in Figure 5.6, we can see that the position of the branches is not significantly changed, instead their values change and the gap closes. Near the top of the plot we can also see an extra branch, related to the oscillatory behavior of the spectral function for high enough  $\mu$ . In [26] there is a more in depth explanation and analysis of this effect.

Finally, in (c) we have significantly increased the chemical potential to  $\mu = 12$ , and only plotted the upper half plane. In this case we can clearly see that the gap is completely closed, and the density of states has spread significantly near the origin.

## 5.2 Semi-holography

Moving on to the more general case, we will consider a finite  $g$  and its effects in the spectral function. We will follow a similar procedure as the one presented for the holographic limit, but now focusing more in discussing how they change as a function of  $g$ .

### 5.2.1 Dependence on $g$

Even though in the next few sections we will analyze the behavior of  $\rho(\omega, k_3)$  for different values of  $g$ , first we will consider some simple situations in which we can clearly see how  $g$  affects the spectral function, having fixed  $\tilde{g} = 1$  and  $\mu = 0$ .

We will begin presenting the results of computing the spectral function at  $k_3 = 0$ , for several values of  $g$ , and determine the mass dependence with it. In Figure 5.8 we can see what we have found in this calculation.

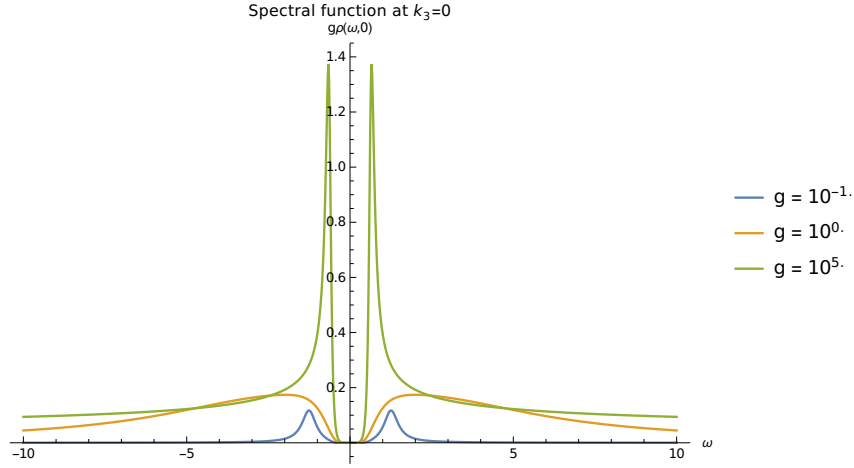


Figure 5.8: Here we can see the result of computing  $g\rho(\omega, 0)$  for several values of  $g$ , at a fixed  $\tilde{g} = 1$  and  $\mu = 0$ . Since we have multiplied by  $g$ , the ARPES sum-rule should now integrate to this constant instead of 1. Notice the difference both in width and height of the peaks as  $g$  changes from  $10^5$  (the holographic limit) to  $10^{-1}$ .

The effect of  $g$  in the spectral function is significant, as we could have expected. It introduces a dramatic widening for values around  $g \sim 1$  without changing the position of the maximum too much. However, considering that the density of states is very spread the notion of a peak becomes blurrier.

In addition, notice that even though the peaks spread, they maintain a mass gap of the same size, the same that we have computed from the holographic limit. On the other hand, when  $g \rightarrow 0$  the only contribution is the bare mass which expressed in units of  $M_0$  is one. Therefore, as we increase  $g$  from zero to  $\infty$  we should see a continuum of effective masses connecting these two extremes.

In Figure 5.9 we can see the same behavior shown previously in Figure 5.8, but in a larger range of values.

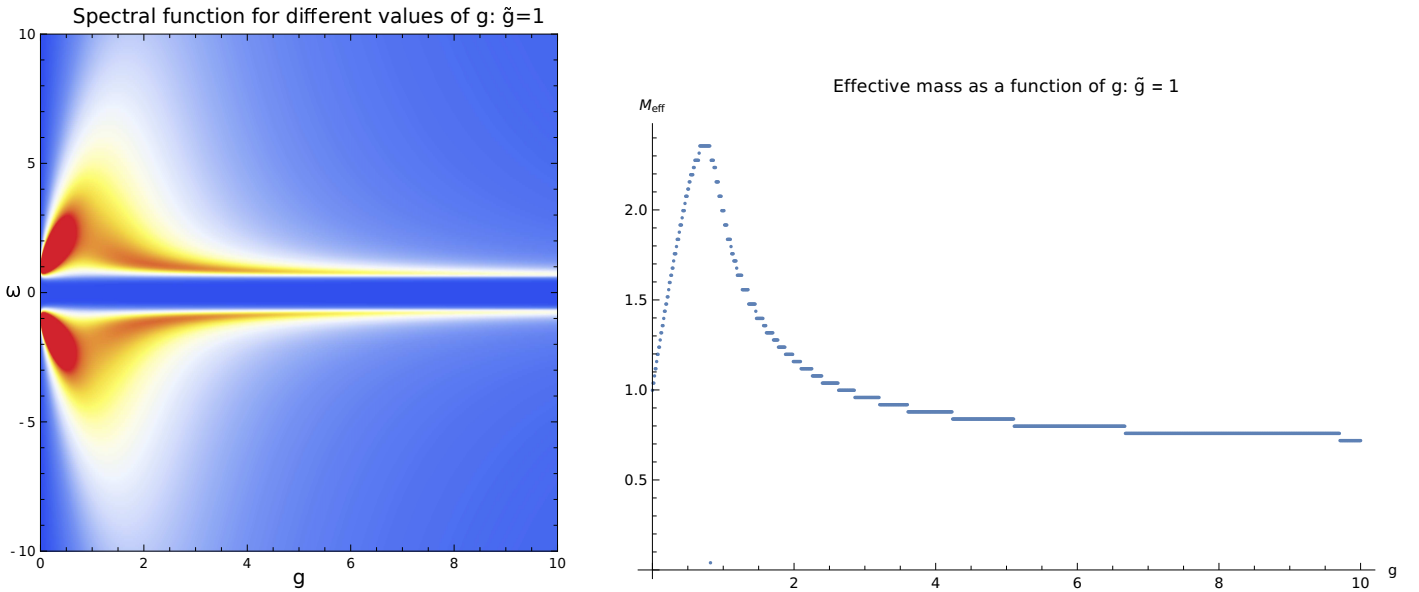


Figure 5.9: (left) Here we present an extension to Figure 5.8, computing the spectral functions for a range of values of  $g$ , showing the dependence of the peak spreading and the peak position. (right) From this data we then compute the mass gap as the distance between peaks. Notice that because of the presence of  $g$  in the denominator of the spectral function we can find a maximum gap around  $g \sim 1$ .

Considering first 5.9(left), notice that as we expected at  $g = 0$  the peaks are exactly at  $\omega = \pm 1$ , and as  $g \rightarrow \infty$  they get closer to the mass gap. The peak spreading happens in a wide region, from  $g \sim \frac{1}{2}$  to  $g \sim 4$ , however we can clearly see that the gap between the branches is constant regardless of  $g$ .

5.9(right) shows the distance between the peaks as a function of  $g$ , indeed following the behavior we were expecting from it. Since we already know the behavior at the holographic limit in terms of  $\tilde{g}$ , we can already predict how these two plots will look like when  $\tilde{g}$  increases. In the next section we will study this behavior.

Before moving on, we present the spectral function in the  $(\omega, k_3)$ -plane, for a fixed  $\tilde{g} = 2$  and several values of  $g$  in Figure 5.10.

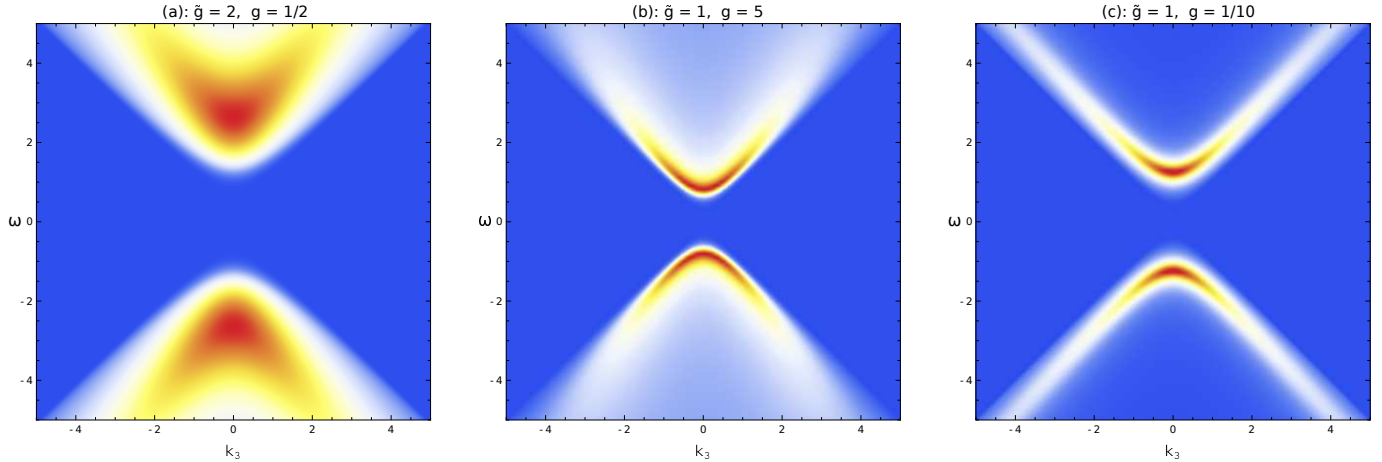


Figure 5.10: In these plots we can see the spectral function in the  $(\omega, k_3)$ -plane for several values of  $g$ . Notice that as we saw previously the peaks are significantly more spread for  $g \sim 1$ .

Notice that in 5.10(a) we can see the expected peak spread filling the inside of the branch. Therefore, unlike in the holographic limit, states will not be sharply defined at one value of the mass, but rather in a very broad region.

On the other hand, in 5.10(b) the parameter  $g$  is now increased and we can see that the density of states starts condensing near the edge, which as we have seen when  $g \rightarrow \infty$  will become the well-defined branch we have shown in the holographic limit. Finally, when we take  $g = \frac{1}{10}$  the branch is sharp and the peaks are very close to  $\omega = \pm 1$ , as we were expecting.

### 5.2.2 Dependence on $\tilde{g}$

Now that we understand better the effect of  $g$  in the spectral function, we can consider different values of  $\tilde{g}$ . In the holographic limit we showed the linear dependence of the mass gap with  $\tilde{g}$ , now we will begin by checking that indeed that is still the same regardless of our choice of  $g$ .

In Figure 5.11 we present these results, computing  $\rho(\omega, 0)$  for several values of  $\tilde{g}$  and  $g$ .

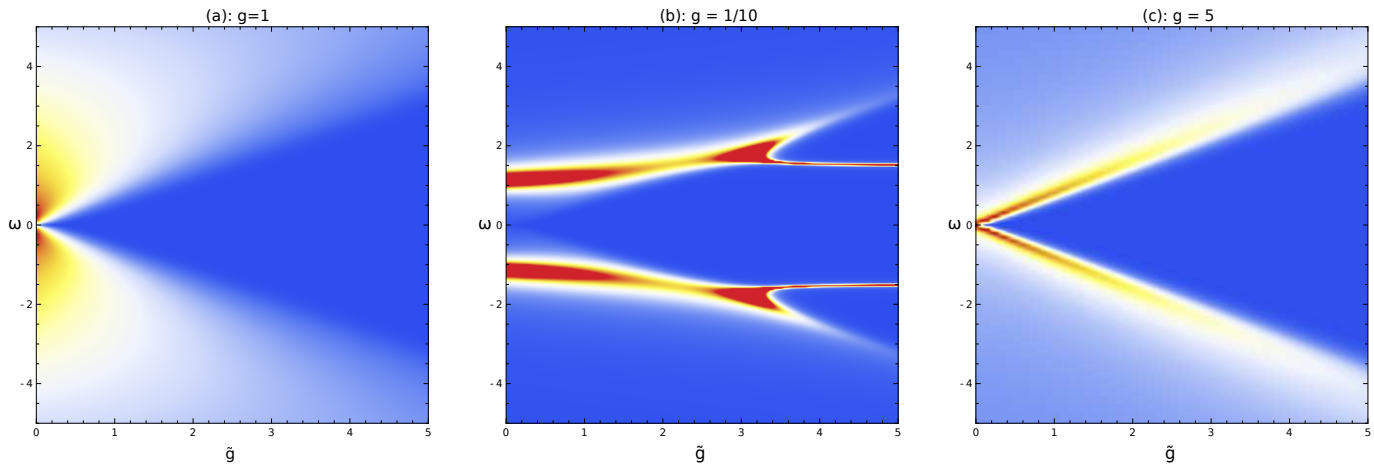


Figure 5.11: In analogy to Figure 5.1 in the holographic limit, now we repeat the results for several values of  $g$ . Notice that the mass gap follows the same linear dependence as before, “pushing away” the peaks.

Indeed, here we can see that for different values of  $g$  the mass gap follows a similar behavior we have seen in Figure 5.9, but in this case the gap is linearly growing with  $\tilde{g}$ . Notice that the position of the peaks is not growing linearly, only the region in which the spectral function is zero grows like that.

In addition to the gap, the peaks themselves are also more spread when  $\tilde{g}$  increases, especially when  $g \sim 1$ . This spreading also occurs when  $g$  is larger, but much less significantly.

Now, notice that in the plot 5.11(b) we can see a fairly interesting band structure that is not appearing in the others. The only difference being that in this plot  $g = \frac{1}{10}$ , significantly smaller than the others. What we are seeing here we can interpret as an avoided crossing of two poles, one peak starting from  $\omega = 0$  at  $\tilde{g} = 0$  and another one starting from  $\omega = 1$ . Then, as  $\tilde{g}$  increases we can see that the lower peak’s growth saturates and becomes a very thin band at a constant  $\omega$ , while the other grows linearly.

In Figure 5.12 we can see the details of this plot. Because of the extreme thinness of the lower branch, measuring it is fairly difficult when the other one is too close, and therefore we can only see it when they are enough far away from each other.

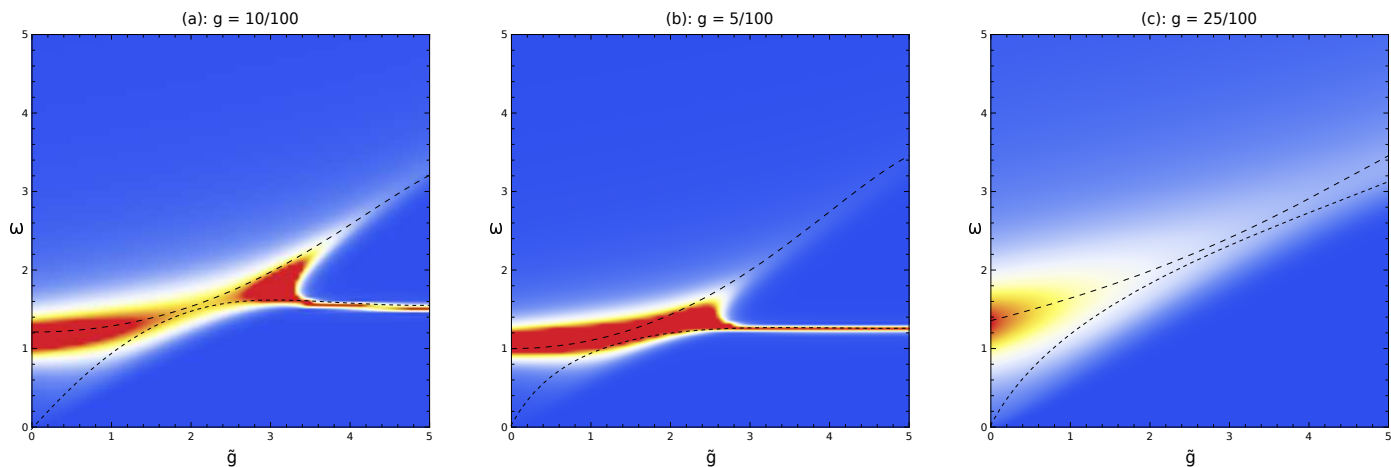


Figure 5.12: Here we can see a close up of the avoided crossing at low  $g$ , where the dashed lines are visual indicators of where the poles are supposed to be, each described by the position of the band we can see in the limit  $g = 0$  and the CFT band. Notice that this branching only happens at small enough  $g$ , hence it is not visible in other plots.

This structure is also highly sensitive to temperature, and one possible approach to determine more accurately how the position of each peak depends on  $\tilde{g}$  would be to decrease  $T$  significantly. However, doing so increases the computation time dramatically, and more analysis of this is necessary.

Next, we will analyze the spectral function in the plane, again for several values of  $\tilde{g}$  and  $g$ .

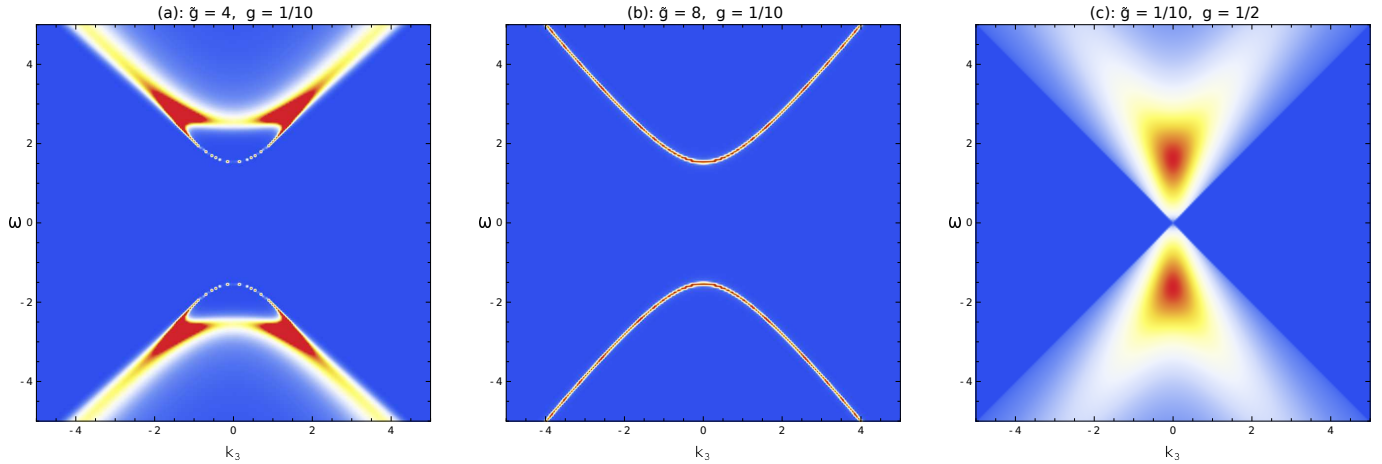


Figure 5.13: In these plots we can see the spectral function in the  $(\omega, k_3)$ -plane for several values of  $\tilde{g}$  and  $g$ . Notice the presence in plots (a) and (b) of the band structure, while in (c)  $g$  is large enough for the density of states to be filling the light-cone.

In 5.13(a) we can clearly see the band structure hinted at in Figure 5.12. The bottom branch is indeed very thin and follows the usual dispersion relation for massive particles, in this case with effective mass  $M_{\text{eff},1} \approx 1.5$ . Notice now that the shape of the top branch is not exactly parabolic, however we can associate it an effective mass of  $M_{\text{eff},2} \approx 2.5$ , and they both merge for high enough  $|\mathbf{k}|$ .

This band structure is an interesting characteristic of the model, that only appears in a very specific regime, and one possible physical interpretation is the following. Consider that, in the boundary, we are describing a massive fermion with interactions. Then, for low enough energies these fermions could form long-lived bound states with an effective mass higher than the bare mass of the propagator. If that is indeed the case, it is reasonable to think that the strength of that bound will be related to the coupling constants  $g$  and  $\tilde{g}$ .

We have noticed that these two bands are kept together as only one peak, in terms of  $\tilde{g}$  as shown in Figure 5.12, longer when  $g$  is large. Going back to the holographic limit, we can indeed see that there are no band structure in any of the plots, we can only see both bands separated when  $g$  is closer to zero. Notice as well that the bottom band does not depend on  $\tilde{g}$ , since it saturates quickly and remains constant. This is clearly the product of a combination of both the self-energy and the semi-holographic contribution, perhaps best understood as a perturbation of the usual spectral function for massive fermions.

In 5.13(b) we have increased  $\tilde{g}$  enough to clearly see the bottom band, showing that indeed its effective mass does not change significantly with that parameter.

In 5.13(c) on the other hand we can see the complete opposite effect. Here, a very small  $\tilde{g}$  makes the spectral function to fill the region inside the light-cone because of the peak spreading. Therefore, any possible band structure is impossible to measure, and even though we can find a peak, it is not significantly above its surroundings.

### 5.2.3 Dependence on $\mu$

Following the same structure as before, we will now consider the case  $\mu \neq 0$ . Since for certain values of  $g$  the spectral function is not a well-defined band anymore, we want to study the effects of having a chemical potential on that regime.

For this purpose, we start by showing in Figure 5.14 what happens with the spectral function for several values of  $\tilde{g}$  when the chemical potential is increased to  $\mu = 1$ .

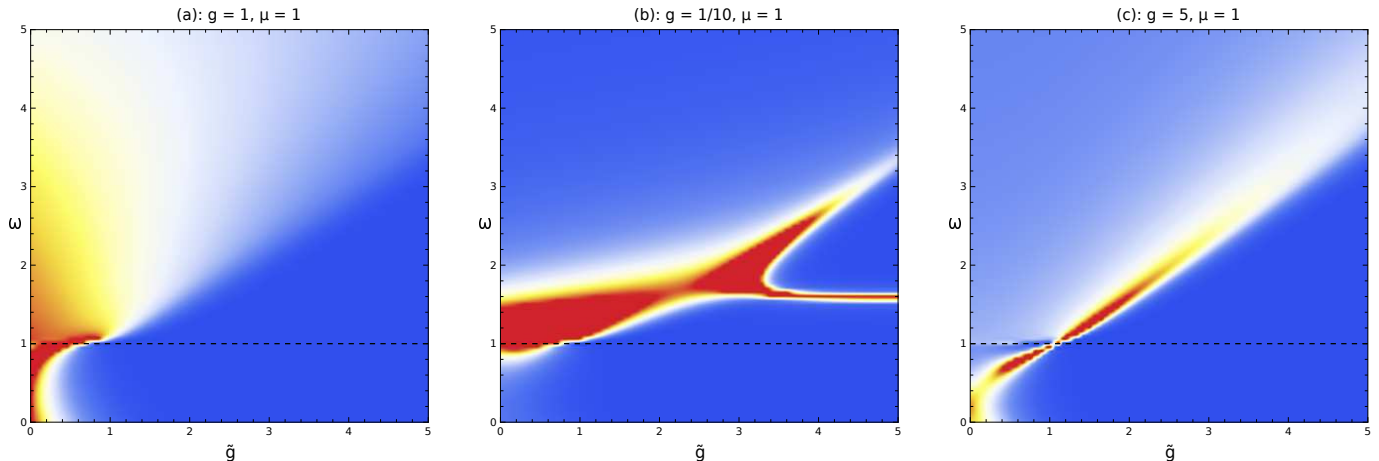


Figure 5.14: Here we can see three significant cases of the spectral function that we have introduced before, now with  $\mu = 1$ . The dashed line marks the points with  $\omega = \mu$ . In (a) we set  $g = 1$ , and thus a large spread of the peaks, with the chemical potential “pushing up” the density of states from the region  $\omega < \mu$ . In (b) we have the band structure case, however  $\mu$  here is too small to produce a significant change on it. Lastly, in (c) we have increased  $g$  to 5, thus now resembling more the holographic limit as we have seen before.

For a more complete analysis of the effects of the chemical potential on the spectral function, we consider here the three most relevant cases we have seen. First, in 5.14(a) we choose  $g = 1$ , for which the peaks spread greatly, and set the chemical potential to  $\mu = 1$ . What we can see in the plot is that when the density of states is non-zero below  $\omega = \mu$ , happening when  $\tilde{g}$  is small enough, these states are shifted towards  $\omega \sim \mu$  and form a peak at that energy. If  $\tilde{g}$  is high enough however, they are not shifted and remain near the origin thus describing nearly massless particles.

In 5.14(b) on the other hand, because  $g$  is very close to zero the effective mass of the particles is close to  $\omega = 1$ , therefore not being affected significantly by the chemical potential. In Figure 5.15 we will take another look at this situation with a higher  $\mu$ .

Finally, in 5.14(c) we can see the expected result we could have predicted from Figure 5.4, since  $g$  is already large enough to be close to the holographic limit. Next, we will consider again (a) and (b) for a higher chemical potential.

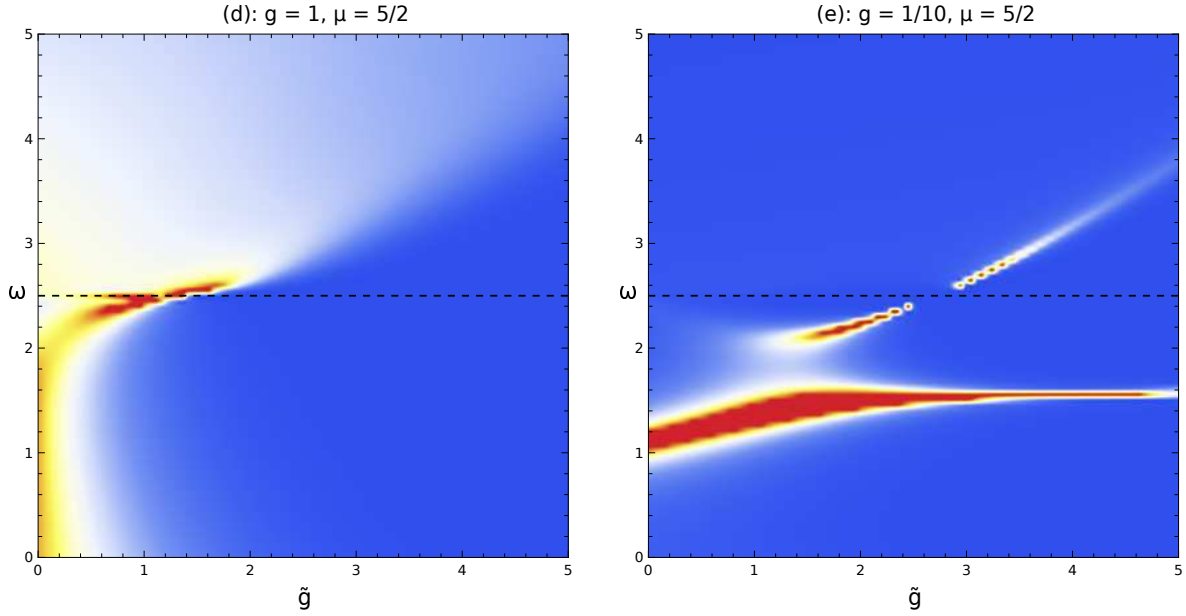


Figure 5.15: Considering only plots (a) and (b) from Figure 5.14, here we show the effect of increasing the chemical potential to  $\mu = 5/2$ . In (d) the spread spectral function follows a behavior similar to what we have seen before, while in (e) now  $\omega = \mu$  crosses the top band, showing the usual effect of reducing its value to zero, while leaving the lower band largely unaffected.

In Figure 5.15(a) we show that the behavior of the spectral function at  $g = 1$  does not change significantly when the chemical potential is increased. Since  $\mu$  is now larger, it is necessary for  $\tilde{g}$  to be larger as well so the main volume of the spectral function is not affected.

On the other hand, 5.15(b) shows that when the chemical potential is increased, only the top band is significantly affected by it. We can also see that because states are being pushed towards  $\omega = \mu$ , when the effective mass is smaller than the chemical potential (around  $\tilde{g} \sim 2$  in the plot), the density of states shifts towards the top band, clearly showing that there are two poles interacting in that regime.

Next, we will consider a fixed  $g$  and  $\tilde{g}$ , and compute the spectral function for a range of values for  $\mu$ . Considering again these three important cases, we will analyze their behavior as a function of the chemical potential.

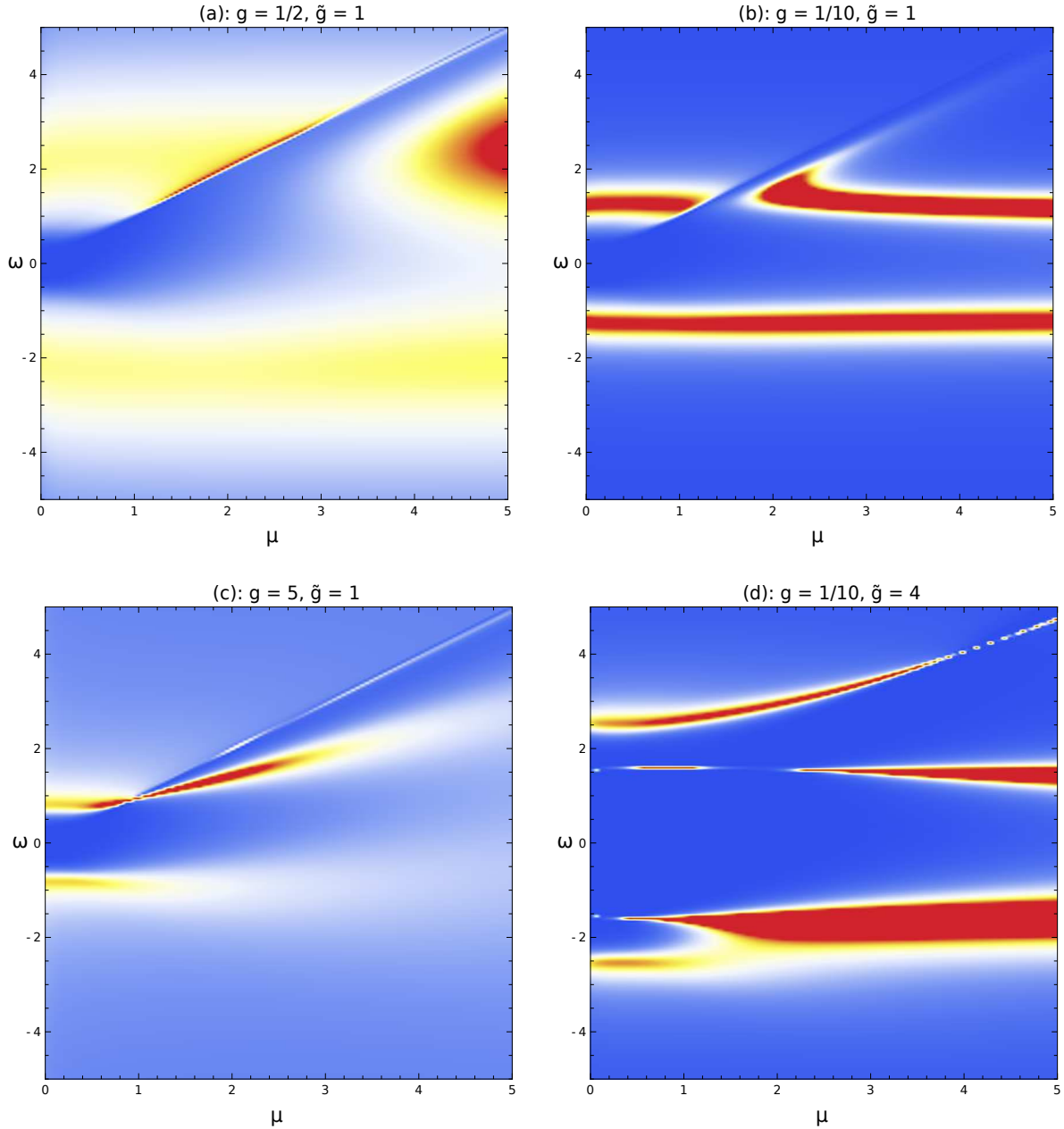


Figure 5.16: Here we present a different perspective on the three cases relevant for this discussion. In (a) we have the spread case, in (b) and (d) we have the band structure at two different  $\tilde{g}$ , and in (c) we have the situation closest to the holographic limit.

Considering 5.16(a) in the first place, we find the normal behavior at small  $\mu$ , and around the point in which the chemical potential is large enough to affect the spectral function we see the states getting closer together slightly above the line  $\omega = \mu$ . Then, when  $\mu$  is large enough particles begin behaving as if they were massless, which we can see from the increasing value of the spectral function around  $\omega = 0$  for  $\mu > 4$ . At these values we also start seeing how the bottom branch gets shifted upwards, which in this plot we can see as a bulge below the  $\omega = \mu$  line.

On the other extreme, in 5.16(c) we present the near-holographic limit case. Its behavior is exactly what we could have predicted, and no new effects are visible.

Lastly, in plots 5.16(b) and 5.16(d), we focus on the regime in which the band structure is visible. Specifically,

in (b) the two poles are very close together thus forming only one peak. In this case when the chemical potential crosses the peak it gets distorted, making the spectral function at the points  $\omega = \mu$  go to zero, however as  $\mu$  keeps increasing the peak returns back to normality, remaining mostly unaffected by the high value of the chemical potential.

In the last plot, (d), we have increased  $\tilde{g}$  enough for the two bands to be far away from each other, and again we see an interesting behavior. As the chemical potential increases, the bottom branch, with two bands, merge together in one broad peak as we would expect, since we are creating more particles than antiparticles. It remains at roughly the same energy, mostly widening with  $\mu$ .

On the other hand, the top branch keeps its band structure as  $\mu$  changes, with the bottom one widening as the chemical potential moves past its effective mass. The top band however, is being warped upwards in  $\omega$  as  $\mu$  increases, crossing once the line  $\omega = \mu$  and then continuing right below it.

Let us compare now this last plot, (d), with (a) and (b). In (a) we see that the spectral function gets pushed towards  $\omega > \mu$ , in the same way that the top band in (d) does. At the same time, in (b) we can see that even though there is some pushing when the line  $\omega = \mu$  crosses the band, it remains essentially at the same energy regardless of the chemical potential. Connecting these two behaviors then, we can see that for higher  $g$  the density of states is mostly on the top band making the bottom one basically undetectable, while for smaller  $\tilde{g}$  the behavior of the peak is driven by the bottom band.

To better visualize this dependence, in Figures 5.17 and 5.18 we plot the spectral function in the plane  $(\omega, k_3)$  in these different situations.

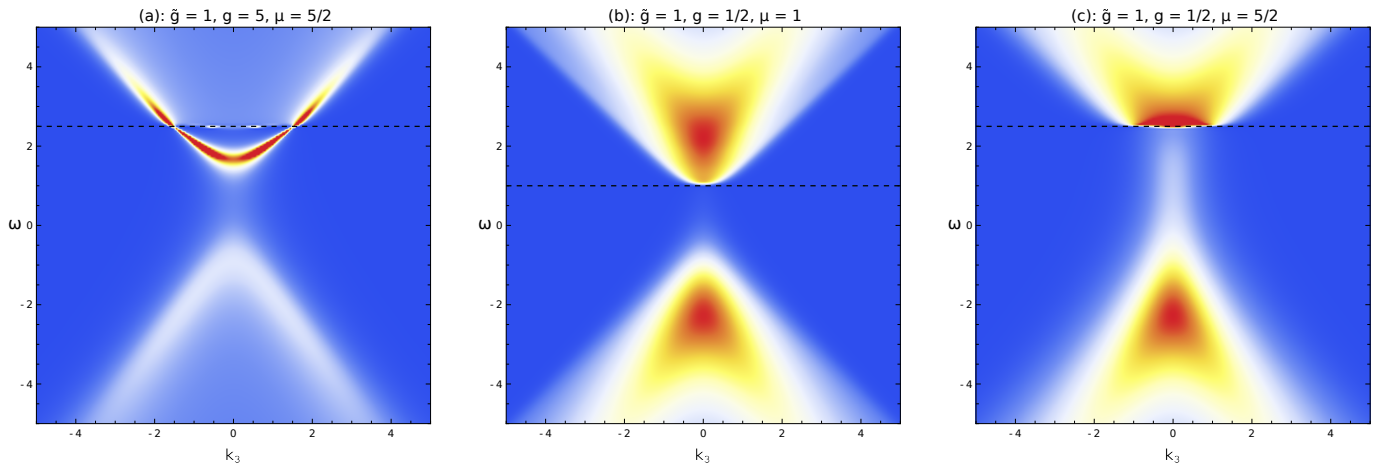


Figure 5.17: Here the spectral function in the  $(\omega, k_3)$ -plane is shown. In (a) we have the simple near-holographic limit behavior. In (b) and (c) we show how the density of states is pushed upwards with increasing  $\mu$  in the spread peaks regime.

First, in (a) we show the usual behavior associated with large  $g$  that we have been seeing, nothing remarkably different is happening here.

Next, in (b) the chemical potential is not high enough to affect the top branch, but we can already see some effects in the bottom branch. A blurriness is noticeable, meaning that the spectral function is closer to zero, in agreement with what we can see in plot (a) and others. From plot (a) in Figure 5.16 we can see that at  $\mu = 1$  the top branch is slightly affected by the chemical potential, but it is not visible in this plot.

Now, in plot (c) we take  $\mu = 5/2$  to show how the states concentrate right above the line  $\omega = \mu$ , completely distorting the parabolic shape of plot (b). In addition, the lower branch becomes stretched and a bridge between

the two is clearly visible. However, the region  $\omega > \mu$  contains most of the volume of the spectral function, and therefore most of the states will be found there.

The behavior shown in these plots is in perfect agreement with our predictions by analyzing Figure 5.16, plots (a) and (c). We can move on then to the band structure case in Figure 5.18.

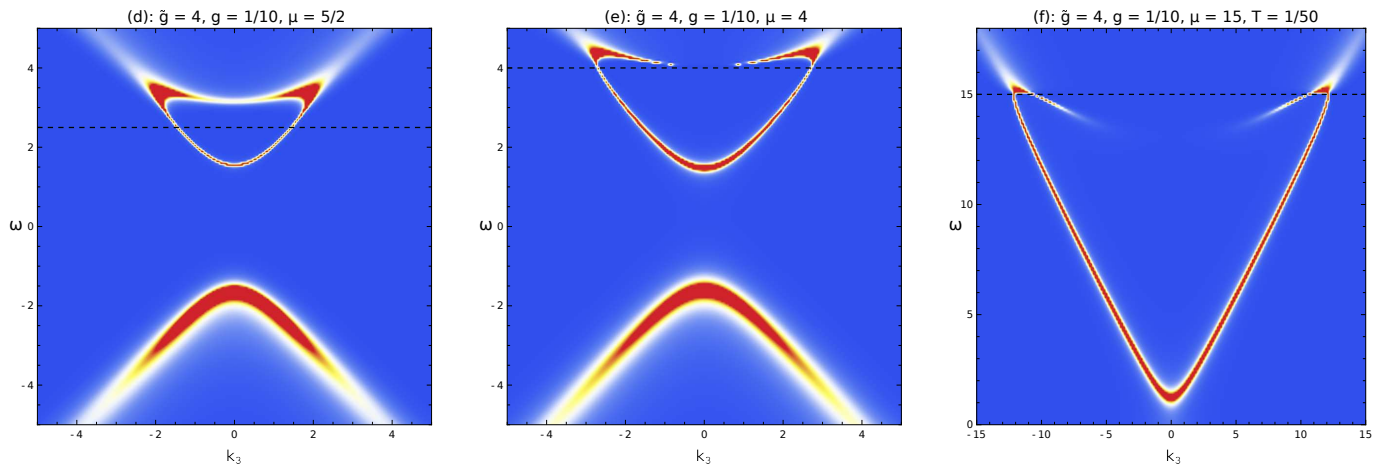


Figure 5.18: Continuing with Figure 5.17's plots, in (d), (e) and (f) we show the behavior of the band structure for several different values of  $\mu$ . Notice that in (f) we increased the chemical potential significantly, and we had to reduce the temperature to  $\frac{1}{50}$  so that we could find the set of initial conditions associated with these parameters.

In these three plots we can see significantly different values of the chemical potential affecting the band structure we have been studying. Starting with plot (d), we have chosen a value for  $\mu$  in between the effective masses of both bands, showing that the bottom band is not significantly affected by the chemical potential. The negative branch, however, is dramatically changed as the density of states has shifted from being mostly on the most negative band to the least negative.

Then, in plot (e) we have increased the chemical potential further to  $\mu = 4$ , showing that the top band is indeed slightly above the line  $\omega = \mu$ . In addition, the bottom band is wider as the states are more short-lived because the chemical potential is fairly higher than the effective mass. Notice however that its position has barely changed with  $\mu$ , and even though in other situations we would have started seeing a bridge between the top and bottom branches that is not the case here.

Finally, dramatically increasing the chemical potential to  $\mu = 15$  shows that the top band is now below the line  $\omega = \mu$ , however both bands still merge at a higher energy. At this point we can notice that the bottom branch has slightly moved down, however particles are still behaving as massive ones as the parabolic dependence is clearly visible.

## 6 Conclusion

In this section we will briefly review what we have done in this thesis and, in general, discuss what we have found. Then, we will present some possible outlooks of this work, both as a direct consequence of what we have done and future developments.

### 6.1 Discussion

The AdS/CFT correspondence is indeed a very fruitful field of research, with a large potential for explaining very complex systems in a straightforward manner. However, because of its intrinsic limitations there is still much work to do, and in the future we will continue getting insights into Condensed Matter Theory because of it.

In this thesis we applied the AdS/CFT correspondence to a very specific case: describing massive atoms in a Fermi gas. The final goal of this approach is to describe cold atom gases, or as we have explained in the introduction, cold Fermi mixtures. Even though the amount of work ahead of us is very significant, this is a small step in the right direction.

Our contribution has been to introduce a static background for the bulk that encodes the information about several parameters of the boundary theory, such as temperature and chemical potential, as well as the bare mass of the atoms. Since we work with systems in equilibrium, we extract the information encode in the geometry using a probe field, which we let propagate from the horizon of the black hole all the way to the boundary, where the massive fermions propagate.

As we have seen however, correctly deriving a method to describe this bulk theory is non-trivial, and required a development and generalization of some techniques used in simpler cases. For this we considered the case of massless boundary fermions and recomputed it using our new method, clearly showing its advantages when we applied it to the more general case of massive atoms.

Although, extracting this geometric information using a probe field is not enough, since we still need to compare our results with experiments. For this we computed the Green's function and spectral function, which we can compare with RF spectroscopy experiments and therefore check and correlate that our results are indeed describing the physical system. In the results we have indeed found a mass gap that depends linearly on the parameter  $\tilde{g}$ , and the interesting behavior shown when  $g$  is small enough as an avoided crossing.

Comparing with experiments requires a good understanding of the results we have found, and that was our goal in the last section. We considered several of the most important parameters of the theory,  $g$ ,  $\tilde{g}$ ,  $T$  and  $\mu$ , and analyzed how the spectral function is affected by changes in them. Moreover, we studied in depth how the effective mass of the boundary fermions depends on those parameters, so that we understand the details of this mechanism for introducing a mass.

### 6.2 Outlook

However, there is still work to do. In this thesis we have not looked at every possible parameter dependence, for example  $M$  and  $q$ , but as we explained before they non-trivially define the scaling behavior of the boundary operators, and therefore understanding how the theory changes in terms of critical exponents and other quantities can give more physical insights into the procedure.

Related to this, we have given a possible explanation for the band structure we have found, but more analysis is definitely necessary to completely understand it. Determining what are the consequences in the boundary

theory and studying how is this behavior related to the propagation in the bulk would be good starting points, but many others are possible.

Besides this, we have not looked at any thermodynamic quantities such as conductivity in the boundary, which would be another way of checking this model's predictions with experiments. Several of these can be computed using the Green's function, so this would be very clear next step from this thesis.

Also related to thermodynamic quantities, we focused this thesis in the static probe limit, in other words, we considered the background geometry to be static. To describe phase transitions we need however to move away from the probe limit. In AdS/CFT this is equivalent to considering a non-static background for the fermionic field to propagate, that is, consider the back-reaction in the geometry. We briefly mentioned before that the fermionic case is not as simple as the bosonic, as it requires additional considerations regarding the ground-state, but there are several possible techniques that can be used.

In the introduction we also mentioned that we are not very interested in the relativistic behavior of atoms, but in the non-relativistic limit of the theory. From our results we can already see that for small enough  $|\mathbf{k}|$  the spectral function reduces to what we would expect from a non-relativistic theory, but the next proper step would be to consider the limit  $c \rightarrow \infty$  and extract this behavior.

Slightly further down the road, now that we have developed a method to describe one species of massive fermions in the boundary, the next step is to introduce another species to complete the Fermi mixture picture. It would involve adding a new coupling operator between the fermions in the boundary, which should be dual to some field in the boundary. Since in this case we have two Dirac fermions in the boundary, with possibly two different masses, it would be necessary to again double the number of degrees of freedom in the bulk by introducing another two fermionic fields, as well as possibly another scalar field.

Once we can describe interacting species of fermions in the boundary using the AdS/CFT correspondence however, we are a step closer to start describing proper physical systems. This is clearly not a simple task, but step by step we continue developing the necessary tools to start predicting their behavior.

## References

- [1] J. Bardeen, L. N. Cooper, J. R. Schrieffer, *Phys. Rev.* **108** (1957) 1175.
- [2] A. J. Leggett, *Modern Trends in the Theory of Condensed Matter*, Springer-Verlag, Berlin, 1980, p. 13.
- [3] C. A. Regal, M. Greiner, D. S. Jin, *Phys. Rev. Lett.* **92** (2004) 040403.
- [4] M. W. Zwierlein, C. A. Stan, C. H. Schunck, S. M. F. Raupach, A. J. Kerman, W. Ketterle, *Phys. Rev. Lett.* **92** (2004) 120403.
- [5] M. W. Zwierlein, A. Schirotzek, C. H. Schunck, and W. Ketterle, *Science* **311**, 492 (2006).
- [6] G. B. Partridge, W. Li, R. I. Kamar, Y. A. Liao, and R.G. Hulet, *Science* **311**, 503 (2006).
- [7] K. B. Gubbels and H. T. C. Stoof, *Phys. Rev. Lett.* **100**, 140407 (2008).
- [8] E. Burovski, N. Prokof'ev, B. V. Svistunov, M. Troyer, *Phys. Rev. Lett.* **96**, 160402 (2006).
- [9] C. Lobo, A. Recati, S. Giorgini, and S. Stringari, *Phys. Rev. Lett.* **97**, 200403 (2006).
- [10] S. A. Hartnoll, *Lectures on holographic methods for condensed matter physics*, 17 Jan 2010. [arXiv:0903.3246v3 [hep-th]]
- [11] J. M. Maldacena, *The large N limit of superconformal field theories and supergravity*, *Adv. Theor. Math. Phys.* **2**, 231 (1998), [*Int. J. Theor. Phys.* **38**, 1113 (1999)];
- [12] S. S. Gubser, I. R. Klebanov and A. M. Polyakov, *Gauge theory correlators from noncritical string theory*, *Phys. Lett. B* **428** (1998) 105.
- [13] E. Witten, *Anti-de Sitter space and holography*, *Adv. Theor. Math. Phys.* **2** (1998) 253;
- [14] Kostas Skenderis, *Lecture Notes on Holographic Renormalization*, 11 Oct 2002. [arXiv:hep-th/0209067v2]
- [15] David Tong, *Lecture Notes on Quantum Field Theory*, 2006 and 2007.
- [16] Yoran Tournois, *The Holographic Electron Star*, 30 June 2015. Master's Thesis for Utrecht University.
- [17] N. W. M. Plantz, H. T. C. Stoof, and S. Vandoren, *Order parameter fluctuations in the holographic superconductor*, 16 Jan 2017. [arXiv:hep-th/1511.05112v4]
- [18] S. Carroll, *Spacetime and Geometry: An Introduction to General Relativity*, Pearson Education, San Francisco (2004).
- [19] J. Zaanen, Y. Sun, Y. Liu and K. Schalm, *The AdS/CMT manual for plumbers and electricians*, [<https://web.science.uu.nl/drstp/Postgr.courses/SPTCM/2015/adscmtreview.pdf>]
- [20] Amadeo Jimenez-Alba, Karl Landsteiner, Yan Liu, Ya-Wen Sun, *Anomalous magnetoconductivity and relaxation times in holography*, 4 May 2015. [arXiv:1504.0656 v2 [hep-th]]
- [21] R. Contino and A. Pomarol, *Holography for fermions*, *JHEP* **0411** (2004) 058 [arXiv:hep-th/0406257].
- [22] Sergej Moroz, *Below the Breitenlohner-Freedman bound in the nonrelativistic AdS/CFT correspondence*, 27 Mar 2010. [arXiv:0911.4060v2 [hep-th]]
- [23] Umut Gürsoy, Erik Plaushinn, Henk Stoof, Stefan Vandoren, *Holography and ARPES sum-rules*, 18 Apr 2012. [arXiv:12.5074v3 [hep-th]]
- [24] D. T. Son, A. O. Starinets, *Minkowski-space correlators in AdS/CFT correspondence: recipe and applications*, 29 Sep 2002. [arXiv:hep-th/0205051v2]

- [25] Palash B. Pal, *Representation-independent manipulations with Dirac matrices and spinors*, 14 May 2015. [arXiv:physics/0703214v4]
- [26] U. Gürsoy, V. Jacobs, E. Plauschinn, H. Stoof and S. Vandoren, *Holographic models for undoped Weyl semimetals*, J. High Energy Phys. **04** (2013) 127.